CANADIAN THESES

THÈSES CANADIENNES

NOTICE

The quality of this microfiche is heavily dependent upon the quality of the original thesis submitted for microfilming. Every effort has been made to ensure the highest quality of reproduction possible.

If pages are missing, contact the university which granted the degree.

Some pages may have indistinct print especially if the original pages were typed with a poor typewriter ribbon or if the university sent us an inferior photocopy.

Previously copyrighted materials (journal articles, published tests, etc.) are not filmed.

Reproduction in full or in part of this film is governed by the Canadian Copyright Act, R.S.C. 1970, c. C-30. Please read the authorization forms which accompany this thesis.

AVIS

La qualité de cette microfiche dépend grandement de la qualité de la thèse soumise au microfilmage. Nous avons tout fait pour assurer une qualité supérieure de reproduction.

S'il manque des pages, veuillez communiquer avec l'université qui a conféré le grade.

La qualité d'impression de certaines pages peut laisser à désirer, surtout si les pages originales ont été dactylographiées à l'aide d'un ruban usé ou si l'université nous a fait parvenir une photocopie de qualité inférieure.

Les documents qui font déjà l'objet d'un droit d'auteur (articles de revue, examens publiés, etc.) ne sont pas microfilmés.

La reproduction, même partielle, de ce microfilm est soumise à la Loi canadienne sur le droit d'auteur, SRC 1970, c. C-30. Veuillez prendre connaissance des formules d'autorisation qui accompagnent cette thèse.

THIS DISSERTATION
HAS BEEN MICROFILMED
EXACTLY AS RECEIVED

LA THÈSE A ÉTÉ
MICROFILMÉE, TELLE QUE
NOUS L'AVONS REÇUE

Canada

National Library
of Canada

Bibliothèque nationale
du Canada

Ottawa, Canada
K1A 0N4

CANADIAN THESES ON MICROFICHE SERVICE – SERVICE DES THÈSES CANADIENNES SUR MICROFICHE

PERMISION TO MICROFILM – AUTORISATION DE MICROFILMER

• Please print or type – Écrire en lettres moulées ou dactylographier

AUTHOR – AUTEUR

Full Name of Author – Nom complet de l'auteur

John Steven Kirk

Date of Birth – Date de naissance

Sept 03, 1961

Canadian Citizen – Citoyen canadien

☑ Yes / Oui   ☐ No / Non

Country of Birth – Lieu de naissance

Canada

Permanent Address – Résidence fixe

#25-6215-98 avenue
Edmonton, Alberta
T6A 0A3

THESIS – THÈSE

Title of Thesis – Titre de la thèse

Laboratory Study of Mineralogical Changes During Steam Condensate Flooding of Cold Lake Oil Sands

Degree for which thesis was presented
Grade pour lequel cette thèse fut présentée

M. Sc.

Year this degree conferred
Année d'obtention de ce grade

1985

University – Université

University of Alberta

Name of Supervisor – Nom du directeur de thèse

Fred. J. Longstaffe

AUTHORIZATION – AUTORISATION

Permission is hereby granted to the NATIONAL LIBRARY OF CANADA to microfilm this thesis and to lend or sell copies of the film.

The author reserves other publication rights, and neither the thesis nor extensive extracts from it may be printed or otherwise reproduced without the author's written permission.

L'autorisation est, par la présente, accordée à la BIBLIOTHÈQUE NATIONALE DU CANADA de microfilmer cette thèse et de prêter ou de vendre des exemplaires du film.

L'auteur se réserve les autres droits de publication; ni la thèse ni de longs extraits de celle-ci ne doivent être imprimés ou autrement reproduits sans l'autorisation écrite de l'auteur.

▶ ATTACH FORM TO THESIS – VEUILLEZ JOINDRE CE FORMULAIRE À LA THÈSE ◀

Signature

Date

October 7, 1985

NL-91 (r. 84/03)

Canada

THE UNIVERSITY OF ALBERTA

"Laboratory Study of Mineralogical Changes During Steam
Condensate Flooding of Cold Lake Oil Sands"

BY

John S. Kirk

A THESIS
SUBMITTED TO THE FACULTY OF GRADUATE STUDIES AND RESEARCH
IN PARTIAL FULFILMENT OF THE REQUIREMENTS FOR THE DEGREE
OF Master of Science

Department of Geology

EDMONTON, ALBERTA
Fall, 1985

THE UNIVERSITY OF ALBERTA

RELEASE FORM

NAME OF AUTHOR: John S. Kirk

TITLE OF THESIS: "Laboratory Study of Mineralogical Changes During
Steam Condensate Flooding of Cold Lake Oil Sands"

DEGREE: Master of Science
YEAR THIS DEGREE WAS GRANTED: Fall, 1985

Permission is hereby granted to THE UNIVERSITY OF ALBERTA
LIBRARY to reproduce single copies of this thesis and to lend or sell
such copies for private, scholarly or scientific research purposes
only.

The author reserves other publication rights, and neither
the thesis nor extensive extracts from it may be printed or otherwise
reproduced without the author's written permission.

(SIGNED) ....

PERMANENT ADDRESS:

#25-6215-98 ave.
Edmonton, Alberta
Canada,   T6A OA3

DATE: ...Oct. 4...198 5

THE UNIVERSITY OF ALBERTA

FACULTY OF GRADUATE STUDIES AND RESEARCH

The undersigned certify that they have read, and recommend to the Faculty of Graduate Studies and Research for acceptance, a thesis entitled "Laboratory Study of Mineralogical Reactions During Steam Condensate Flooding of Cold Lake Oil Sands" submitted by John S. Kirk in partial fulfilment of the requirements for the degree of Master of Science.

....
(Supervisor)

....

....

....

....

Date: ......Oct. 1/85...

DEDICATION

This thesis is dedicated to my wife, Jacqueline Kirk, and my parents Rose and Jack Kirk who patiently supported me and were able to cope with the schedule, or lack thereof, of a graduate student engrossed by his work.
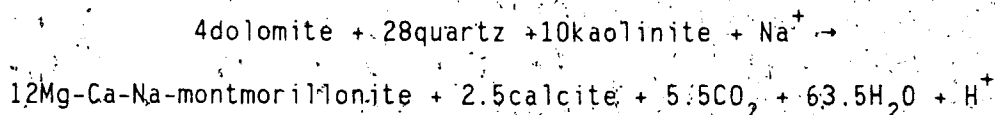
ABSTRACT

A laboratory study was completed, to determine the interaction between steam condensate and Cold Lake oil sand during steam stimulation. Four separate flow experiments at $265°C$ and 6.2 to 8.3 MPa pressure passed injection fluids of either pH 11.0 or 6.3 through Clearwater Formation sand at either 1.2 or 4.8 pore-volumes/day. Cores were prepared from sand with bitumen removed and with bitumen in-place.

The results indicate that the following changes occurred to all four cores during the course of the experiments: (1) a decrease in grain size; (2) a decrease in dolomite content; (3) a decrease in kaolinite content in the finer fractions; (4) CO_2 production; (5) precipitation of smectite rims on framework grains; (6) precipitation of calcite in pore spaces; and (7) a reduction in permeability. The $\delta^{18}O_{SMOW}$ values of the calcites (-9.4 to -10.8 permill) indicate that they formed between $240°$ and $275°C$ (i.e., at experimental temperatures).

Based on the above observations, two reactions are proposed:

$$2.5 \text{dolomite} + 32 \text{quartz} + 28 \text{kaolinite} + Na^+ \rightarrow$$
$$24 \text{Mg-Ca-Na-beidellite} + 1.5 \text{calcite} + 3.5 CO_2 + 95.5 H_2O + H^+$$

and/or

$$4 \text{dolomite} + 28 \text{quartz} + 10 \text{kaolinite} + Na^+ \rightarrow$$
$$12 \text{Mg-Ca-Na-montmorillonite} + 2.5 \text{calcite} + 5.5 CO_2 + 63.5 H_2O + H^+.$$
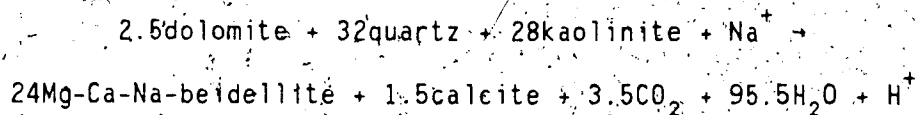
The above reactions occurred to a greater extent when the high pH fluid was used instead of the low one. Higher flow rate promoted more

mineral growth indirectly because greater volumes of fluid were passed through the core. Bitumen decreased the extent to which the reactions occurred by armouring the grains.

Smectite growth was the main cause of permeability reduction because it increased the amount of material in the pore space and it created a microporosity network that restricted flow. Fines migration and accumulation at pore throats contributed to permeability reduction. Low injection fluid salinity caused greater osmotic swelling of smectite and therefore decreased porosity and permeability.

The bitumen-free core subjected to high pH, low salinity injection fluid at low flow rates suffered the greatest permeability reduction (98%). The second greatest permeability decrease (85%) occurred in the core subjected to the same fluid but at higher flow rates implying that high injection rates minimize the damaging effects of high pH injection fluids. The permeability of the core subjected to neutral pH injection fluid decreased by 50%. Visual observations indicated that the permeability of the bitumen-saturated core decreased the least.

ACKNOWLEDGEMENTS

TABLE OF CONTENTS

LIST OF FIGURES

xiv

LIST OF PLATES

I. INTRODUCTION

Athabasca, Peace River, Wabasca and Cold Lake are the four main oil sand deposits of Alberta (Figure 1). The combined resources of these deposits have been estimated as high as 196.7 billion m^3 (1237 billion barrels) of crude oil (Energy Resources Conservation Board, 1983). Less than ten percent of these resources are shallow enough (<50 m of overburden) to be produced by surface mining methods (Farouq Ali, 1974). The more deeply buried deposits (>200 m of overburden) must be produced by _in situ_ techniques. Secondary and tertiary recovery methods must be used because the bitumen lacks a natural drive mechanism and it is too viscous to be produced by standard methods.

Two such _in situ_ recovery techniques are steam flooding and cyclic steam stimulation; both involve adding heat and large volumes of fluids to the reservoir system. These techniques decrease the viscosity of the bitumen, allowing it to flow. However, under these artificial hydrothermal conditions, mineral solution and precipitation can occur resulting in detrimental changes (i.e., a reduction) in the porosity and permeability of the reservoir. One result of this formation damage is high residual oil saturation (Sedimentology Research Group, 1981; Boon _et al._, 1983).

A greater insight into the mineral reactions that occur as steam condenses during a steam flood is required in order to better understand the reservoir system during such a recovery. The understanding of the effects that these reactions or "artificial diagenesis" have on the porosity and permeability of the reservoir can lead to more optimal use of the steam injection methods.

1
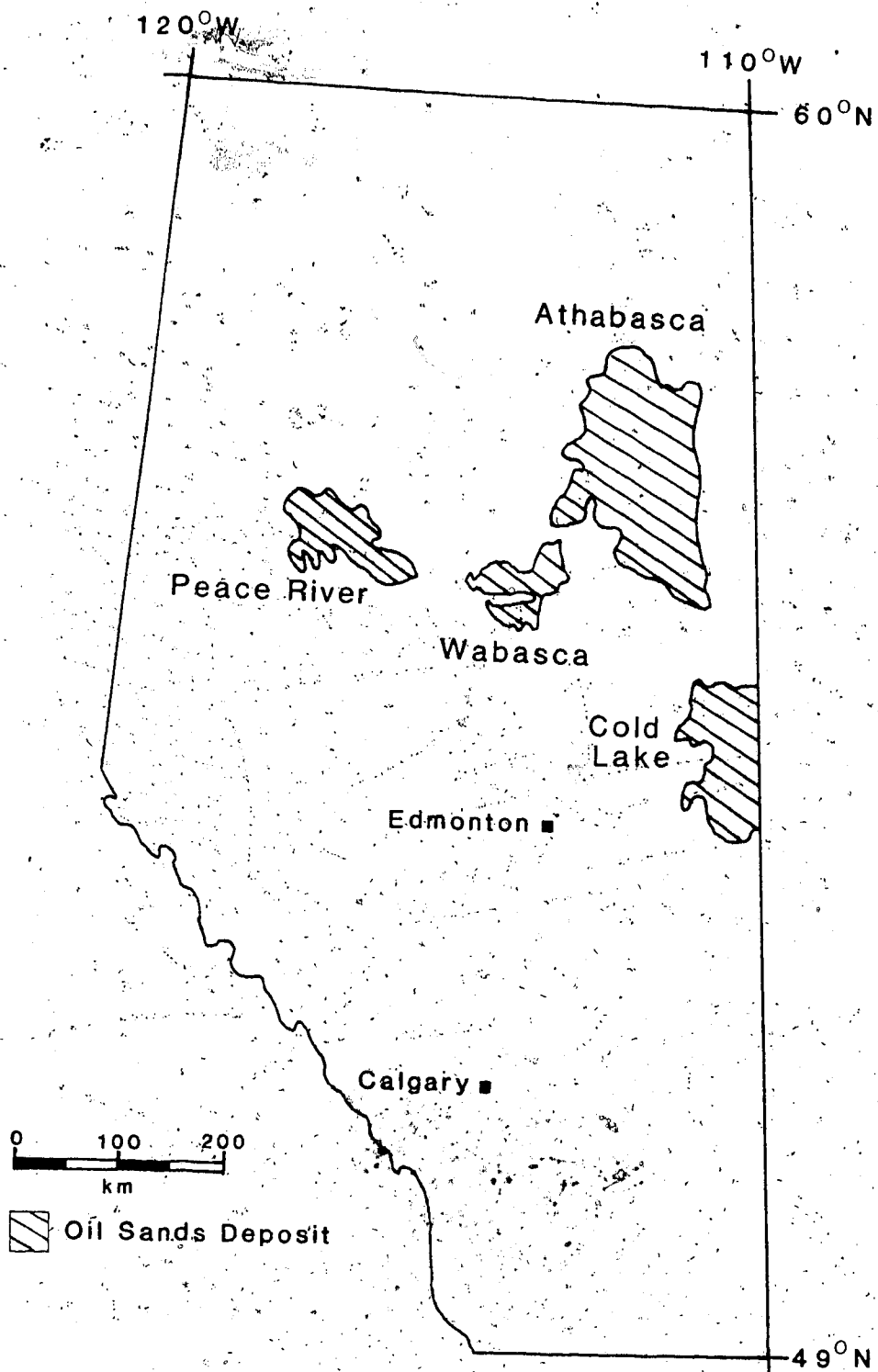
Figure 1. The four main oil sand deposits of Alberta.

A. Location of Study Area

Samples for the experimental study were collected from a well (11C-30-64-4W4) at the Husky Oil Tucker Lake pilot plant located approximately 225 km northeast of Edmonton in the Cold Lake oil sands deposit (Figure 2). At the well site, the Clearwater Formation is 44 m thick and covered by 455 m of overburden.

B. Steam Injection Recovery Methods

Cyclic Steam Stimulation

There are three main problems to overcome when applying an _in situ_ recovery method to an oil sands reservoir: (1) the high viscosity of the bitumen rendering it almost immobile; (2) the lack of communication that exists between injection and production wells because bitumen plugs the pore spaces; and (3) lack of reservoir depth needed to provide sufficient overburden pressure to contain the pressures needed to displace the bitumen (Farouq Ali, 1974).

Cyclic steam stimulation ("huff and puff") is a type of steam injection process where steam is injected into the formation through production wells for a period of approximately one week. The reservoir is then shut-in for a soak period of two to three weeks while the steam condenses and heats the bitumen. When the soak period is completed, the viscosity of the bitumen has decreased and it is produced through the injection wells (Figure 3). After production rates drop, the entire cycle may be repeated. Since this type of recovery method is operational on a single well basis, the problem of reservoir communication is not severe (Farouq Ali, 1974).
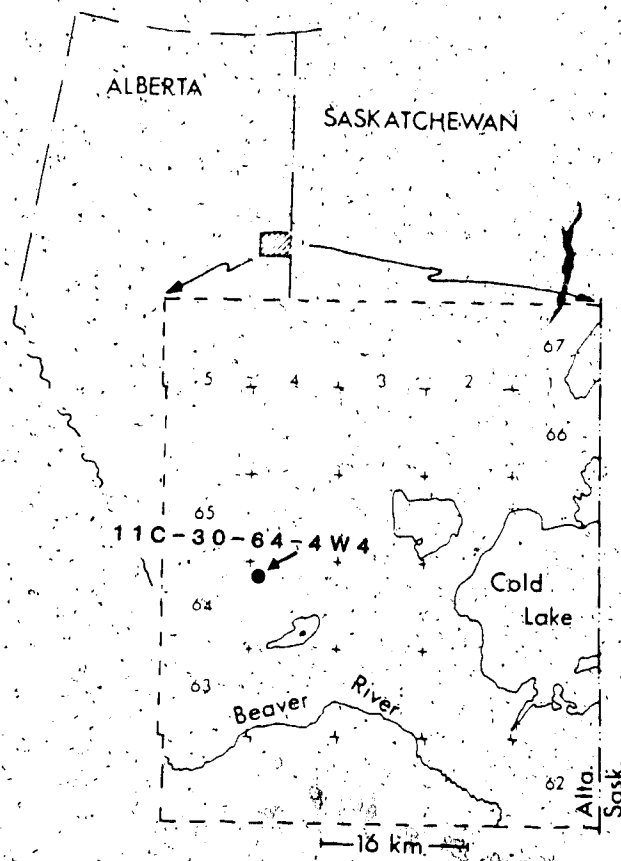
Figure 2. Location of the well (11C-30-64-4-W4) from where the sample material was collected (modified after The Sedimentology Research Group, 1981).
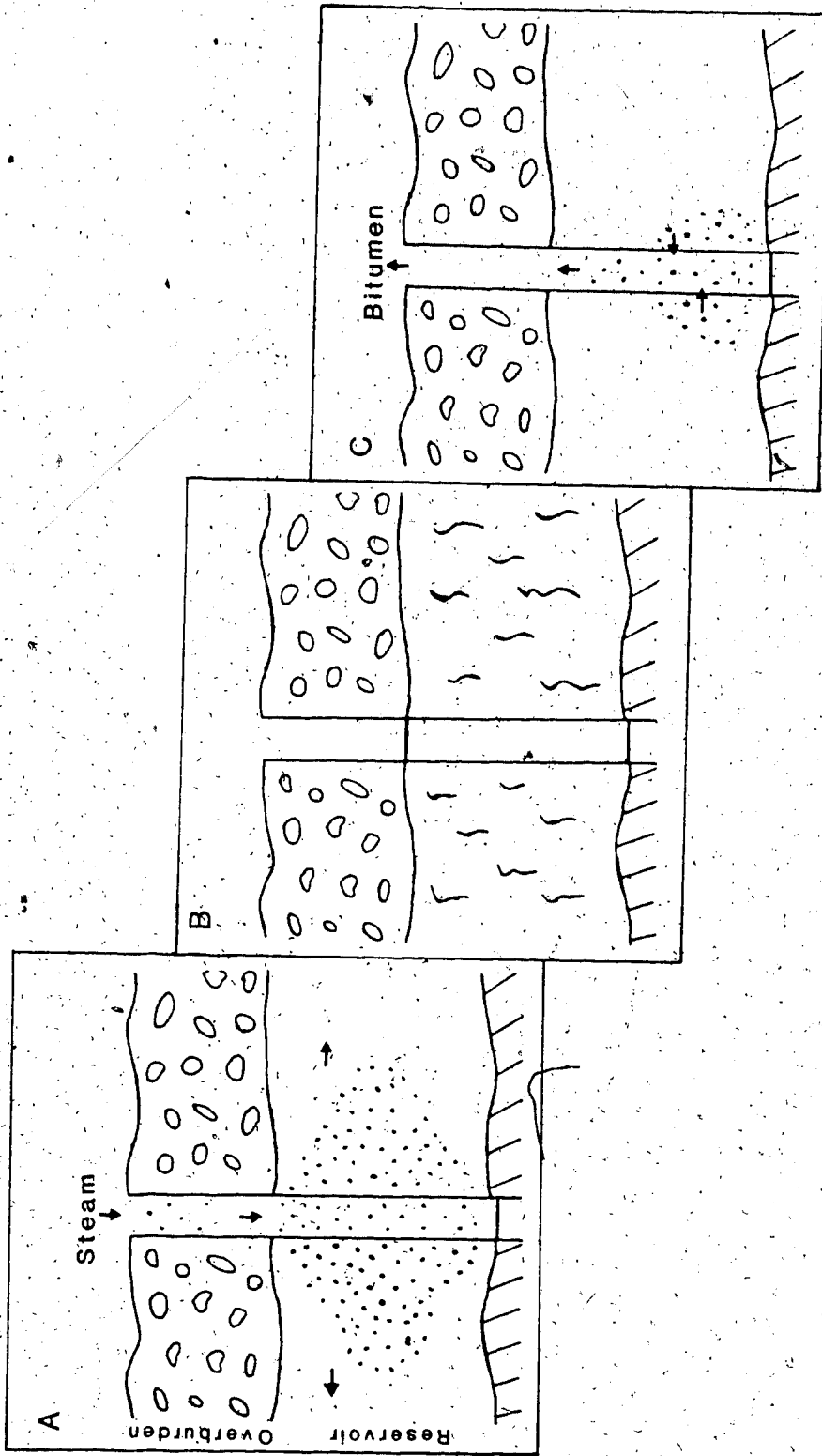
Figure 3: Schematic sections showing the three main stages of a steam injection cycle: (a) injection; (b) soak period and (c) production.

There are some disadvantages to cyclic steam stimulation. The area affected by the single well process is small compared to multiple well recovery techniques, therefore limiting the amount of bitumen that can be produced. Also, since this procedure does not involve a drive process to push the bitumen to the producing well, it relies on the inherent reservoir pressure. Therefore, shallow formations are poor candidates for cyclic steam stimulation (Schumacher, 1978, p. 70). This process is usually the initial production method, preceding other thermal recovery techniques. Recovery is of the order of 5 to 10 percent of the bitumen in-place (Farouq Ali, 1974).

Steam Flood (Drive) Recovery

During a steam flood, steam is injected into a series of outlying wells to drive the bitumen inward toward the production wells (Schumacher, 1978, p. 72). The main difference between this process and cyclic steam stimulation is that the former is a multi-well or pattern injection (Figure 4) and the latter is a single well recovery method. Because of this difference, communication between injection and production wells is required during a steam flood. This communication path is created by a fracture either prior to or simultaneous with the initial injection of steam (Settari and Raisbeck, 1981).

In the steam saturation zone (Figure 5), the reservoir temperature is approximately the temperature of the injected steam causing bitumen viscosity to decrease. The bitumen is then moved to the production well by gas drive and by distillation of the bitumen (Schumacher, 1978, p. 72). Recovery efficiency can range from 35 to 50 per cent of the bitumen in-place (Schumacher, 1978, p. 72; Farouq Ali, 1974). Steam
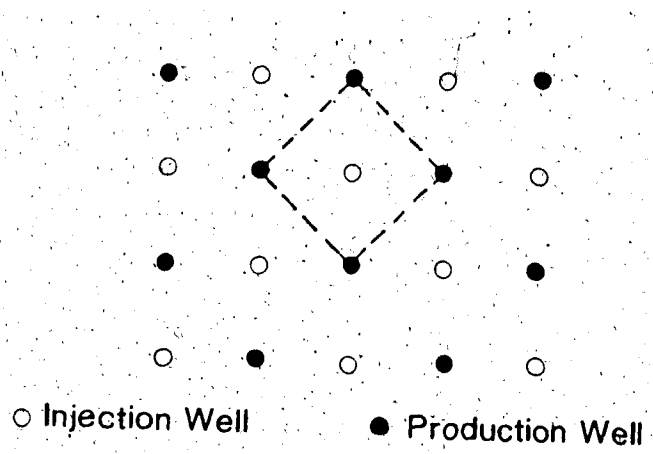
Figure 4. Map view of a pattern grid used during steam drive production. The area enclosed by the dashed lines is a "five spot" pattern.
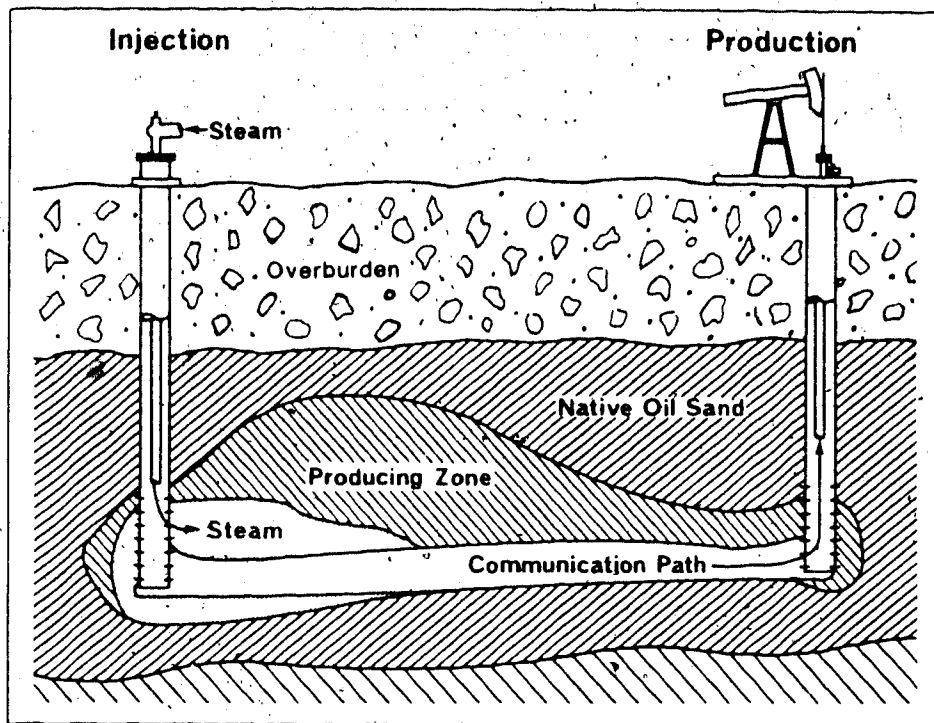
Figure 5. Schematic cross-section between adjacent injection and production wells during a steam drive. The different zones present in the reservoir are shown (modified after Tremaine et al., 1983).

flood projects are usually employed in conjunction with steam stimulation production.

C. Recovery Methods at the Tucker Lake Pilot Plant

Cyclic steam injection is employed at the Tucker Lake pilot site. The injection fluid is 60% quality steam (60% steam and 40% water) made from non-saline water. The soak period is approximately five days. Overburden pressure on the Clearwater Formation is about 11.9 MPa.

D. Problems Associated with Thermal Recovery Methods

A number of problems are associated with the introduction of hot injection fluids into the reservoir (Boon, 1977). Chemical reaction (mineral solution and precipitation) between the fluids and the formation can reduce porosity and permeability. Permeability reduction is undesirable because it leads to lower production rates and higher residual oil saturations (Boon et al., 1983). These effects are most pronounced as the steam condenses to liquid.

E. Purpose of Study

The purpose of this study is to determine mineralogical changes that occur in the Clearwater Formation at the Tucker Lake pilot site during steam flood recovery as the steam condenses and to determine the specific effects that these changes have on reservoir permeability.

This goal has been approached by three main avenues of study: (1) the mineralogy of the Clearwater formation at the study area was determined; (2) mineral reactions that can occur during a steam flood were investigated experimentally in an autoclave laboratory; and (3) these

reactions were related to changes in the porosity and permeability of the formation during a steam flood.

The experiments were designed to dynamically simulate the steam injection process and to determine the specific effects this process has on the Clearwater Formation.' Fluids were passed through 31 cm cores at elevated temperature and pressures . After the experiments, each core was studied at different intervals, to observe changes or trends along the core. These differences would exist because injection fluid chemistry changes as the fluids pass through and react with the core.

A. Clearwater Formation

Stratigraphy

Sample material was collected from the lower Albian Clearwater Formation. In the Cold Lake area it is overlain by the Grand Rapids Formation and underlain by the McMurray Formation. All three formations comprise the Mannville Group (Figure 6). The contact with the Grand Rapids Formation is diachronous and transitional (Kramers, 1974). The basal contact with the McMurray Formation is either gradational (Mellon, 1967) or interfingering (Carrigy, 1963).

In the Cold Lake area, the Clearwater Formation is dominantly sands. Shales from the Grand Rapids and McMurray Formations bound these sands (Kramers, 1974) (Figure 6).

A glauconitic sandstone unit occurs at the base of the Clearwater Formation in the Athabasca oil sand deposit. This sand unit is designated as the Wabiskaw Member of the Clearwater Formation (Figure 6). This member is not present in the Cold Lake area (Kramers, 1974).

Sedimentology and Provenance

The maximum southward transgression of the Boreal Sea during the Albian between the rising Cordillera to the west and the North American craton to the east occurred during Early Clearwater time (Kramers, 1974). The underlying and overlying formations are non-marine (Outtrim and Evans, 1977; Putnam and Pedskalny, 1983; Minken, 1974). The retreat of the Boreal Sea resulted in the sequential deposition of

11

PERIOD	STAGE	NORTHWEST ALBERTA PEACE RIVER	NORTHEAST ALBERTA		EAST CENTRAL ALBERTA COLD LAKE
			WABASCA	ATHABASCA	
LOWER CRETACEOUS	ALBIAN	SHAFTESBURY FM / PEACE RIVER M. / SPIRIT RIVER FM / BLUESKY FM	LA BICHE FM / PELICAN FM / JOLI FOU FM / GRAND RAPIDS FM / CLEARWATER FM / WABISKAW MBR / McMURRAY FM	LA BICHE FM / PELICAN FM / JOLI FOU FM / GRAND RAPIDS FM / CLEARWATER FM / WABISKAW MBR / McMURRAY FM	VIKING FM / JOLI FOU FM / UPPER GRAND RAPIDS / LOWER GRAND RAPIDS / CLEARWATER FM / McMURRAY FM
	ALBIAN AND OLDER	GETHING FM / CADOMIN FM			
PALEOZOIC					

Legend: OIL SAND, BARREN SAND, SHALE, CONGLOMERATE, UNCONFORMITY

Figure 6. Stratigraphic correlation chart for the four main oil sand deposits of Alberta (modified from Kramers, 1974).

shales, silty and sandy shales, interbedded shales and sands, massive sands and non-marine sandstones (upper Grand Rapids Formation) in the Wabiskaw area. To the south and east, the Clearwater is dominated by sands and shales associated with transitional marine environments.

The facies contained in the Clearwater in the Cold Lake area are delta-fringe shales and silts, lower delta front shales and sands, and upper delta front beach and stream-mouth bar sands (Harrison 1981).

Two source areas have been proposed based on the large amount of volcanic rock fragments in the sands. One proposed source is the igneous terranes associated with the Cordillera in British Columbia such as the Omineca and Nelson Batholiths (Putnam and Pedskalny, 1983). The other possible source is the emergent Precambrian Shield to the east (Harrison et al., 1981).

Mineralogy

The Clearwater sands have been described as feldspathic litharenites and litharenites (Putnam and Pedskalny, 1983 after Folk, 1968) and lithic sands and rock fragment sands (Williams, 1963 after Travis, 1955). The classification scheme of Folk (1968) is employed during this study.

Table 1 is a summary of the petrographic studies and Table 2 is a summary of the x-ray diffraction (XRD) studies that are in the literature concerning the Clearwater in the Cold Lake area. The results of the two types of studies differ because XRD determines sample mineralogy whereas petrography determines lithology. XRD classifies rock fragments by their mineral constituents whereas petrography classifies

Table 1. Constituents of the Clearwater Formation sands in the Cold Lake area. Abundances determined using petrographic techniques (Harrison et al., 1981; Bowman et al., 1983, p. 3.14).

	Abundance (%)	
	Harrison et al.	Bowman et al.
Quartz	21	20 - 35
Feldspar	28	10 - 15
Volcanic Fragments	23	
Metasediment Fragments	5	
Argillite Fragments	3	
Total lithic Fragments	31	30 - 50
Chert	20	0 - 10
Carbonates		0 - 5
Mica		1
Glauconite		2 - 5
Heavy Minerals		tr
Siderite Cement		0 - 3
Calcite Cement		0 - 5

Table 2. Mineralogy of the Clearwater Formation sands in the Cold Lake area. Abundances determined using XRD techniques (Bayliss and Levinson, 1976; Perry and Gillott, 1979).

	Abundance (%) (range)	
	Perry and Gillott	Bayliss and Levinson
Quartz	52	75 (30 - 98)
Plagioclase	17	7 (0 - 27)
K-feldspar	2	7 (0 - 19)
Dolomite	15	0.6 (0 - 5)
Calcite	0	0.1 (0 - 2)
Kaolinite	7	3 (0 - 11)
Mica	3	0.6 (0 - 3)
Illite	2.5	3 (tr - 13)
Montmorillonite	1	3 (0 - 17)
Chlorite	0.5	1 (tr - 7)

rock fragments as individual constituents. Other discrepancies exist because of lateral and vertical variation in mineralogy within the formation. Some variation may be due to sample preparation and actual methods employed.

Putnam and Pedskalny (1983) completed a detailed petrographic study of the Clearwater Formation in the same township that the sample material for this study was taken (64-4W4). The most abundant constituents of the formation are rock fragments of which there are four types: (1) volcanic (acid volcanic, zoned grains, porphyries and vesicular grains); (2) sedimentary (chert, sandstone, siltstones and shales); (3) plutonic; and (4) metamorphic rock fragments. The most abundant volcanic rock fragment type has a partially chloritized, aphanitic groundmass that contains oriented feldspar microlites. Following labile rock fragments in decreasing order of abundance are quartz, feldspar (plagioclase and K-feldspar) and accessory minerals such as biotite, zircon, tourmaline, zeolite, and hornblende. Cement, when present, consists of calcite, siderite, silica and zeolite.

B. Previous Studies in Experimental Systems

Studies completed that are related to this study can be catagorized as: field or experimental studies, physical or mathematical models, static or dynamic models, or experiments using actual core material or experiments using pure minerals to act as reactant materials. This study is a dynamic, physical study using actual oil sand.

The earliest studies of potential reactions between minerals and fluids in oil sand type environments were static experiments that involved placing mixtures of pure minerals in bombs or autoclaves with

a fluid of known composition. The bombs were then heated in ovens to desired temperatures for set durations and then the materials in the bombs were re-analyzed to determine changes (Levinson and Vian, 1966; Bayliss and Levinson, 1971).

More recently Boon (1977), Perry and Gillott (1979), Boon and Hitchon (1983a, b) and Hebner et al. (1985) conducted such studies keeping within the context of steam injection into an oil sand reservoir. Results from such experiments are applicable to closed geological systems.

In similar studies, Levinson and Vian (1966) and Bayliss and Levinson (1971) placed kaolinite, quartz and various carbonates in bombs with distilled water. The mixtures were heated and after three or six weeks, the solids were re-analyzed. In the earlier study it was determined that dolomite was the most reactive of the carbonates and that the following unbalanced reaction could describe the system:

$$\text{dolomite + kaolinite + quartz + } H_2O =$$
$$\text{trioctahedral smectite + calcite + } CO_2. \tag{1}$$
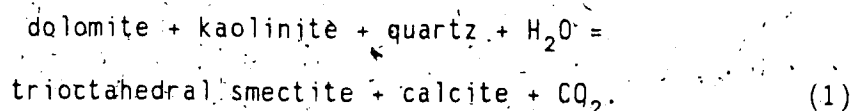
Bayliss and Levinson (1971) proposed reactions (2) and (3) for the same system containing either dolomite (2) or calcite (3) respectively:

$$24MgCa(CO_3)_2 + 28SiO_2 + Al_2Si_2O_5(OH)_4 + 6H_2O =$$
$$8Ca_{1/8}Mg_3(Si_{15/4})Al_{1/4})O_{10}(OH)_2 + 23CaCO_3 + 25CO_2 \tag{2}$$

$$CaCO_3 + 8SiO_2 + 7Al_2Si_2O_5(OH)_4 =$$
$$6Ca_{1/6}AL_2(Si_{11/3})Al_{1/3})O_{10}(OH)_2 + CO_2 + 8H_2O \tag{3}$$
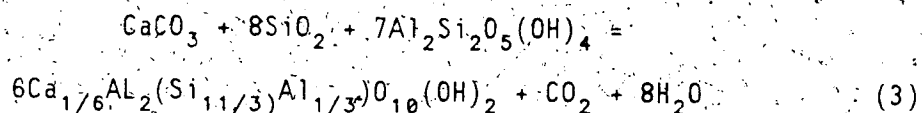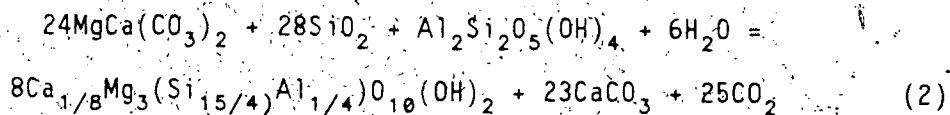
In a similar study, Perry and Gillott (1979) studied the formation of montmorillonite and also noted that only small amounts of dolomite (<2.5% by weight) are necessary to produce significant amounts of montmorillonite.

Hebner et al. (1985) tested the effects that starting mineralogy, solution pH, salinity, temperature and run duration have on new mineral phases in the oil sand system. In runs with 5% (by weight) dolomite, analcime (with trace amounts of smectite) formed in pH 10 and 12 fluids but in neutral (pH=7) solutions only smectite formed. By increasing the starting amount of dolomite to 33 1/3 weight percent, more analcime and smectite were produced in the respective experiments and calcite became a common product. Analcime was the more abundant mineral in runs with high salinity and high pH.

Boon (1977) used experiments in static autoclaves to determine mineralogical changes that occur in an oil sand reservoir (McMurray Formation, Athabasca deposit) when injected with steam. He determined that quartz solubility increases with temperature while bitumen decreases quartz solubility. Boon (1977) maintained that montmorillonite formation is probable during in situ steam injection of the Athabasca oil sands and that silica reprecipitation significantly reduces formation porosity and permeability.

Boon and Hitchon (1983a, b) conducted similar experiments using shale from an Athabasca reservoir and made the following observations. Greater salinity (NaCl) in injection fluids results in increased Ca concentration and lower pH because of Na^+ exchange for Ca^{2+} and H^+ on clay minerals (also Boon et al., 1983). Al^{3+} decreases with increasing salinity because it is closely associated with colloidal material

flocculated by NaCl. They described the formation of montmorillonite by the following unbalanced reaction:

$$2Al_2Si_2O_5(OH)_4 + 8H_4SiO_4 + 2M^+ =$$
$$6M_{0.33}Al_{2.67}Si_{3.67}O_{10}(OH)_2 + 23H_2O + 2H^+ \qquad (4)$$
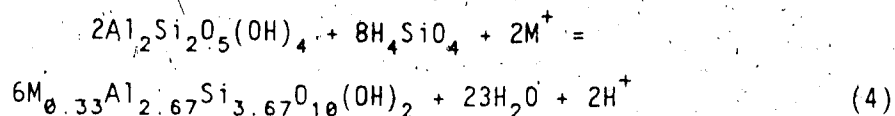
where M^+ represents either one monovalent or half of a divalent cation.

Waldorf (1965) passed air, water and steam through natural cores (lithology not specified) to test the permeabilities to the different fluids at various temperatures. He determined that a fifty-fold permeability decrease occurred in cores with montmorillonite when those cores were exposed to water rather than air.

Reed (1979), McCorriston et al. (1981) and Sydansk (1982) all passed fluids through sandstone (non-oil sand) cores at elevated temperatures and pressures and collected the effluent for analysis. It was determined that silica concentration decreased with increasing flow rate (decreased fluid contact time) (Reed, 1979; Sydansk, 1982). Silica dissolution increased with pH (Reed, 1979; Sydansk, 1982). Phillipsite and other authigenic zeolites were observed as products in Berea sandstone (85% quartz + feldspar, carbonate and clays) and these zeolites had lower Si/Al ratios than the clays that were dissolved (Sydansk, 1982). Alumina compounds can precipitate when pH and temperature increase. Furthermore, $Mg(OH)_2$ is an insoluble salt that can form when mixing injection fluids with formation fluids (McCorriston et al. 1981).

Relating their work to field experiences, McCorriston et al. (1981) maintained that as injection fluids move from the injection well, pH

and temperature decrease resulting in precipitation of minerals in the pore space, specifically amorphous silica. Amorphous silica is potentially more harmful than quartz because it is less dense, therefore occupying more volume. Injection fluids with pH levels between 9 and 10 can lead to irreversible permeability reduction of up to 50%. Overall, they claim that the use of injection fluids with high alkalinity and low ionic strength greatly increases the potential for fluid-rock interactions, clay swelling and dispersion of fines. Sydansk (1982), however maintained that consumption of caustic by cation-exchange with the core reduces dissolution by forming insoluble precipitates such as $Ca(OH)_2$. The decrease in pore space due to the precipitation of the salt was not considered.

The Sedimentology Research Group (1981) conducted an on-site study involving the examination of two cores. One core was taken prior to any continuous-drive steam injection while the other was taken after almost two years of the recovery process. Both cores were from the Clearwater Formation (Cold Lake), laterally separated by 15 m. Comparing the two cores, it was evident that the framework grains were largely unaltered and showed very little textural change. However thick layers of smectite developed on most of these grains. The large surface area combined with the microporosity network of the smectite morphology may have resulted in the retention of bitumen in the pore spaces. Porosity was reduced by smectite growth and compaction of framework grains after the removal of bitumen. Smectite reduced the effective porosity by: (1) increasing the amount of material in the pore space, (2) creating a microporosity network and (3) forming clay

mineral bridges. Smectite was formed in the pore space by reaction of kaolinite on the surfaces of volcanic rock fragments:

$$2Na^+ + 8SiO_2 + 7Al_2Si_2O_5(OH)_4 =$$
$$6Na_{1/3}Al_{7/3}Si_{11/3}O_{10}(OH)_2 + 7H_2O + 2H^+ \qquad (5).$$
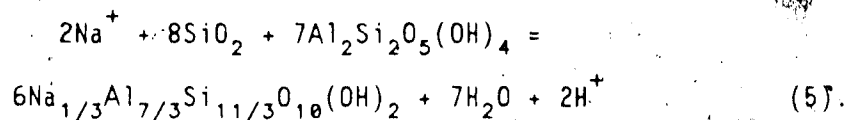
In a study incorporating both static and dynamic experiments, Boon et al. (1983) studied the reactions between Cold Lake (Clearwater) oil sand and injection fluids of varying pH and salinities. The latter part of their study (dynamic or flow experiments) parallels this present study more so than any of the others. They found that the products of their reactions were analcime, calcite, montmorillonite and chlorite. Dolomite and kaolinite were consumed. Increased amounts of calcite and montmorillonite were formed at higher pH (not quantified). Based on thermodynamics, it was possible that albite could have formed by:

$$kaolinite + 2Na^+ + 4H_4SiO_4 = 2albite + 2H^+ + 2H_2O \qquad (6).$$
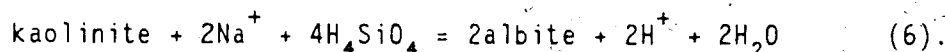
However it was not readily apparent that feldspar had formed. Its absence was attributed to either kinetic effects or problems with thermodynamic data used to predict albite formation.

The second part of the study by Boon et al. (1983) indicated a number of interactions between the cores and the fluids that were passed through them. They found that similar mineral reactions occurred during the core floods as during the static autoclave experiments. The main factors affecting the reactions were salinity,

temperature and pH. Bitumen had only minor effects on the reactions. Silica concentration in the effluent samples decreased with increased flow rate, which was similar to the findings of Reed (1979) and Sydansk (1982). Permeability reduction was attributed mainly to dispersion of fines (noted in all post-experiment cores).

C. Studies in Natural Systems: Diagenesis of Volcanoclastic Rocks

Because of the high abundance of volcanic rock fragments in the Clearwater Formation, the natural diagenesis of volcanoclastic sediments should provide information concerning their behavior during "artificial diagenesis". Two geologic environments will be related to the dynamic experiments of this study: diagenesis of volcanoclastic sediments initiated under marine conditions and alteration of this sediment type by supersaline fluids.

Surdam and Boles (1979) claimed that more than just the geothermal gradient must be considered when determining the equilibria associated with burial diagenesis. Pore-fluid chemistry is also an important consideration. Davies et al. (1979) stated that pore-fluid chemistry is a function of residence time of the fluids, starting fluid composition and rock composition. Early diagenetic reactions such as the hydrolysis of silicates or volcanic glass are important because they increase solution pH (Surdam and Boles, 1979):

$$Ca-silicate + H_2O = H-silicate + Ca^{2+} + 2OH^- \qquad (7).$$
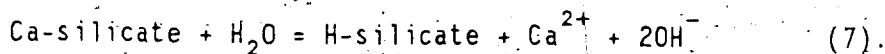
They found that the most abundant alteration products of volcanogenic sandstones are zeolites, clays, calcite, albite and K-feldspar.

The hydrolysis of glass increases solution pH (Surdam and Boles, 1979). The precipitation of montmorillonite initially consumes all the available silica and alumina which releases H^+. However the solution pH does not decrease because the hydrolysis of the glass consumes more H^+ than is consumed by the precipitation of montmorillonite (Davies et al., 1979). The net effect of combined solution of andesitic glass and precipitation of montmorillonite is a gradual increase in solution pH (Davies et al., 1979). The latter authors also attribute the precipitation of heulandite to an increasing concentration of silica and aluminate.

Galloway (1979) studied arc-derived sandstones ranging in composition from quartz-poor litharenites to quartz-poor plagioclase arkoses (overall feldspar was the most dominant constituent; volcanic rock fragments were second in abundance). He determined that four main diagenetic stages had occurred: (1) early pore-filling calcite, (2) chlorite or montmorillonite rims around detrital grains, (3) pore-filling laumonite or phyllosilicates (montmorillonite, chlorite or kaolinite) and (4) replacement of volcanic rock fragments, feldspar and matrix by calcite and/or chlorite. Quartz overgrowths developed during the last stage. Stages 3 and 4 decreased porosity the most.

The most common environment for zeolite authigenesis is the diagenesis of volcanogenic sediments (Hay, 1978). Clinoptilolite and phillipsite are generally the first zeolites to form during the alteration of volcanic glass and may eventually be replaced by K-feldspar and analcime (Sheppard and Gude, 1968; Boles, 1977; Hay, 1978). Because of the low temperatures involved, Boles (1977) conjectured that this was a kinetic effect and that phillipsite was

metastable.   Phillipsite. is more commonly associated with mafic
volcanoclastic rocks, clinoptilolite is usually associated with silicic
volcanoclastic rocks (Hay and Sheppard, 1977; Hay, 1978).

Both zeolites and phyllosilicates can form from the same material.
Pore fluid composition controls the type of mineral that is favored.
Zeolites are more stable under conditions of high Na^+, K^+ and Ca^{2+}/H^+
ratios and low magnesium activities (Hay, 1966; Hay, 1978).

Sheppard and Gude (1968) studied the diagenesis of rhyolitic tuffs
in a saline environment. Phillipsite was the most abundant zeolite.
Because of the shallow burial (and therefore little or no pressure and
temperature gradients), they maintained that diagenetic facies distri-
bution is controlled by pore-fluid chemistry. Phillipsite was favored
over clinoptilolite by a relatively high K/Na+Ca+Mg ratio and by low
silica activity.

III. EXPERIMENTAL AND ANALYTICAL METHODS

The experiments conducted during this study were designed to dynamically simulate the interaction between the Clearwater Formation and steam condensate. Material used in the experiments was collected from an oil sands pilot plant and was characterized as to its mineralogy, grain size, carbonate chemistry and stable isotope composition. Aqueous solutions similar to injection fluids used in steam injection projects were prepared. These solutions were analyzed for pH and cation concentrations. The sand was packed into core sleeves and placed in an apparatus that allowed injection fluids to pass through the core at elevated temperature and pressures. Production fluids were collected throughout the experiment and analyzed for pH and cation concentrations. After the run was completed, the core material was re-analyzed in order to determine changes that occurred during the course of the experiment. The permeability of the core material to the injection fluids at room temperature was measured before and after the experiments.

A. Sample Collection and Preparation

Sand used in the experiments was taken from a cored interval of the Clearwater Formation from well 11C-30-64-4W4 (Figure 2). The core was stored in sample bags when the samples were taken. Approximately 1 kg of core material was taken from each of three depth intervals (456.0 m, 470.5 m and 476.5 m) in order to represent the entire reservoir, thereby reducing the possibility of studying a mineralogically anomalous section of Clearwater Formation at the pilot site.

25

After the sample material was collected, the bitumen was removed at room temperature using toluene. All the sand was then combined and homogenized into one sample using sample quartering techniques. From this large sand sample, three aliquots were taken to determine the mineralogy and grain size of the sand and to ascertain if the three intervals were homogeneously mixed into one sample.

B. Grain Size Analysis

Two methods were used to determine the grain size distribution of the sample; hydrometer and wet sieving. The details of these two methods are given in Appendix 1. Wet sieve analysis determines the minimum dimension of a particle (i.e., the dimension which passes through the finest sieve). Hydrometer analysis determines the equivalent to spherical diameter of a particle.

C. Mineralogical Analysis

The mineralogy of the sand was determined using petrographic, x-ray diffraction and chemical (gravimetric CO_2 analysis) techniques. The <2 µm, 2-5 µm and 5-20 µm size fractions were separated using sett methods and the clay mineralogy of these fractions was studied using x-ray diffraction. Scanning electron microscopy was used to identify pore space mineralogy and textures. The stable isotope compositions of the carbonates were also determined. The details of all these methods are given in Appendix 1.

D. Fluid Preparation and Analyses

The injection fluids were prepared by adding concentrated NaOH and/or dissolving NaCl in deionized water in specific quantities to achieve the desired pH and salinity. The pH of the solutions was checked with a Corning pH/ion meter 135, using a two-point calibration.

Cation and CO_2 concentrations of the fluids were determined using Inductively Coupled Argon Plasma (ICP) and Total Inorganic Carbon (TIC) analyses, respectively. These two analytical methods are outlined in Appendix 1.

E. Permeability Determinations

The permeability of each core (except for the bitumen-saturated one) was determined before and after the corresponding core flood using the differential pressure transmitter loop described below. The details of the determinations and the permeability calculations are given in Appendix 1.

F. Experimental Procedures

Four separate flow experiments were completed, each using fresh sample material. Four parameters were controlled to determine the effect that each parameter had on the type and extent of mineral reactions and the subsequent permeability change that occurred in each core. These variables were: (1) presence or absence of bitumen, (2) salinity (NaCl concentration) of injection fluids, (3) pH (controlled by NaOH concentration) of injection fluids, and (4) flow rate of the injection fluids (Table 3).

Table 3. The values of the parameters for each experiment. trace = those cores packed with toluene-cleaned sand. saturated = the core packed with oil sand.

	RUN #1	RUN #2	RUN #3	RUN #4
Presence of bitumen	trace	trace	trace	saturated
Salinity (NaCl mg/kg)	3000	1400	1400	1400
pH (NaOH control)	6.3	11.0	11.0	11.0
Flow Rate (ml/hr)	5	5	20	5
Porosity (%)	27	27	27	27[1]
Pore Volume[2] (ml)	101	101	113	111
Cumulative Fluid Injected				
(ml)	3211	3261	10148	3288
(pore volumes)	31.8	32.3	89.9	29.6
Average Temperature (°C)	267	267	265	261
Duration (days)	21	21	21	21
Length of sand in core (cm)	23.23	23.30	22.60	23.00

[1] porosity of core #4 assumed equal to the other cores.

[2] $PV = CV - SV$; SV = (weight of sand in core)/(density of sand) where: PV = pore volume, CV = inner volume of core, and SV = volume of sand in core. Sand density was assumed to be 2.65 g/cm^3.

Three cores were made of sand essentially free of bitumen while one core contained bitumen-saturated sand (Table 3). Modifications were made to the experimental apparatus to accommodate the viscous bitumen.

Procedure for Bitumen-free Cores

Cores were made by brazing an endcap into a stainless steel sleeve (31 cm long by 5 cm diameter). A sintered filter was placed on the endcap and homogenized sand was pored into the sleeve. The sand, once in the sleeve, was not packed but gently shaken to avoid moving fines in the core before the initiation of the core flood. When the sleeve was full of sand, an endcap with a sintered filter was brazed onto the open end of the core sleeve (Figure 7). The sand was compacted when the core was deformed by overburden pressure in the autoclave (see below).

Experiments were conducted by placing a core on-line in the auto-clave part of the apparatus (described below). The pressure drop across (and therefore the permeability of) the core was determined at room temperature, prior to starting the oven and the ruska pump simul-taneously. It took approximately eight to ten hours for a core to reach experimental temperature. The initial flow rate (the rate at which the injection fluid flowed through the core) for the first three runs was 20 ml/hr (Table 3) to allow CO_2 evolution from the cores to be monitored. Once CO_2 concentration in the effluent decreased to a stable level (32 to 48 hours depending on the run), the flow rate was decreased to 5 ml/hr for the duration of the run. The rate of 20 ml/hr was maintained throughout the second experiment (Table 3). The dura-tion of each experiment was three weeks.
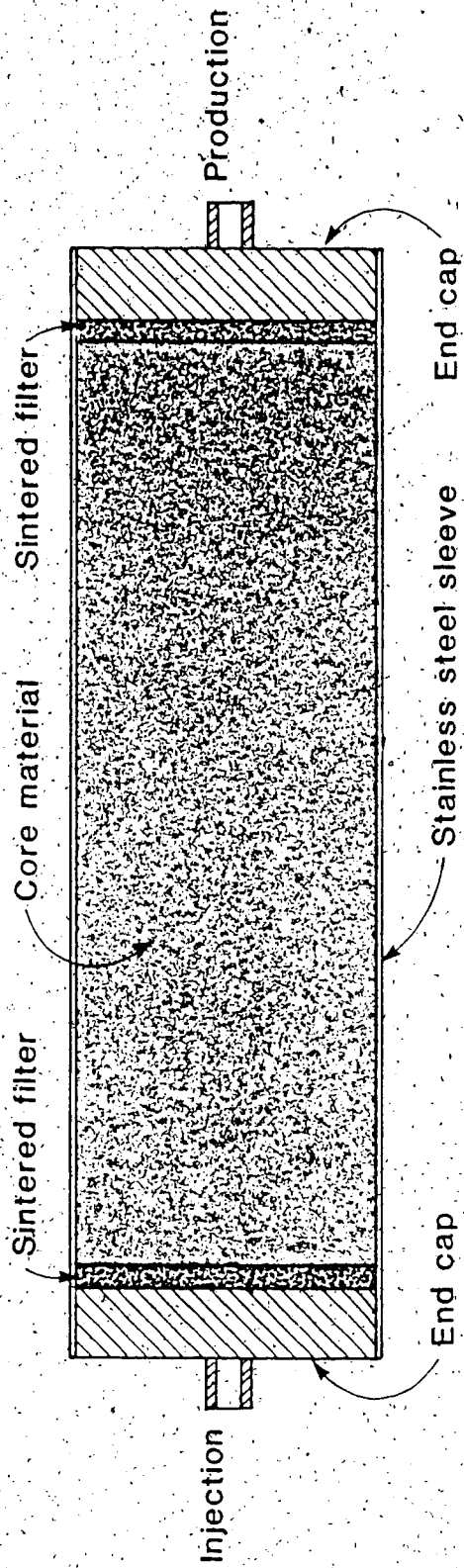
Figure 7. Schematic cross-section illustrating the various parts of the cores used in the experiments.

Labels in figure: Production, End cap, Sintered filter, Core material, Stainless steel sleeve, Sintered filter, End cap, Injection

The equipment used in the flow experiments is shown schematically in Figure 8 and is illustrated in Plate 1. Table 4 lists the make and model of the parts illustrated in Figure 8. The main functions of the apparatus were: (1) to flow injection fluid through the core at elevated temperatures and pressures; (2) to collect effluent after it passed through and reacted with the core; and (3) to measure the change in fluid pressure across the core before and after the experiments so that the permeability could be calculated. All components of the apparatus were stainless steel to limit the reactions between the fluids and the apparatus. The apparatus used in these experiments was similar to those used by Reed (1979), McCorriston et al. (1981) and Boon et al. (1983).

The ruska pump initiated flow by injecting a constant volume flow of distilled water from a reservoir into the lower chamber of the injection fluid accumulator (Figure 8). This action drove the accumulator piston upward, forcing the injection fluid in the upper chamber of the accumulator to flow through the injection line, through a pressure gauge and into the autoclave.

The autoclave was the main part of the experimental system. It was the vessel that held the core (Plate 2) at experimental overburden pressure (8.3 MPa in all four experiments) with N_2 gas and water vapor pressure. The injection line entered the autoclave and was coiled into a heat exchanger before being attached to the core. The fluids passed through the heating coil, into the core sand, and then exited the core into the production line. The autoclave and the lines and core in it were heated in an oven. A cooling coil was set up at the oven entrance
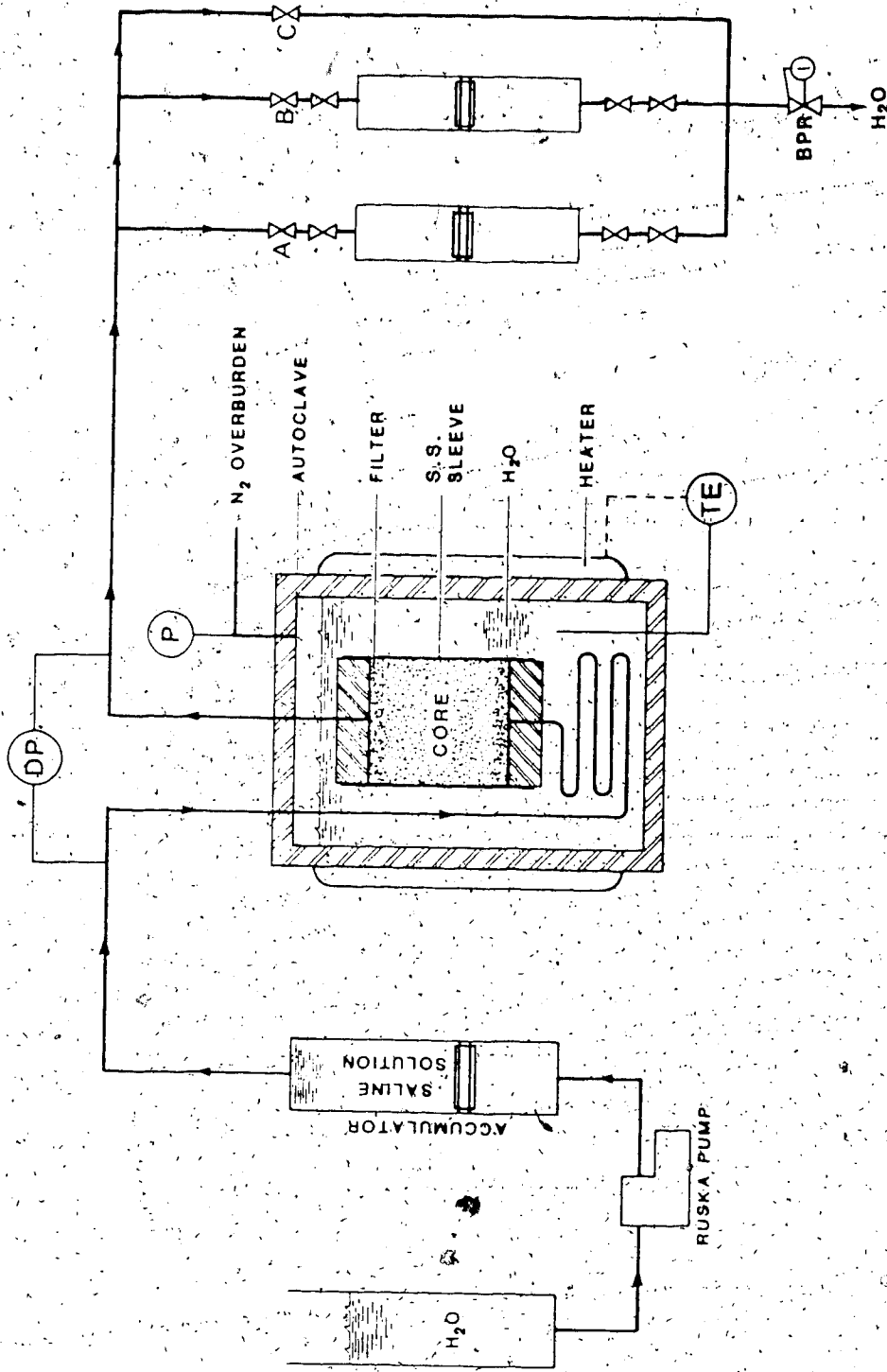
Figure 8. Schematic diagram of the experimental apparatus used in this study. DP = dp cells. P = pressure gauge. TE = thermocouple. S.S. SLEEVE = stainless steel core sleeve. BPR = back pressure regulator.

Plate 1. Flow apparatus used in the experiments. The autoclave (1), containing the core, is in the oven (2) and is attached on-line to the control panel (3). The control panel houses the injection fluid accumulator (4), production fluid accumulators (5), dp cells (6) and neccesary valves and gauges.
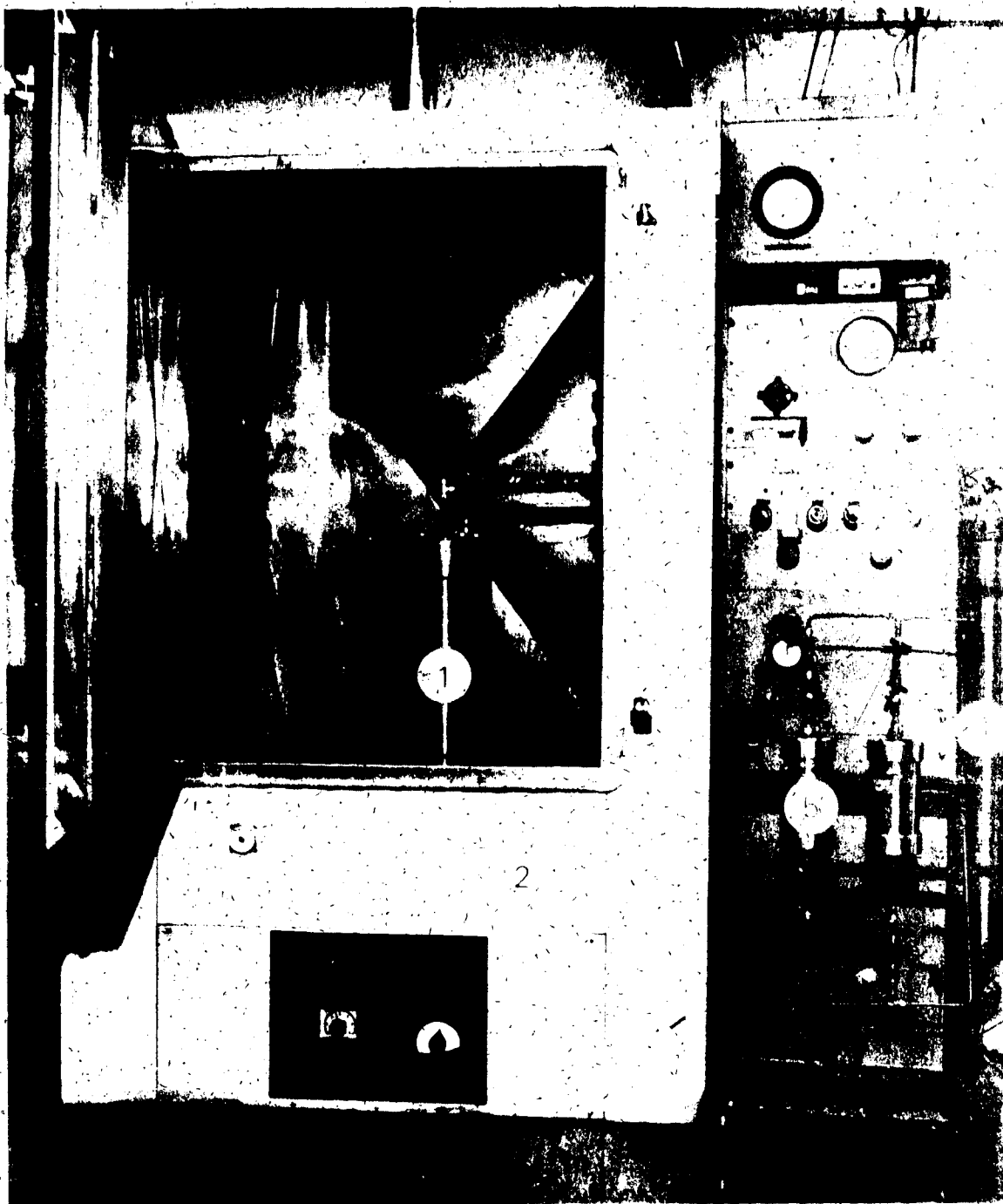
Table 4. Materials used in the experimental flow apparatus schematically illustrated in Figure 8.

MATERIAL	MAKE
line	1/4" type 316 stainless steel tubing
pump	Ruska #2236 WIII single cycle - 1000 ml/cycle
accumulator	Temco #CF-50-250 - 2.5 l capacity
core sleeve	2" schedule 10 pipe - type 316 stainless steel tubing
autoclave	Parr 6" internal diameter - 2 gallon capacity
nitrogen regulator	Tescom Corporation #04-1012-24-003
heater	Hotpack oven #214475
back pressure regulator	Tescom Corporation - maximum regulated 24.1 MPa
thermocouple	Omega 1/16" diameter type
differential pressure transducers	Rosemount Instruments #01199CAP
fittings	Swagelock

Plate 2. The core, 31 cm long (1), is attached to the autoclave head (2). The injection line is coiled into a heat exchanger (3) at the base of the core. Photograph was taken after an experiment showing compression of the core by overburden pressure.
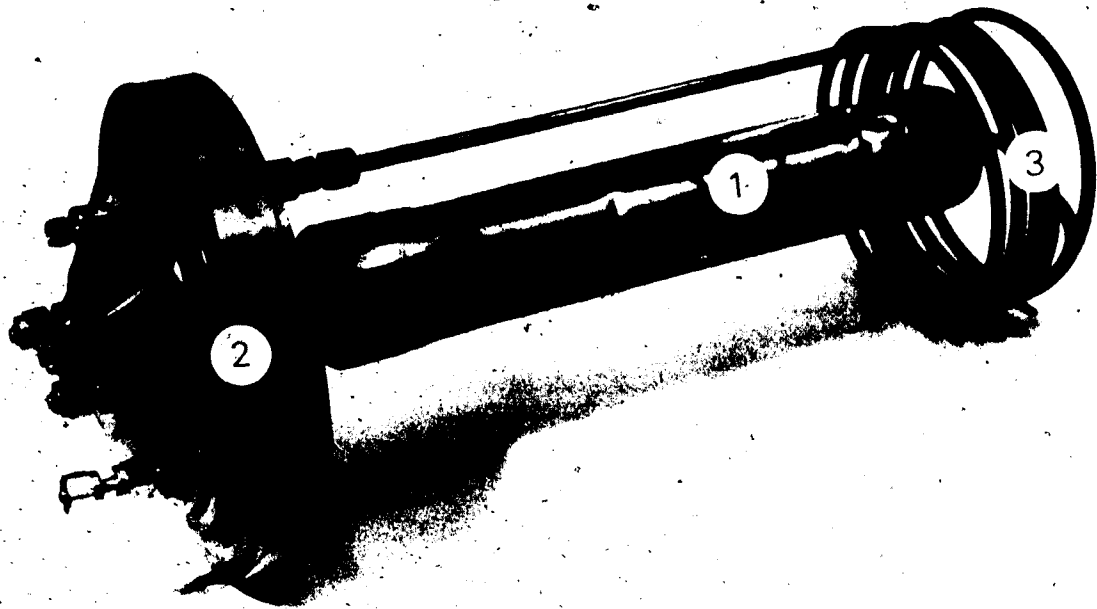
to prevent the fluids in the injection and production lines from flashing to steam.

For bitumen-free cores valves A and B were closed and valve C was opened (Figure 8) so that the production line carried the production fluids (effluent) directly to the back pressure regulator. This valve maintained fluid pressure in the apparatus by allowing fluids to pass only when the pressure was at a minimum threshold. After passing through the back pressure regulator, the effluent samples were collected in sample chambers at the end of the production line. The discrete interval of fluid injected was recorded for each sample taken.

The drop in pressure across the core was determined using differential pressure transmitters (dp cells). The injection line was connected to the upstream side of a dp cell and the production line was connected to the downstream side of a dp cell. The difference in pressure across the cell diaphram that separates the upstream and downstream sides of the dp cell is equal to the pressure drop across the core.

Figure 9 is a detailed schematic diagram of the different pressure and temperature measuring systems. Temperature in the autoclave was measured with a thermocouple connected to recorder #2. There were two pressure transducers in the system that converted pressures to voltage so that these pressures could be recorded on a strip chart. One transducer was on the injection line measuring the injection pressure (recorder #1). The other transducer measured the overburden pressure within the autoclave (recorder #2).

The differential pressure transmitter loop of Figure 8 was set-up in the following manner. A line was connected to the injection line and split to two different dp cells (Figure 9); one used to measure low
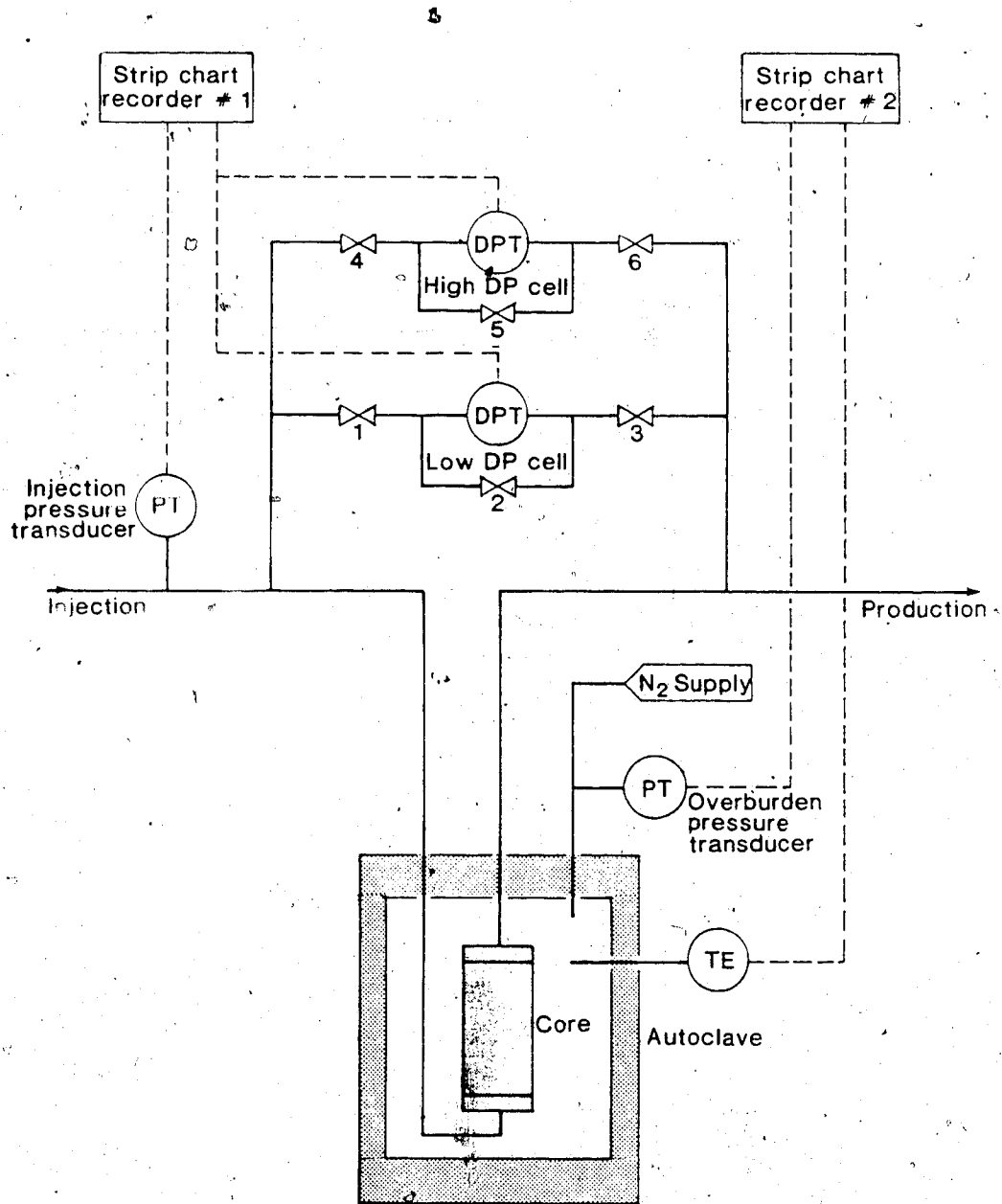
Figure 9. Schematic diagram of the measurement system of the experimental apparatus. Solid lines represent metal tubing. Dashed lines represent electrical wire.

pressure differences (0-27.6 KPa) and the other used to measure higher pressure differences (27.6-165.5 KPa). Likewise, a line was taken from the production line and split to the two dp cells. Only one dp cell was used to measure pressure drops at any one time.

The dp cells measured the pressure difference between two chambers, one on either side (injection and production) of a diaphram. The pressure difference across the diaphram was converted to a current and then to a voltage so it could be recorded on strip chart recorder #1.

Valves 1 and 4 (Figure 9) opened the low and high cell respectively to injection pressure. Valves 2 and 5 are equalization valves. When they were open, both sides of the dp cells were at equal pressure. Valves 3 and 6 opened the low and high cells respectively to production pressure. When no differential pressure was being measured, valves 1, 2, 4 and 5 were open and valves 3 and were 6 closed. To employ the low cell, valves 4 and 2 were closed and valve 3 was opened. Likewise, to use the high cell, valves 1 and 5 were closed and valve 6 was opened.

When the experiments were completed, the oven and the ruska pump were simultaneously turned off. When the autoclave cooled to room temperature (overnight), the pressure drop across the core was once again determined. The core was taken out of the autoclave, frozen and then slabbed along its cylindrical axis. One of the core slabs was quartered perpendicular to the cylindrical axis. Each quarter was labelled (Figure 10) and analyzed separately by the methods used to determine the mineralogy and grain size of the pre-flood sample. The production fluid samples were analyzed using Total Inorganic Carbon and Inductively Coupled Plasma analyses.
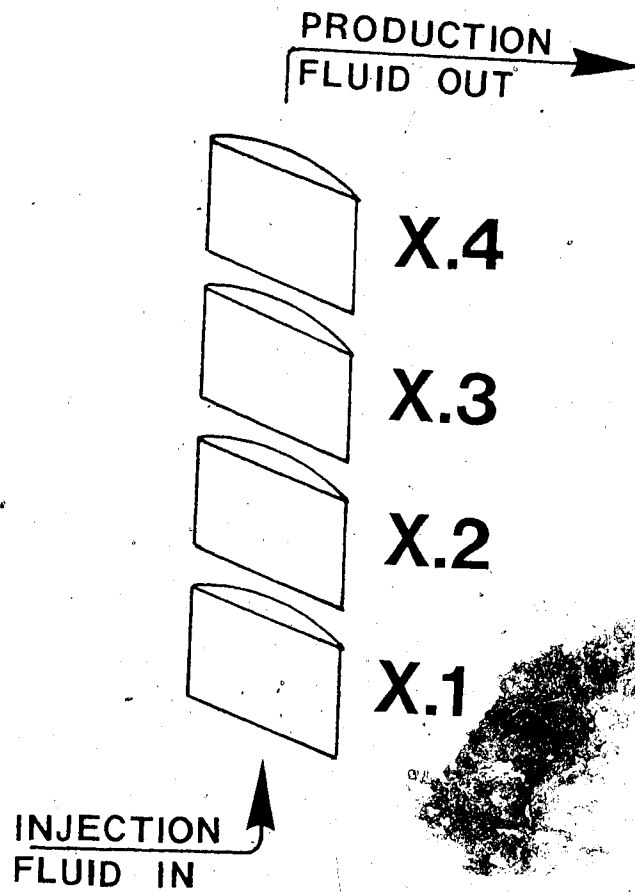
Figure 10. The sample labelling system used for quartered post-flood cores. X = core number. Number .1 designates the injection end of the core and number .4 designates the production end of the core.

Procedure for Bitumen-saturated Core

The fourth experiment was run with core that did not have the bitumen removed. The sample for this experiment was collected from the same depth intervals as the sample for the previous three experiments. This sand was homogenized by kneading in a plastic bag.

A core was made of this material by brazing an endcap into the end of a stainless steel sleeve of similar dimensions as used before. A sintered filter was placed in the sleeve against the endcap. The sleeve was then filled by packing it with seven equal increments of oil sand. Movement of fines was not a concern during the fabrication of this core because of the nature of the material. Before the second filter and endcap were brazed in place, 2 cm of 20 - 40 mesh (0.42 - 0.84 mm) size silica frac sand was packed on the oil sand. This prevented the bitumen from mobilizing and interfering with the solder of the second endcap onto the sleeve. Frac sand was chosen for its silica purity and coarse grain size in order to reduce the effect that it would have on the results of the experiment.

For the bitumen-saturated core, either valve A or B was open and valve C was closed (Figure 8) so that the production fluid flowed into the 500 ml accumulators on-line before the back pressure regulator. The fluids entered the upstream side of one of the 500 ml accumulators pushing the piston down and displacing distilled water out of the bottom chamber of the accumulator. The distilled water passed through the back pressure regulator and was collected to measure the volume of effluent sample in the accumulator. Heating tape on the production line maintained the low viscosity of the bitumen.

IV. RESULTS

A. Grain Size Distribution

Hydrometer

The results of the hydrometer analyses indicate that the grain size distributions of all four cores shifted towards finer grain sizes relative to the pre-flood material (Figure 11). The percentage of fines (material <38 μm) increased two to three times in cores #1, #2, and #3 relative to pre-flood material (Figure 11a and b) but only marginally in core #4 (figure 11c). The weight percent of the <5 and <20 μm fraction increased more in core #3 (Figure 11b) than in cores #1 and #2 (Figure 11a). The increase in the <5 μm fraction of core #4 was minimal compared to the increases observed in the other cores.

Wet Sieve

The wet sieve analyses underrepresent the <38 μm fractions of cores #1, #2 and #3 relative to the hydrometer analyses because preparation for hydrometer analysis by sonication dispersed finer particles more thoroughly than the procedure (boiling) used for wet sieve analysis. However, both hydrometer and wet sieve data indicate that the grain size distributions of the post-flood cores shifted to finer size fractions relative to the pre-flood sand (Figures 11 and 12, respectively).
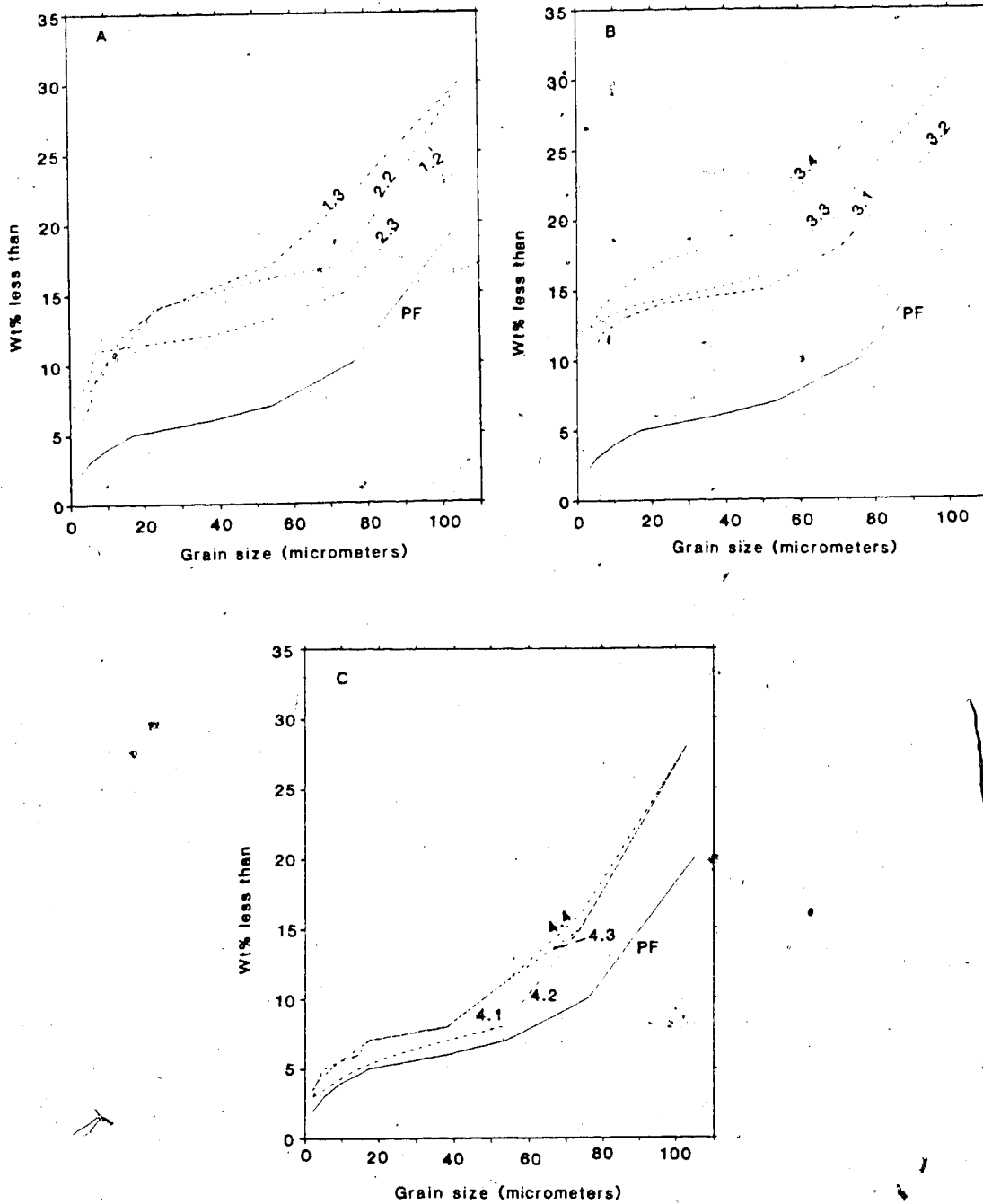
Figure 11. Grain size analyses of (a) core #1 and #2, (b) core #3 and (c) core #4 using hydrometer settling. Data from Tables 2-1 to 2-4.
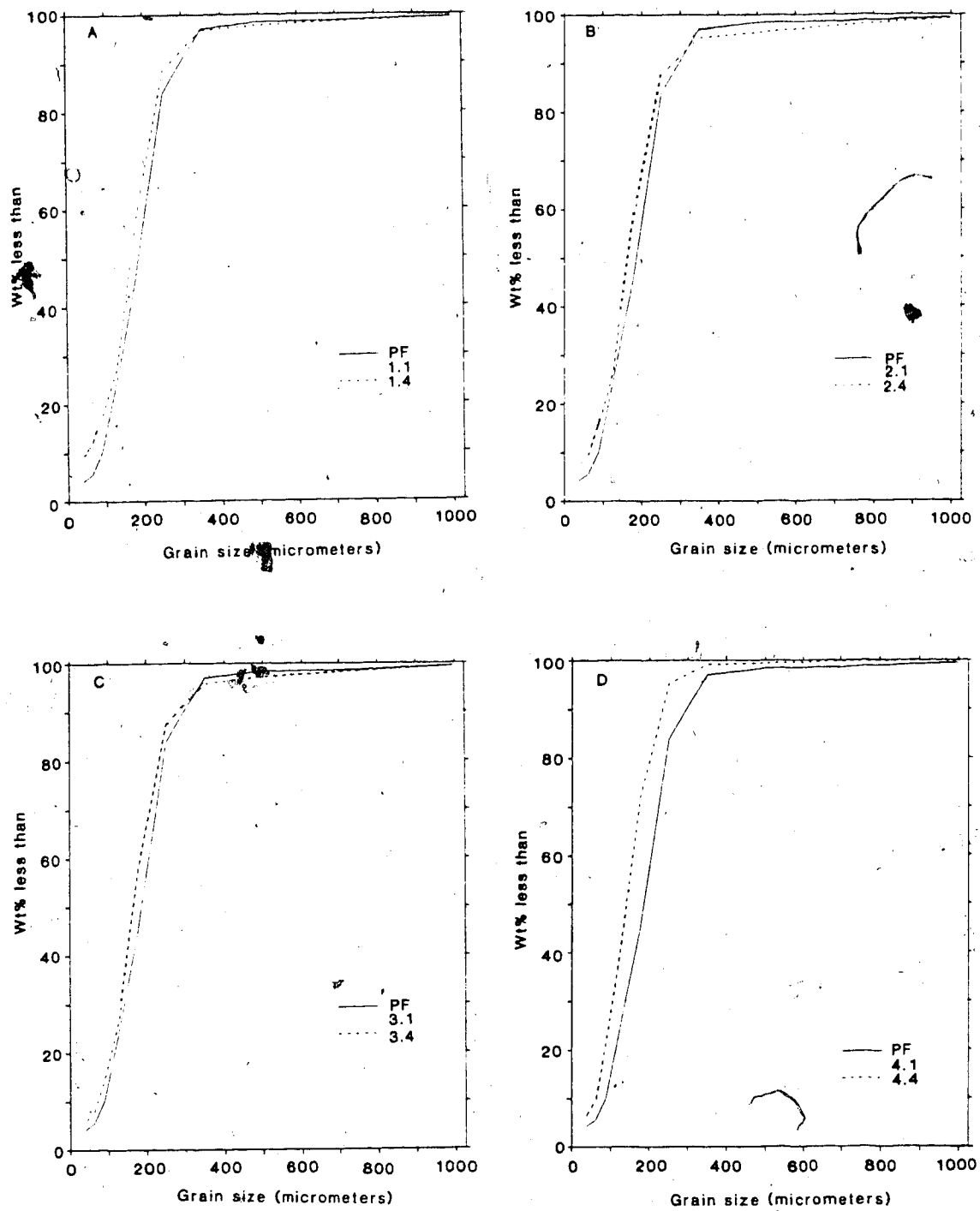
Figure 12. Grain size distributions of (a) core #1, (b) core #2, (c) core #3 and (d) core #4 using wet sieve analysis. Data from Table 2-5.

B. Petrographic Observations

Pre-flood Sand

The mineralogy and grain composition of the pre-flood sand, as determined from point counting, are listed in Table 5. The sand is a non-indurated feldspathic litharenite (Figure 13). Rock fragments are the most abundant constituent. These include volcanic, shale, sandstone, siltstone, and metamorphic rock fragments. The detrital minerals in decreasing order of abundance are quartz, K-feldspar, chert, plagioclase, and carbonate (contrast Putnam and Pedskalny, 1983). Muscovite, biotite, glauconite, opaques and heavy minerals are present in trace amounts.

Volcanic rock fragments have plagioclase microlites in a fine-grained to glassy devitrified groundmass (Plate 3c). The groundmass, light brown or light green in plane polarized light, also contains aligned microlites. Alteration products of the groundmass include chlorite and opaques. The plagioclase microlites are relatively unaltered.

Shale fragments are dark brown in plane polarized light and have mottled or non-uniform extinction with crossed nicols (Plate 3a). Some individual constituents were visible within the grains but could not be identified because of their inherent small size. Siltstone and sand-stone fragments contain rounded quartz or feldspar grains in a fine-grained matrix (Plate 4c).

Metamorphic rock fragments are comprised mostly of quartzite that contains quartz grains with highly sutured boundaries. The quartz

Table 5. Relative abundances of rock fragments and minerals present in the pre-flood sand determined from point counting.

	%
Volcanic Rock Fragments	23
Shale Fragments	5
Siltstone and Sandstone Rock Fragments	4
Metamorphic Rock Fragments	3
Unidentifiable Rock Fragments	4
(Total Lithic Fragments)	(39)
Quartz	21
K-feldspar	13
Chert	12
Plagioclase	9
Carbonate	5
Muscovite	<1
Biotite	<1
Glauconite	<1
Opaques (Pyrite?)	<1
Heavy Minerals	<1
TOTAL	100

Qtz

Quartzarenite

5 / \ 5

Subarkose   Sublitharenite

25 /   \ 25

Arkose   Lithic Arkose   Feldspathic Litharenite   Litharenite

Fdsp   25   50   25   RF+C
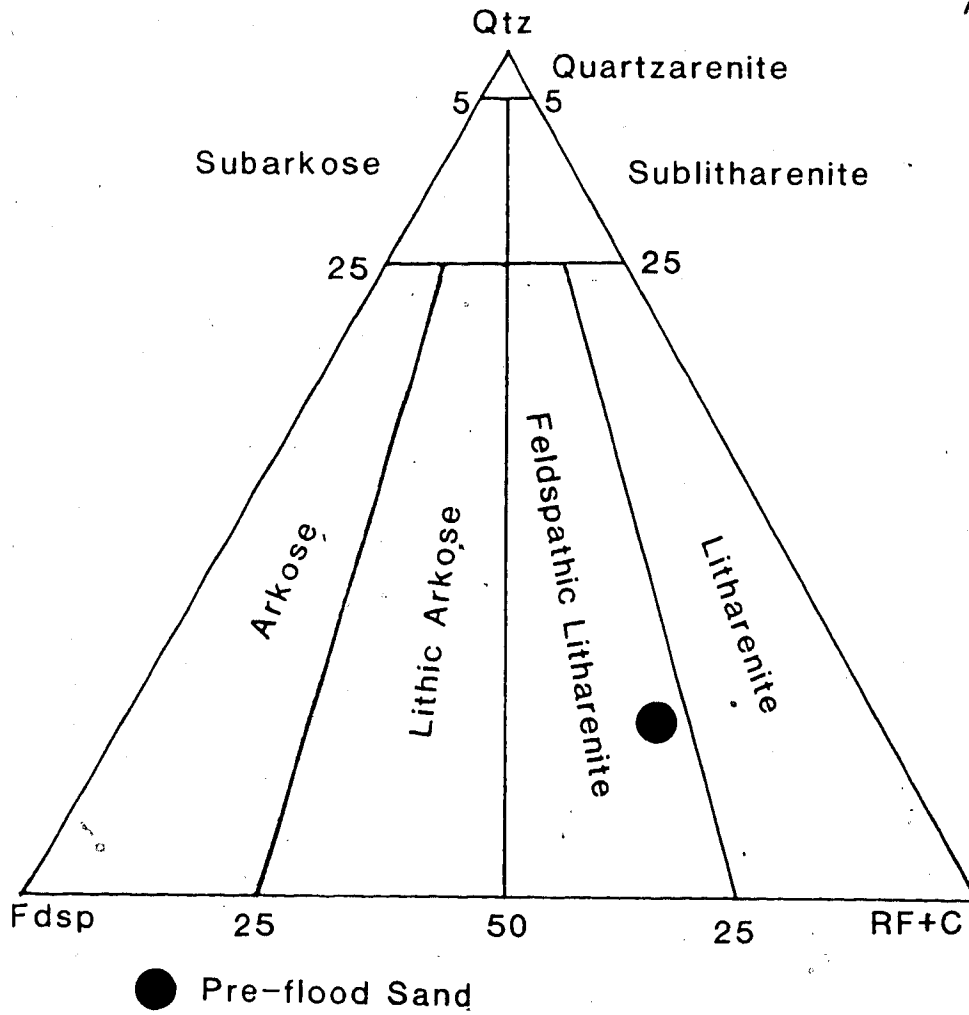
Pre-flood Sand

Figure 13. Classification of the pre-flood sand (after Folk, 1968) based on the point counts in Table 5. Qtz = quartz. Fdsp = feldspars. R.F. = rock fragments. C = chert.

Plate 3. Thin section micrographs of the pre-flood sand. The scale is the same for all micrographs and is located on micrograph C. The blue color in the micrographs is the epoxy mounting medium. It is not a stain nor an indication of porosity since the samples are grain mounts.

A. Some of the residual organic matter (brown) present in the sand after the toluene extraction engulfs plagioclase (Pl) and shale (Sh) grains and finer material (arrows). Plane polarized light. Scale same as C.

B. Same as A but with crossed nicols illustrating the plagioclase twins. Scale same as C.

C. Volcanic rock fragments (V) account for up to 23-25% of the sand. These fragments consist of plagioclase microlites (PH) in a devitrified glass matrix. The volcanic rock fragment partially visible in the right side of the micrograph is more altered (note the opaques) than the other two volcanic rock fragments. The polycrystalline silica grain (PS) is probably a metamorphic rock fragment (see Plate 3D). Some coke is present in the northwest quadrant of the micrograph. Plane polarized light.

D. Same as C but with crossed nicols illustrating the bimodal crystallinity of the metamorphic rock fragment. Scale same as C.

A   B

Pl

Sh

C   D

PS   V

PH   V

V

0.2 mm
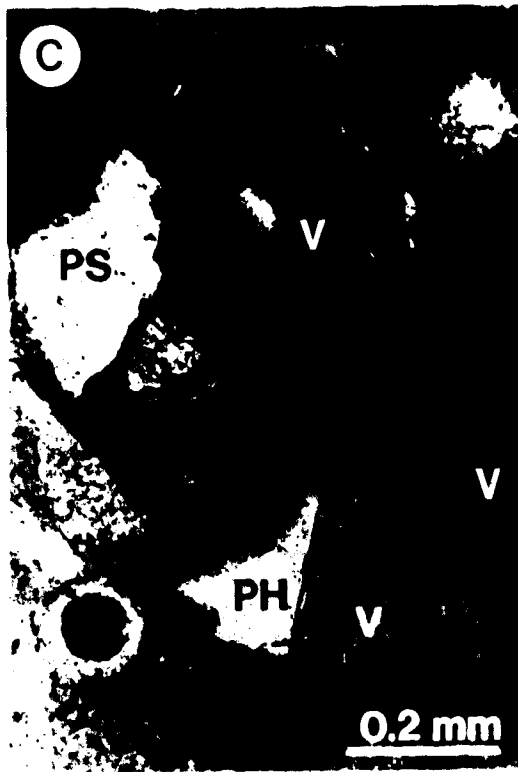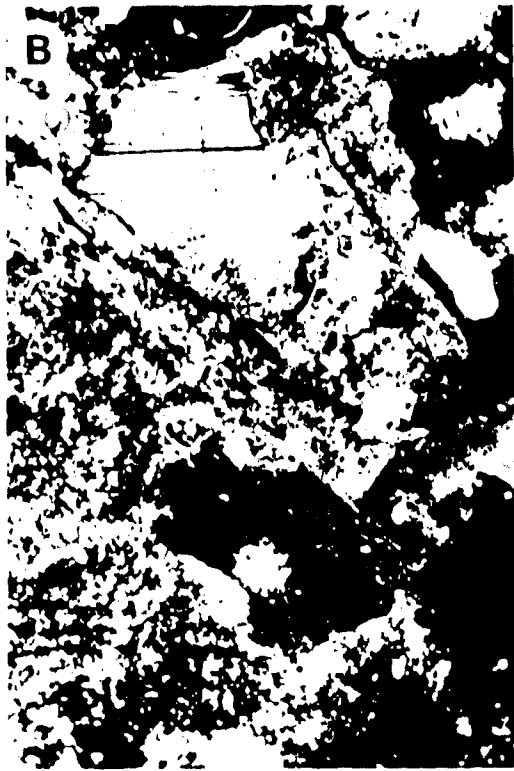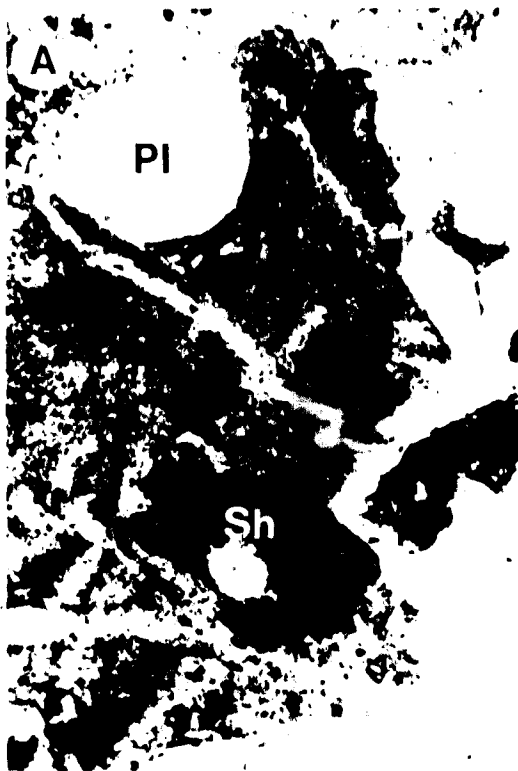
Plate 4. Thin section micrographs of pre-flood (A, B, and C) and post-flood (D) sand. The scale is the same for all micrographs and is located on micrograph A. The blue color in the micrographs is the epoxy mounting medium. It is not a stain nor an indication of porosity since the samples are grain mounts.

A. K-feldspar (KF) is differentiated from quartz (Q) based on alteration. K-feldspar was altered, to a varying extent, to fine-grained mica (A). Quartz grains showed no discoloration. Carbonate (C) is also present. Plane polarized light.

B. Same as A but with crossed nicols illustrating the birefringence of the K-feldspar alteration and the carbonate grain. Scale same as A.

C. Four different types of silica grains are present. Quartz grains (Q) are classified as the monocrystalline grains of silica. Chert grains (Ch) are mosaics of polycrystalline (uniform size) silica. Metamorphic fragments (MF) are quartzites composed of polycrystalline silica that is coarser than chert. Furthermore, the boundaries between the individual quartz grains in the metamorphic fragments are sutured. The last type of silica grain is the sedimentary rock fragment (SF) composed of silt-sized quartz grains set in a fine-grain matrix. Crossed nicols. Scale same as A.

D. Post-flood sand illustrating the brown rims (arrows) developed on the grains during the experiments (compare with Plate 4A). Plane polarized light (sample 1.2). Scale same as A.
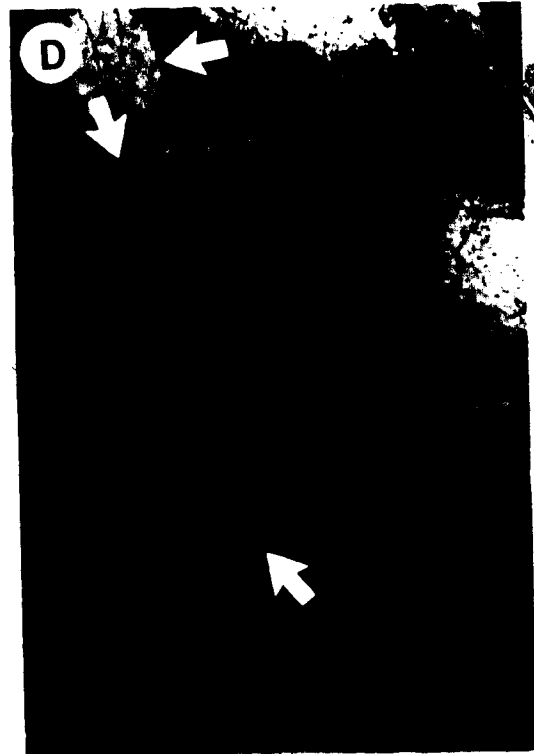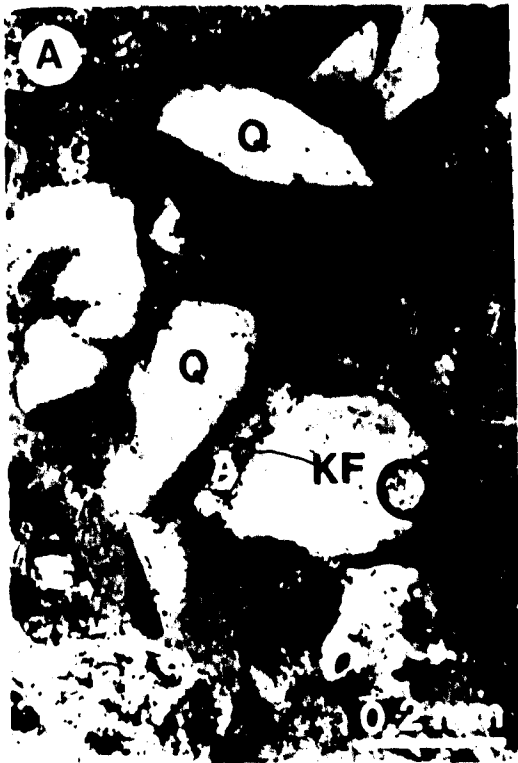
grains in these fragments have undulose extinction caused by stress (Plates 3d and 4c).

Unidentifiable rock fragments are lithic components (chert or volcanic rock fragments) that could not be specifically classified because of their size, fine-crystalline nature, alteration and/or lack of phenocrysts. The more altered (darker under plane polarized light) grains were classified as volcanic rock fragments.

For point-counting purposes, quartz grains were classified as those grains that are composed of monocrystalline silica grains (Plate 4c). These grains are clear under plane polarized light and have either uniform or undulose extinction with crossed nicols. Fluid inclusions are present in some grains.

K-feldspar grains are not twinned. These grains were differentiated from quartz by their alteration to muscovite and lack of clarity in plane polarized light (Plate 4a). The alteration of the grains varies from relatively fresh (some fine-grained muscovite inclusions) to highly altered (almost totally recrystallized to fine-grained muscovite and opaques).

Chert grains are polycrystalline silica that do not have sutured boundaries and are colorless (Plate 4c) to pale brown (Plate 5a) in plane polarized light. The silica mosaic is much finer in the chert grains than in the metamorphic rock fragments.

Two different compositional ranges of plagioclase (Plate 3a) were determined using the Michel-Levy test; An_{10-15} (oligoclase) and An_{30-40} (andesine). Oligoclase is more abundant. Putnam and Pedskalny (1983) also observed a range in plagioclase composition. Plagioclase grains are either fresh or partially altered to a fine-grained birefringent

Plate 5. Thin section micrographs of post-flood sand samples. The scale is the same for A, B, and D (located on A). The scale of micrograph C is located on the micrograph. The blue color in the micrographs is the epoxy mounting medium. It is not a stain nor an indication of porosity since the samples are grain mounts.

A. A small amount of carbonate cement (arrows) was present in most of the post-flood samples. It has a slight brown color compared to the quartz (Q) and feldspar (F) grains. The chert grain (Ch) has a brown discoloration and contains some opaque minerals. Plane polarized light (sample 2.2).

B. Same as A but with crossed nicols showing the high birefringence of the carbonate cement (sample 2.2). Scale same as A.

C. High magnification of carbonate cementing a quartz grain (Q), a shale fragment (arrow) and a volcanic rock fragment (V). The euhedral nature of the cement is illustrated. The relatively colorless cement (CC) grew around a slightly brown carbonate grain (C). Plane polarized light (sample 2.3).

D. The increase in fines during the experiments resulting in partial induration of clusters of grains. The clear quartz, chert and feldspar grains are easily seen set in the brown fines. However, the shale and volcanic rock fragments are hard to distinguish from the fines because of their similar color. Plane polarized light (sample 1.3). Scale same as A.

Ch

Q

F

0.2 mm

C

CC

Q

0.1 mm
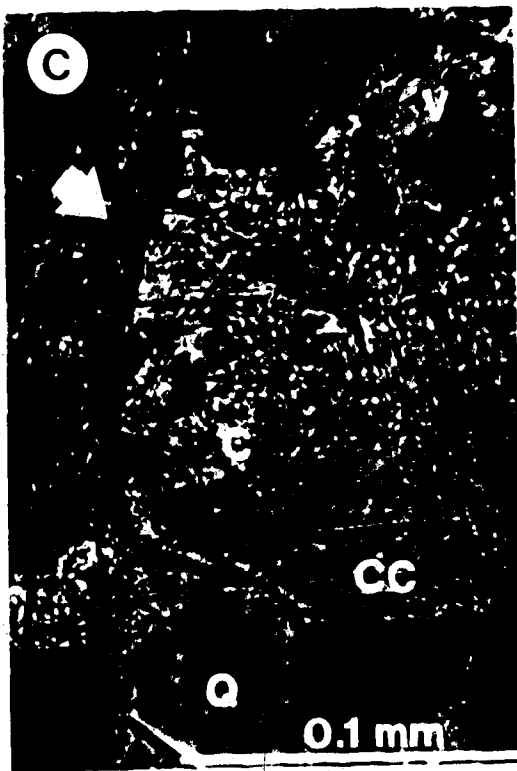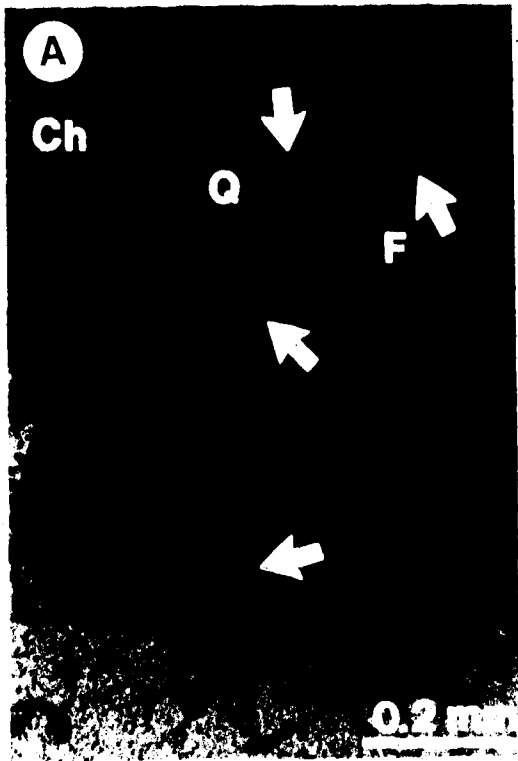
mineral. Some (10%) are altered to the extent that the twin planes are difficult to discern and their color is spotted brown under plane polarized light.

Carbonate grains have high birefringence (Plate 4b). Most of the grains have a brown alteration color in plane polarized light. The average size of the carbonate grains (0.09 - 0.11 mm) is approximately half that of the average grain size for the sand. Carbonate cement is rarely developed.

Mica grains (muscovite and biotite) have planar cleavage that is commonly disrupted because the grains were bent by overburden pressure. Because of their platy habit, they may be underrepresented in the point counts. This possibility became apparent when the pre-flood sand was examined under a binocular microscope and micas (shining flecks) were observed in more than trace percentage.

Glauconite was identified by its pleochroic green-yellow color in plane polarized light. The grains also have high birefringence.

Opaque minerals were observed both as alteration products (mainly on volcanic rock fragments) (Plate 3c). and as discrete grains. Only discrete grains were counted. The majority of these grains have a red rim. Heavy minerals have high positive relief and very low birefringence.

The monomineralic grains (quartz, chert and feldspars) lack overgrowths or clay coatings. However, the more intensely altered rock fragments show these features to some extent. The trace amount of organic material remaining after toluene extraction engulfs the grains (Plate 3a).

Post-flood Sands

Few differences were observed between pre-flood and post-flood sands and between different quarters of the same core. In cores #1, #2 and #3, most of the grains have a dark brown rim (Plate 4d). The grains in core #4 are covered with similar rims but to a lesser extent. The increased amount of fines produced resulted in partial induration of the samples (Plate 5d).

Carbonate grains are less abundant in the post-flood cores than in the pre-flood sand. These grains are most abundant in core #4, followed in decreasing abundances by cores #2, #3 and then core #1.

Carbonate cement is present in all cores in greater abundance than in the pre-flood sand. It is more abundant in cores #2 and #3 than in cores #1 and #4. The cement appears to bind only a few grains (6 grains maximum observed) together (Plate 5a) and when present, encloses one or more relic carbonate grains that are altered to a dark brown color and to an opaque mineral (Plate 5c).

The coarsening of chert mosaics, observed by the Sedimentology Research Group (1981), was not observed in any of the post-flood cores. Two possibilities may account for this discrepancy: (1) two years of steam flooding (Sedimentology Research Group, 1981) allowed more time for the mosaics to coarsen; or (2) the "chert" grains with coarser mosaics may have been siltstone or sandstone fragments.

C. Mineralogy

X-ray Diffraction (XRD)

Data from XRD analyses on the whole sand are consistent with the observations made during the petrographic study. The XRD patterns indicate the presence of quartz, feldspar (oligoclase? and ortho- clase?), dolomite, calcite, kaolinite, illite or muscovite, and chlor- ite and/or smectite in all pre- and post-flood samples. The changes that occurred in the sand during the four experiments are listed in Table 6. Quartz and feldspar peak intensities did not change signifi- cantly between the post-flood and pre-flood samples because the mine- rals were originally present in great abundances.

Smectite, dolomite and calcite abundances changed appreciably during the experiments. The amount of smectite approximately doubled in all quarters of cores #1, #2 and #3 (Table 6). The smectite content in core #4 increased by approximately 60% (Figure 14a).

Dolomite abundance decreased in all post-flood samples (Table 6). The greatest decrease occurred in core #1. The dolomite content in cores #2 and #3 decreased in approximately equal proportions. Of the post-flood samples, dolomite is most abundant in the production half of core #4 (samples 4.3 and 4.4; Figure 14b).

Calcite abundance increased in all the post-flood samples relative to the pre-flood material except for sample 1.4 (Table 6). The trace amount of calcite present in the pre-flood sand doubled in the injec- tion half (samples 1.1 and 1.2) of core #1.

Calcite abundance in core #2 increases to the second quarter (sample 2.2) and then continually decreases through the rest of the

Table 6. I/I_o values for the minerals most abundant in the samples as determined using whole sample XRD. I_o refers to the specified peak height on the diffractogram of the pre-flood sand. I is the intensity of the same peak but on the diffractogram of the specified post-flood sample. $I/I_o < 1$ shows a decrease in abundance, $I/I_o > 1$ shows and increase. Feldspars are not included in the table because of the problems associated with unit cell variation with solid solution. nd = not determinable.

	Smectite (001)	Kaolinite (001)	Dolomite (104)	Calcite (104)	Quartz (101)
1.1	2.1	0.9	0.2	1.8	0.9
1.2	2.0	1.0	0.3	2.0	nd
1.3	1.5	0.8	0.1	nd	1.3
1.4	2.3	1.0	nd	1.0	0.7
2.1	2.3	1.0	0.2	1.3	nd
2.2	2.1	1.0	0.3	2.3	nd
2.3	2.5	1.1	0.2	2.0	0.8
2.4	1.9	0.9	0.2	1.5	0.8
3.1	1.9	0.8	0.3	1.2	nd
3.2	2.5	1.1	0.4	1.7	0.7
3.3	1.8	1.0	0.4	2.8	0.7
3.4	2.0	0.9	0.2	1.6	0.7
4.1	1.8	0.7	0.2	2.4	1.0
4.2	2.0	1.1	0.3	1.5	0.9
4.3	1.6	1.0	0.6	1.5	1.1
4.4	1.0	0.9	0.7	1.6	1.0
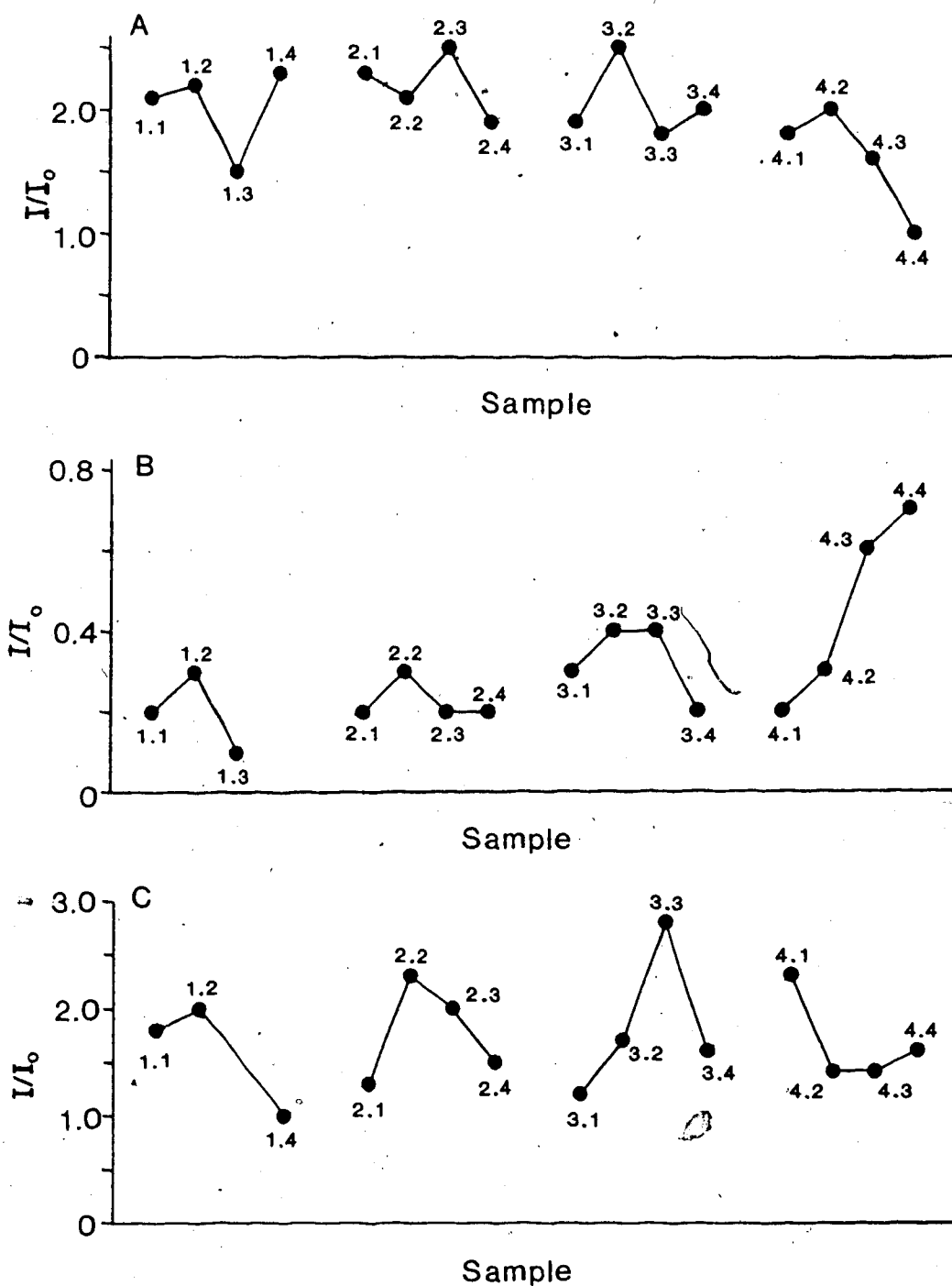
Figure 14. I/I$_o$ values from backpack XRD charts for (a) smectite, (b) dolomite and (c) calcite. Data from table 6.

core (samples 2.3 and 2.4; Figure 14c). The calcite content of core #3 increases gradually to the third quarter (sample 3.3) and then decreases. Calcite abundance in core #4 is greatest in the injection quarter (sample 4.1).

Gravimetric CO_2

Carbon dioxide is 1.7 weight percent of the pre-flood sand. This is equal to 3.6 weight percent dolomite (Table 7).

The amount of CO_2 remaining in cores #1, #2 and #3 is approximately equal having decreased to less than 50% of the pre-flood sand (Figure 15). This corresponds to between 1 and 2 weight percent calcite (Table 7). The amount of CO_2 decreases slightly from the injection quarters to the production quarters in cores #1 and #3. Sample 1.4 contains the least amount of CO_2 (0.21 wt%). In core #2 the amount of CO_2 remains approximately constant throughout the core.

The CO_2 content of core #4 has slightly decreased relative to the pre-flood sand and is approximately double that of cores #1, #2 and #3 (Figure 15). CO_2 content is greatest in samples 4.2 and 4.3 (1.69 and 1.57 wt%, respectively) where abundance has not changed appreciably relative to the pre-flood material. The CO_2 abundances in core #4 correspond to between 2.5 and 3.5 weight percent dolomite (Table 7).

Clay Mineralogy of the <2 μm Fraction

The most abundant clay mineral in the pre-flood sand is smectite (65-70%) followed in decreasing order of abundance by illite, kaolinite and chlorite (Table 8). Quartz and feldspar are also abundant in this portion.

Table 7. Weight percent CO_2 in all samples using gravimetric CO_2 analysis. The wt% CO_2 is recalculated to wt% calcite for cores #1, #2 and #3 since calcite is the dominant carbonate in those cores (determined by XRD). Likewise wt% CO_2 in the pre-flood material and in core #4 was recalculated to wt% dolomite because dolomite is present in greater abundance than calcite. cal=calcite dol=dolomite.

Sample	wt% CO_2	wt% cal	wt% dol
PF	1.70		3.6
1.1	0.75	1.7	
1.2	0.73	1.7	
1.3	0.69	1.6	
1.4	0.21	0.5	
2.1	0.60	1.4	
2.2	0.60	1.4	
2.3	0.56	1.3	
2.4	0.60	1.4	
3.1	0.79	1.8	
3.2	0.70	1.6	
3.3	0.49	1.1	
3.4	0.54	1.2	
4.1	1.34		2.8
4.2	1.69		3.5
4.3	1.57		3.3
4.4	1.38		2.9
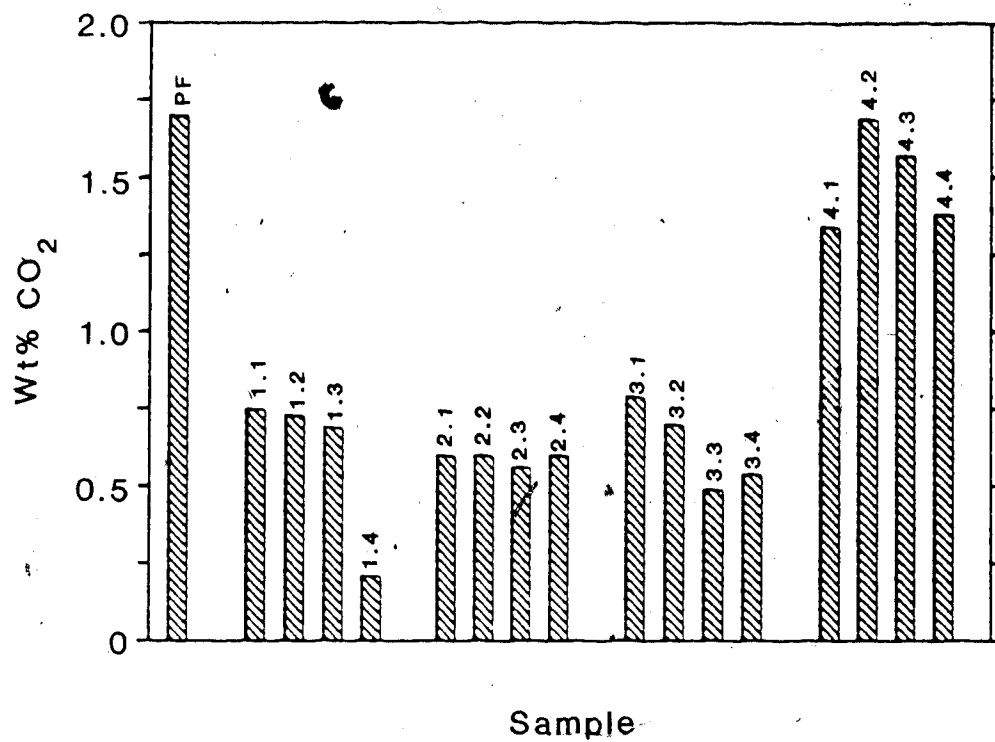
Figure 15. Weight percent CO_2 in each sample determined using gravimetric CO_2 analysis (values from Table 7). PF = pre-flood sand.

Table 8. Relative abundances of clay minerals in the <2 µm size fraction determined using the peak height method (Apppendix 1). PF = pre-flood sand.

	Kaolinite %	Illite %	Smectite %	Chlorite %
PF	12	16	68	4
1.1	12	39	44	8
1.2	10	23	62	5
1.3	7	14	75	4
1.4	9	36	47	8
2.1	2	32	54	12
2.2	6	15	74	5
2.3	9	18	70	3
2.4	13	34	47	6
3.1	5	16	75	4
3.2	6	13	78	3
3.3	6	15	74	5
3.4	7	15	74	4
4.1	10	23	59	8
4.2	11	24	55	10
4.3	9	25	56	10
4.4	10	23	61	6

Smectite is the most abundant clay mineral in all post-flood samples ranging from 40 to 80%. The 060 diffraction peak is at 1.50Å indicating that the smectite is dioctahedral. It is most abundant in core #3 followed by core #2, core #1 and core #4 (Figure 16). In cores #1 and #2, smectite is most abundant in the middle portion of the cores (1.2, 1.3, 2.2, and 2.3). Smectite content is evenly distributed throughout cores #3 and #4 (Figure 16).

Illite abundance increased in all cores relative to the pre-flood sand except for core #3 where illite is present in abundances equal to that of the pre-flood sand (Table 8).

The ratios of smectite:illite for all samples, calculated from the values in Table 8, are illustrated in Figure 17. These two clays are compared against each other because they are the most abundant (accounting for between 75 and 90% of the clay minerals in all pre-flood and post-flood samples). The ratios (Figure 17) reflect the trends in smectite content (Figure 16).

Kaolinite content of cores #1 and #4 did not change relative to the pre-flood sand. It decreased in cores #2 and #3. A trend exists in core #2 where kaolinite abundance increases consistently along the injection path of the core (from sample 2.1 to 2.4). Kaolinite is 50% less abundant in core #3 than in the pre-flood sand (Table 8).

Chlorite content increased in core #4 relative to the pre-flood material but remained unchanged in core #3. In cores #1 and #2, abundance increased in the outer portions (1.1, 1.4, 2.1, and 2.4) but remained unchanged in the inner portions (Table 8).
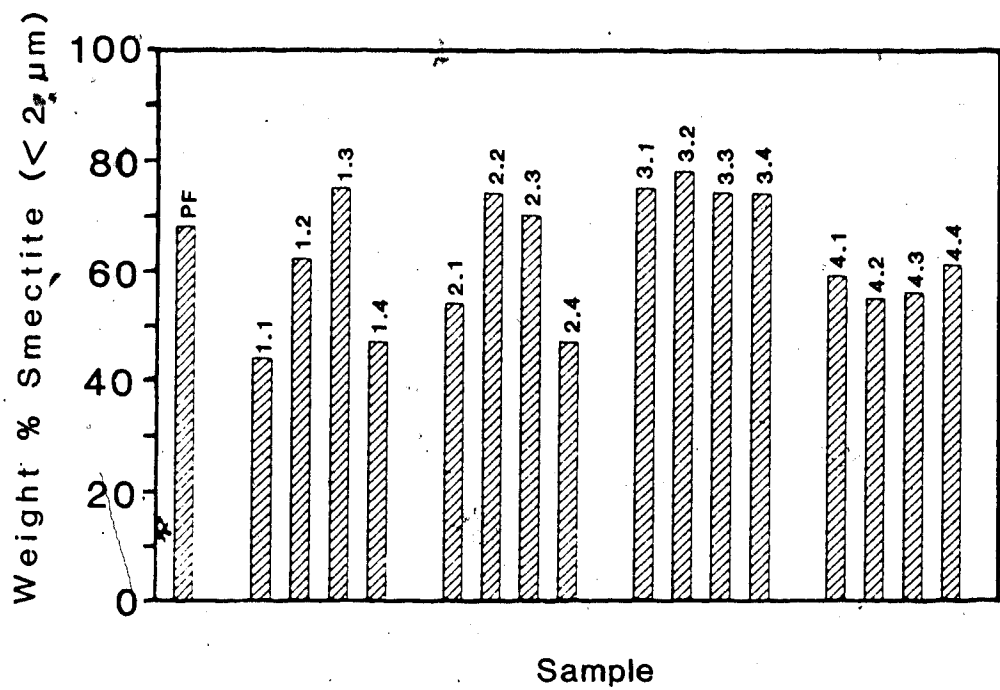
Figure 16. Percentage of smectite in the <2 μm fraction of all samples.
PF = pre-flood sand.
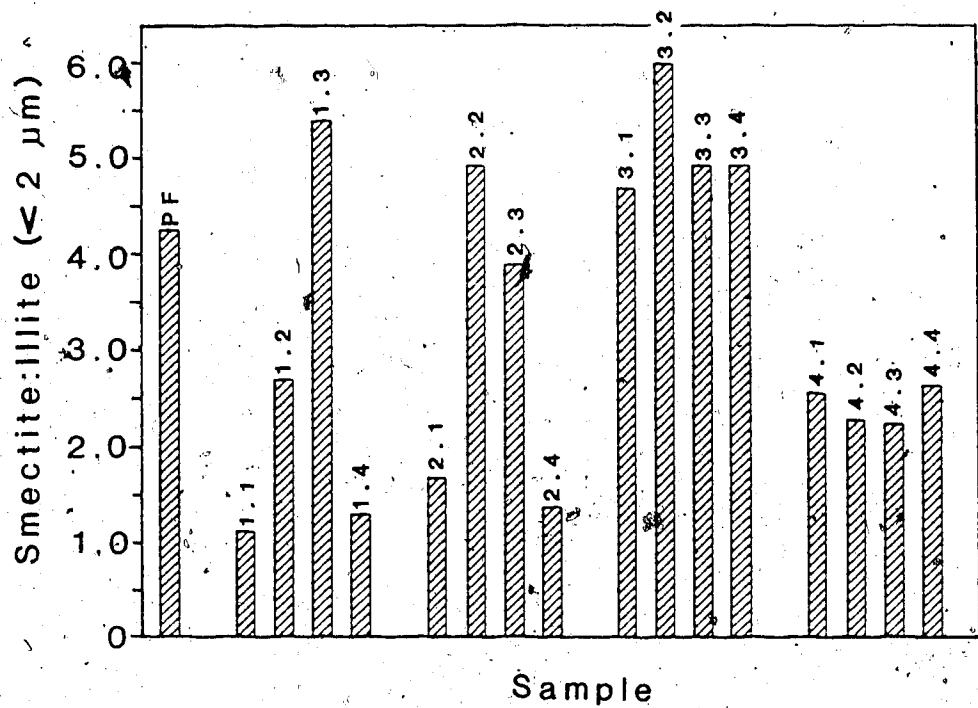
Figure 17. Smectite:illite ratio in the <2 μm fraction of all samples based on the values in Table 8. PF = pre-flood sand.

Clay Mineralogy of the 2-5 μm Fraction

Smectite, illite, kaolinite, and chlorite are present in this fraction of all samples. Quartz and feldspar are also present.

The ratio of kaolinite to illite decreased in all post-flood samples relative to the pre-flood sand (Table 9). In core #3, the ratio consistently increases along the injection path (from sample 3.1 to 3.4).

Similar trends in the smectite:illite ratio developed in cores #1, #2 and core #3. The ratio increased from the injection quarter to the third quarter and then decreases in the production quarter of each core (Figure 18). The final decrease was not as pronounced in the core #3. The ratio is highest in core #3, followed by core #2 and then core #1. In core #4, the amount of smectite relative to illite does not change significantly compared to the pre-flood sand. A slight decrease may exist from sample 4.1 through to sample 4.3 (Figure 18).

Clay Mineralogy of the 5-20 μm Fraction

Smectite, illite, kaolinite, and chlorite are present in the 5-20 μm fractions of all samples. The amount of quartz and feldspar present in this portion of each sample has increased relative to the two smaller portions studied.

The ratio of kaolinite:illite decreased in all post-flood samples relative to the pre-flood sand. This decrease was most pronounced in cores #4 and #2 (Table 9).

The smectite:illite ratio increased in all cores relative to the pre-flood sand. The increase was greatest in core #3. Two exceptions were noted: (1) the increase was not significant in the injection half

Table 9. (001) peak intensity ratios of smectite to illite $(I_{14.5}/I_{10.2})$ and kaolinite to illite $(I_{7.2}/I_{10.2})$ for the 2-5 μm and 5-20 μm fractions of all samples. PF = pre-flood sand.

| Sample | 2-5 μm | | 5-20 μm | |
	$I_{14.5}/I_{10.2}$	$I_{7.2}/I_{10.2}$	$I_{14.5}/I_{10.2}$	$I_{7.2}/I_{10.2}$
PF	3.8	1.8	3.1	2.7
1.1	3.8	1.5	9.6	2.0
1.2	7.4	1.6	5.0	2.0
1.3	8.1	1.5	8.2	1.8
1.4	2.7	2.1	3.7	1.0
2.1	5.7	1.2	3.5	1.7
2.2	6.5	1.5	3.3	1.1
2.3	9.4	1.5	8.5	1.3
2.4	5.6	1.5	4.7	1.5
3.1	6.6	1.1	6.9	1.6
3.2	9.2	1.4	15.5	1.7
3.3	10.8	1.5	8.4	1.8
3.4	10.2	1.7	9.0	1.8
4.1	4.8	1.1	5.3	1.0
4.2	4.0	1.5	3.7	1.1
4.3	3.1	1.2	2.0	1.8
4.4	4.0	1.3	2.3	1.3
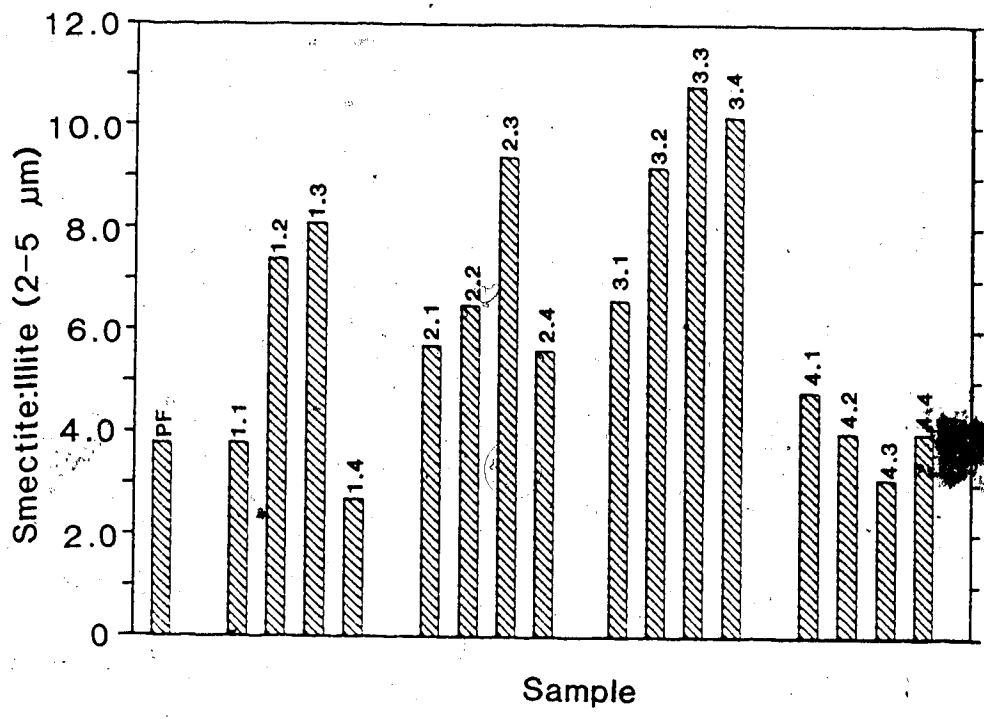
Figure 18. Smectite:illite ratio in the 2-5 μm fraction of all samples based on data from Table 9. PF = pre-flood sand.

of core #2 (samples 2.1 and 2.2) and (2) a decrease was observed in the production half of core #4 (samples 4.3 and 4.4; Figure 19).

Scanning Electron Microscopy (SEM)

A number of diagenetic minerals and textures were identified in the pre-flood sand using SEM. Plate 6 shows the texture of the pre-flood sand with bitumen (Plate 6a) and without (Plate 6b). Three diagenetic clay minerals were identified: smectite, illite and kaolinite (Plate 6c, d and e, respectively). K-feldspar overgrowths, clinoptilolite, pyrite or marcasite (Plate 6f, g and h, respectively), and calcite cement were also identified as diagenetic minerals.

The amount of mineral matter in the pore space increased in core #1 relative to the pre-flood sand (Plate 7). Formation of smectite, with honeycomb texture, analcime, phillipsite and/or clinoptilolite, and illitization of feldspars were also noted (Plate 7f, c, e and g, respectively). Open pores (Plate 7h) are more abundant in core #1 than in the other bitumen-free cores.

Smectite + analcime zeolite (see below) is a common assemblage in the injection half of core #2 (Plate 8; the latter two minerals were not identified using XRD). In the production half of the core, the authigenic suite consists mainly of smectite with minor amounts of analcime. All three minerals are present in core #2 sand in greater abundance than in core #1 sand.

Energy dispersive spectrometry (EDS) completed on the zeolite laths in core #2 (Plate 8d and f) indicated an abundance of K. Upon closer inspection, the laths were observed to have double prismatic terminations that were split along cleavage planes. These observations are
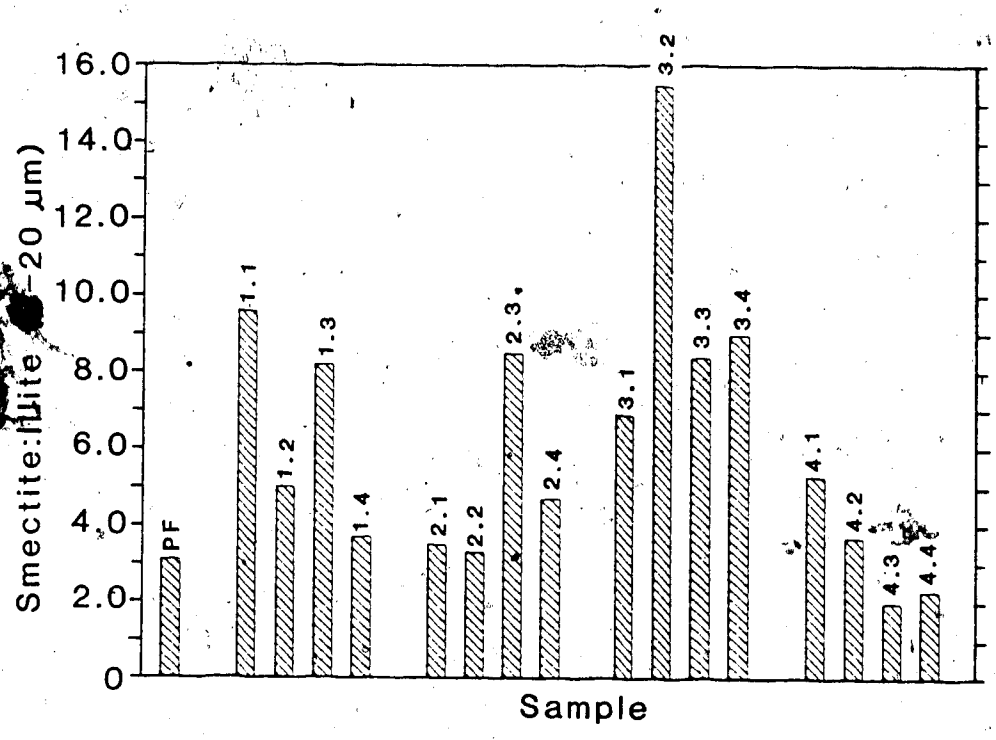
Figure 19. Smectite:illite ratio in the 5-20 μm fraction of all samples based on data from Table 9. PF = pre-flood sand.

Plate 6. Scanning electron micrographs of the pre-flood sand. Scale bars located below each micrograph.

A. The texture of the sample with bitumen in place is illustrated. Relief of the grains is detectable through the oil coatings which are joined by oil bridges (arrows).

B. The pre-flood material is relatively clean of coatings. With the bitumen removed, the different types of grains can be seen including quartz (Q), feldspar (F), volcanic (V) and shale (S) rock fragments and carbonate (C). An important feature to be noted in this photograph is the lack of sample induration.

C. Smectite (and possibly illite) coats on the volcanic grains are common.

D. Fibrous illite (arrows) "healing" a grain fracture. This mineral was also observed to bridge across pores in a similar fashion.

E. Booklets of kaolinite occur as pore-filling material.

F. K-feldspar overgrowths (KF) developed non-continuously on a detrital feldspar grain (F). The smectite also present on the grain inhibited the full development of the overgrowth (Sedimentology Research Group, 1981). This texture was observed throughout the sample.

G. The characteristic monoclinic symmetry of clinoptilolite is illustrated by the coffin-shaped crystals. The lath-shaped crystals are also clinoptilolite. This zeolite is a common alteration product of volcanic sediments (Hay, 1978).

H. The cluster of cubic crystals is authigenic marcasite (or pyrite?).

Plate 7. Scanning electron micrographs of post-flood core #1 sand. Scale bars are located below each micrograph.

A. General view of core #1 (sample 1.3). The <38 μm fraction doubled relative to the pre-flood sand enabling partial induration of the core #1 sand. The pore space material has a massive texture. Note the difference between this micrograph and Plate 6b (approximately the same scale).

B. Higher magnification view of the pore-filling material. A honeycomb fabric was formed by smectite plates growing perpendicular to grain surfaces (arrows). This texture develops a microporosity which entraps the bitumen; this contributes to high residual oil saturation (Sedimentology Research Group, 1981).

C. Authigenic analcime crystals (arrows) developed in the pore spaces only in trace amounts. These crystals, when observed, were associated with volcanic fragments and smectite. A quartz grain (Q), clean of any type of coating, is present at the bottom of the micrograph.

D. Detail of the well-developed cubic-octohedral symmetry of the analcime crystals. The average size of the crystals is approximately 5 μm.

E. The authigenic minerals formed during the experiment can constrict pore-throats. Zeolite crystals (phillipsite and/or clinoptilolite) (Z) are trapped between a quartz grain (Q), a feldspar grain (F), and a smectite-covered volcanic rock fragment (V).

F. Detail of the honeycomb smectite form grown on a volcanic rock fragment. In core #1, this texture is relatively open because of the thin nature of the plates. The average width of the plates is less than 5 μm.

G. Plagioclase feldspars dissolved along twin planes and partially altered to illite (arrows). Minor smectite coats developed along the surfaces.

H. An open pore space between a quartz grain and a volcanic rock fragment.
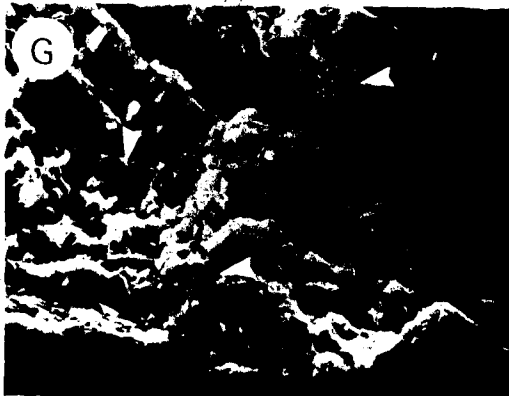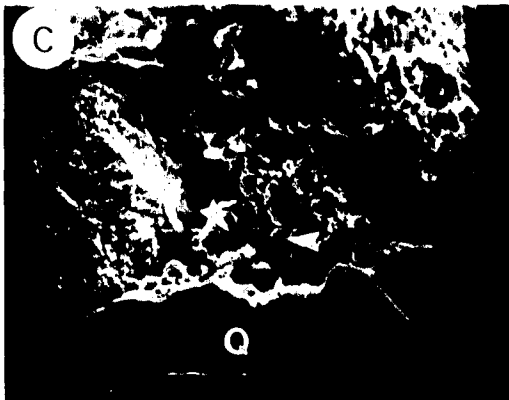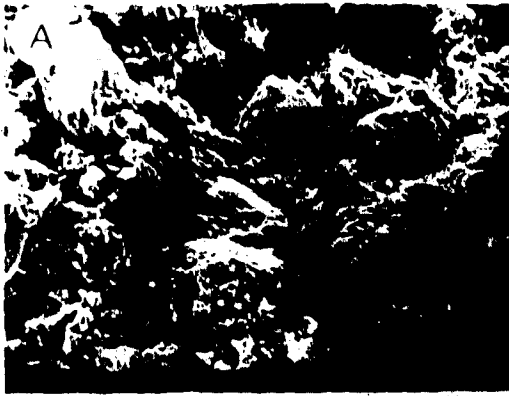
Plate 8. Scanning electron micrographs of post-flood core #2 sand. Scale bars are located below each micrograph.

A. General view of core #2 sand (sample 2.1). The grains are coated to a much greater extent than the grains in the pre-flood sand (Plate 6c). The coatings do not appear as extensive as those in Plate 7a because fewer framework grains are present in the micrograph.

B. A tighter honeycomb fabric of smectite. EDS indicated the presence of Ca, Mg, Na and Fe as probable interlayer cations.

C. Smectite was abundant and well developed in the injection half of this core. The individual flakes appear thicker thus filling in the honeycomb fabric more than the smectite in core #1 (Plate 7b). Analcime crystals are present (arrows). Small lath-like zeolites (clinoptilolite or phillipsite) are dispersed throughout the honeycomb structure of the smectite.

D. A higher magnification view of the honeycomb smectite texture indicates that the average width of the flakes is approximately 5 μm. This size is larger than the smectite in core #1 (Plate 7f). The zeolite laths are intermeshed in the honeycomb structure. These zeolites may have been caught in the honeycomb "net" as they passed through the pore rather than actually forming at the sites they now occupy.

E. Volcanic rock fragments are the most common of the framework grains to be covered with authigenic minerals. The coatings on the volcanic fragment (V) have filled the pore space between that fragment and grains to the right of it. The coatings include smectite (Sm), psite (laths) (P) and/or clinoptilolite (plates). The presence of earlier diagenetic smectite prevents these flood-induced minerals from covering the entire grain.

F. Massive zeolite (phillipsite or clinoptilolite) (Z) coatings were present on volcanic fragments in the injection half of the core. The prisms are aligned perpendicular to the grain surface allowing for easy dislogement and subsequent pore clogging. The fact that these crystals can be dislodged and transported may account for their coating of other authigenic material (eg., micrograph d). A large analcime crystal (An) and a cluster of large smectite flakes (Sm) are also present on the grain surface.

G. A K-feldspar grain is partially dissolved (arrows). No authigenic mineral is evident on the grain.

H. A plagioclase grain dissolves along twin planes and is partially replaced by smectite and/or illite.
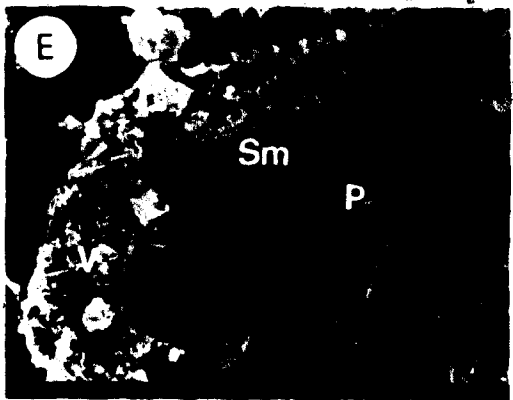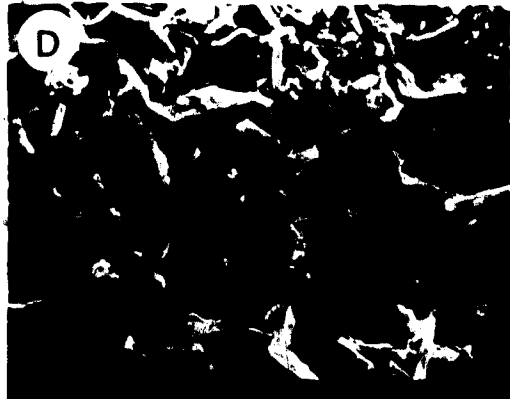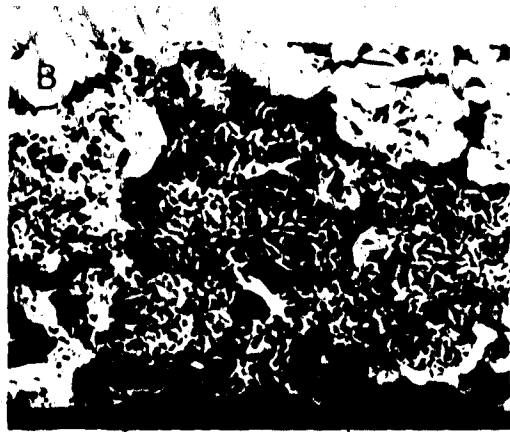
more characteristic of phillipsite than clinoptilolite (Mumpton and Ormsby, 1976). Sydansk (1982) reported the formation of phillipsite during similar experiments.

The majority of volcanic rock fragments in core #2 are coated with authigenic materi▰▰. This armouring may have prevented further solution of the▰▰▰s (Sedimentology Research Group, 1981).

Analcime, ▰▰ present, occurs on smectite indicating that analcime formed after th▰ smectite.

Albite ov▰▰rowths are unique to core #3 (Plate 9). K-feldspar overgrowths were dissolved (Plate 9g and h). Smectite and analcime were observed in similar abundances as in core #2 but phillipsite was rarely observed. Quartz grains in this core were dissolved more than in any other core (Plate 9d).

Authigenic smectite and analcime are present in core #4. Analcime is more abundant in core #4 than in any other core. Authigenic quartz was also noted (Plate 10g).

Stable Isotopes of Carbonate Minerals

The pre-flood dolomite has a $\delta^{18}O_{SMOW}$ of 24.4 permill and $\delta^{13}C_{PDB}$ of 0.0 (Figure 20). All post-flood dolomite samples are significantly depleted in ^{18}O ($\delta^{18}O_{SMOW}$ = 1.7 to 19.0 permill) relative to the pre-flood material (Figure 20). The post-flood calcite is extremely depleted in ^{18}O ($\delta^{18}O_{SMOW}$ = -9.4 to -10.8 permill) relative to both the pre-flood and post-flood dolomite but only very slightly depleted in ^{13}C ($\delta^{13}C_{PDB}$ = -3.1 to -1.9 permill; Figure 20).

Plate 9. Scanning electron micrographs of post-flood core #3 sand. Scale bars are located below each micrograph.

A. General view of core #3 material. The scale is approximately equal to that used in Plate 6c.

B. Smectite rims were well developed on volcanic fragments. EDS indicated Mg, Ca and Fe are present in approximately equal abundances in the smectite.

C. Smectite (Sm) completely covers a volcanic rock fragment. Analcime (arrows), as in most cases, crystallized on the smectite suggesting that it formed later than the smectite. Some bitumen (B) is retained in the pore space.

D. A cluster of analcime crystals (An) and phillipsite and/or clinoptilolite laths grow on a quartz grain (Q) in the injection quarter of core #3 (sample 3.1). The quartz grain shows evidence of solution pitting by its rougher surface (compared to Plate 7c and e).

E. Albite overgrowths (Ab) were noted throughout core #3 (more so than any other core). Their abundance suggests that they formed during the core flood. The lath-like zeolites (phillipsite?) (arrows) are also present in this core but in lesser abundance than in core #2.

F. A feldspar grain is covered by different authigenic minerals including albite overgrowths (Ab), analcime (An), zeolite (Z) and illite (arrows).

G. Solution and illitization of a K-feldspar overgrowth (KF) and the host feldspar grain (F). The contact between the overgrowth and the host grain also appears to be dissolving. Overgrowth surfaces are much rougher than those in Plate 6f. Minor amounts of smectite are present on the adjacent grain (arrows).

H. A higher magnification of the overgrowth observed in micrograph g. The intense solution pitting on the facing surface and the irregularity of the upper surface are evident.
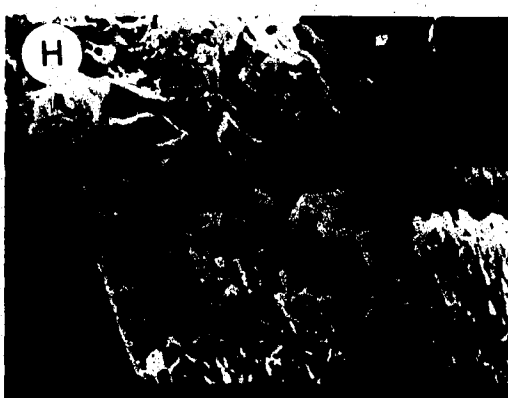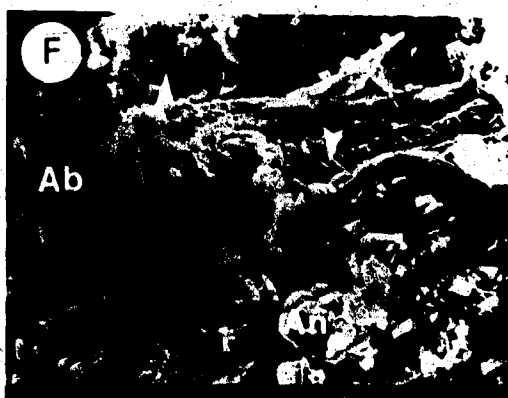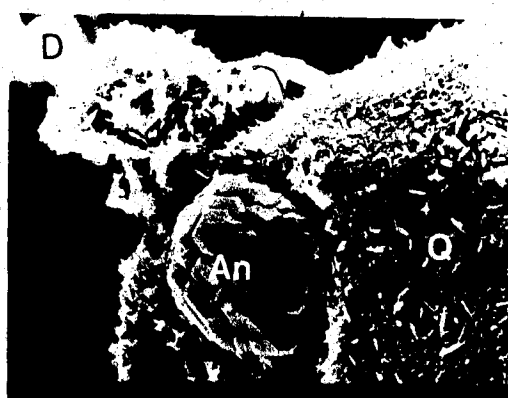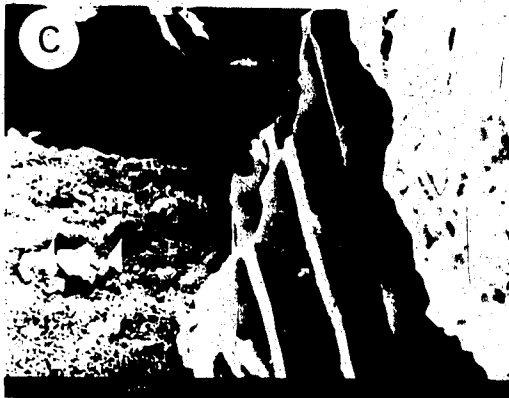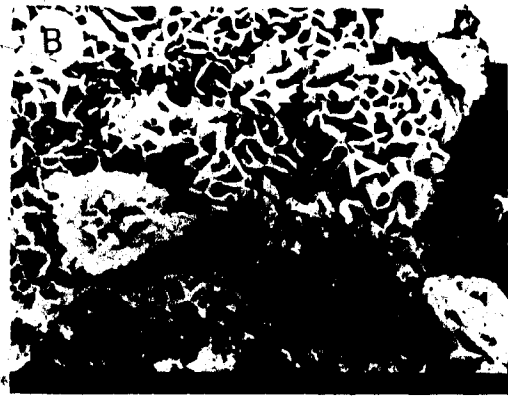
Plate 10. Scanning electron micrographs of post-flood core #4 sand. Bitumen removed from sand after the run using drops of toluene. Scale bars located below each micrograph.

A. General view of core #4 sand (sample 4.4) with similar scale as Plate 6c. The grains are coated more than the pre-flood sand. Bitumen and fines partially indurate a cluster of grains.

B. Smectite (Sm), with honeycomb structure, has developed in the bitumen saturated core. The bitumen (B) that remains in the pore space reflects the texture of the underlying authigenic clay. The average width of the individual smectite flakes is approximately 2 µm.

C. Analcime crystals (An) were most abundant in this core. Bitumen (B) covers these crystals in the northwest corner of the micrograph.

D. Bitumen covers analcime and lath-like zeolite (clinoptilolite?) crystals at a pore throat. These fines have migrated with the bitumen but have become lodged. As a result, the bitumen is retained at the pore throat thereby creating an even more effective pore seal by "cementing" the fines.

E. Dissolution of a K-feldspar overgrowth (KF) is illustrated by solution pitting (large arrows). Small analcime crystals (small arrows) have grown on the grain adjacent to the overgrowth.

F. Irregular texture of smectite (Sm) honeycomb fabric in contact with authigenic calcite (C). The smectite appears to partially cover the calcite.

G. Small authigenic quartz crystals (Q) on the surface of a volcanic rock fragment within a grain cavity. It is not apparent whether these crystals precipitated during diagenesis or during the core flood.

H. Analcime (An) acts as a cement, partially indurating a number of grains including quartz, volcanic rock fragments and feldspar. Smaller analcime crystals are visible on the framework grains including dolomite (D).
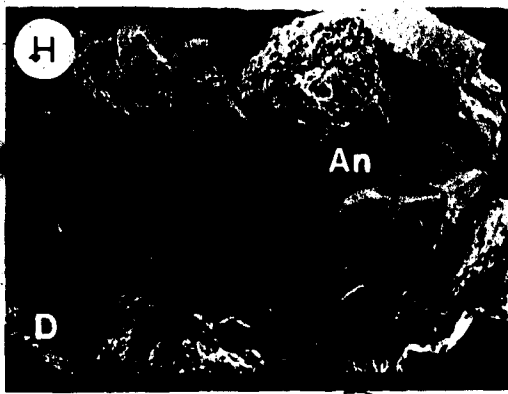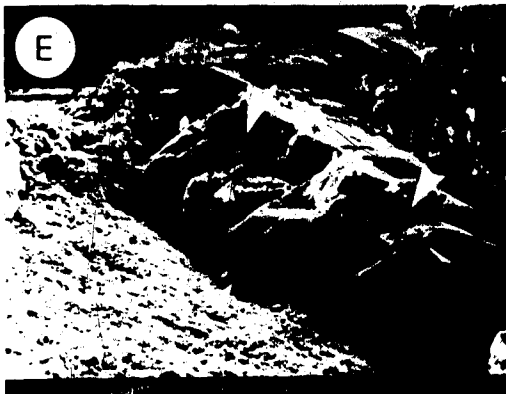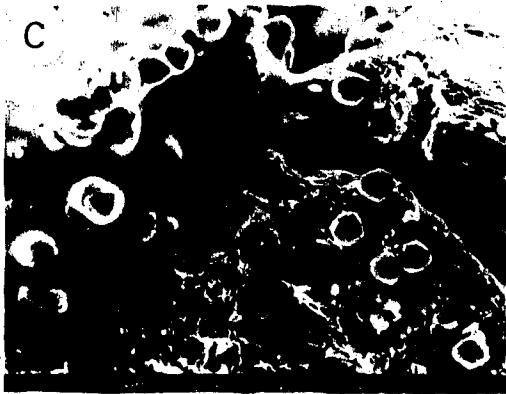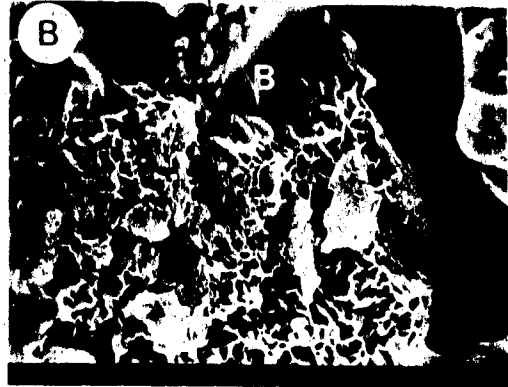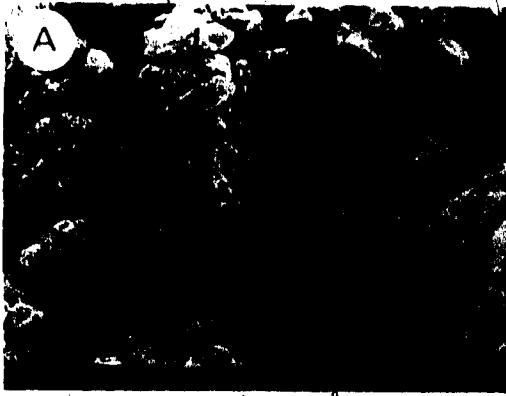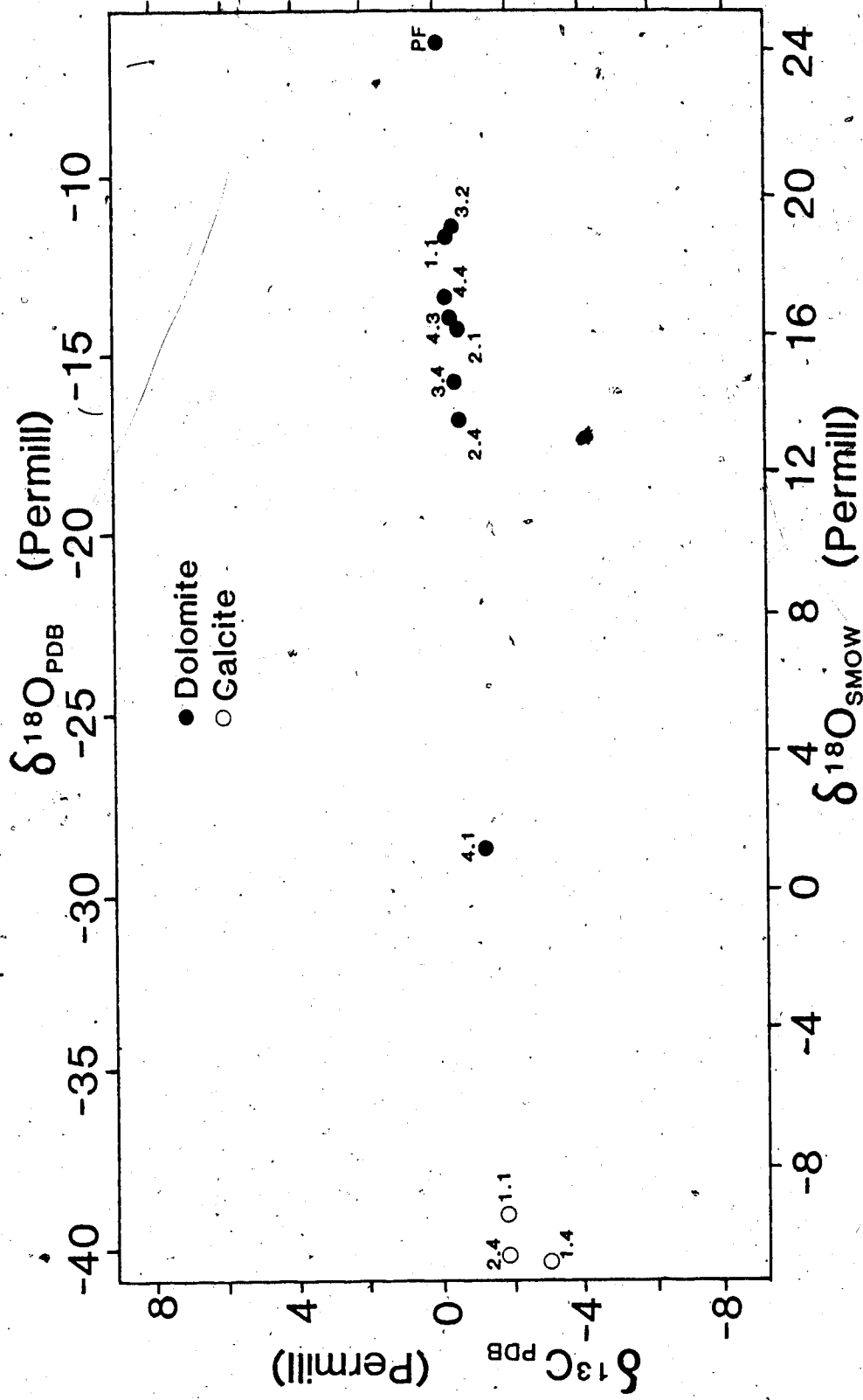
Figure 20. $\delta^{18}O_{SMOW}$ and $\delta^{18}O_{PDB}$ vs $\delta^{13}C_{PDB}$ for dolomite and calcite in selected samples.

D. Production Fluid Chemistry

The starting concentrations of CO_2, Ca, Si, and K in the injection fluids are 6.3, 0.4, 1.0, and 1.7 mg/kg, respectively. The production fluid analyses (Figures 21 to 24) of these species were not corrected for the starting concentrations because of the low initial values. Tables 2-7 to 2-10 in Appendix 2 contain the data that are illustrated in Figures 21 to 24.

Carbon Dioxide

The results of the Total Inorganic Carbon (TIC) analyses for run #1, #2 and #3 production fluids are illustrated in Figure 21. The curves represent the concentration measured in each sample plotted against the volume interval during which it was collected. The results for run #4 are not presented because of problems encountered preparing these fluids for TIC analysis.

The shape of the CO_2 concentration curves for the first three runs is similar. CO_2 concentration rose rapidly and reached a peak before 250 ml of fluid were injected through the cores. During run #1, the amount of CO_2 in solution decreased sharply from the peak value to a level between 1100 and 1300 mg/kg. CO_2 concentration decreased continuously from the peak values during runs #2 and #3 to values below 400 mg/kg. The highest recorded CO_2 concentrations for runs #1, #2 and #3 were 8625 mg/kg (Figure 21a), 10500 mg/kg (Figure 21b) and 15200 mg/kg (Figure 21c), respectively.
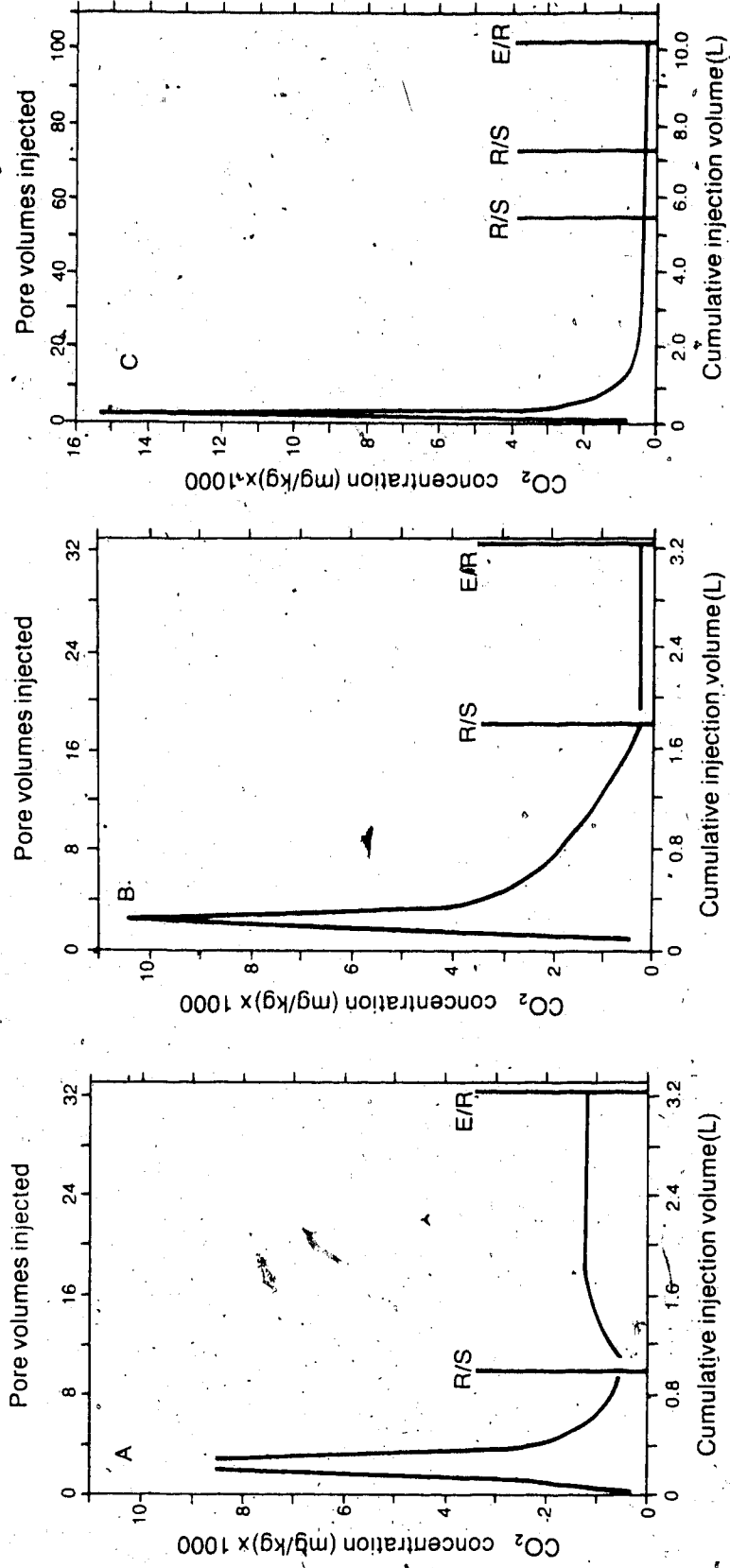
Figure 21. CO_2 concentration in effluents of (a) run #1. (b) run #2 and (c) run #3. R/S = forced shutdown and restart. E/R = end of run.
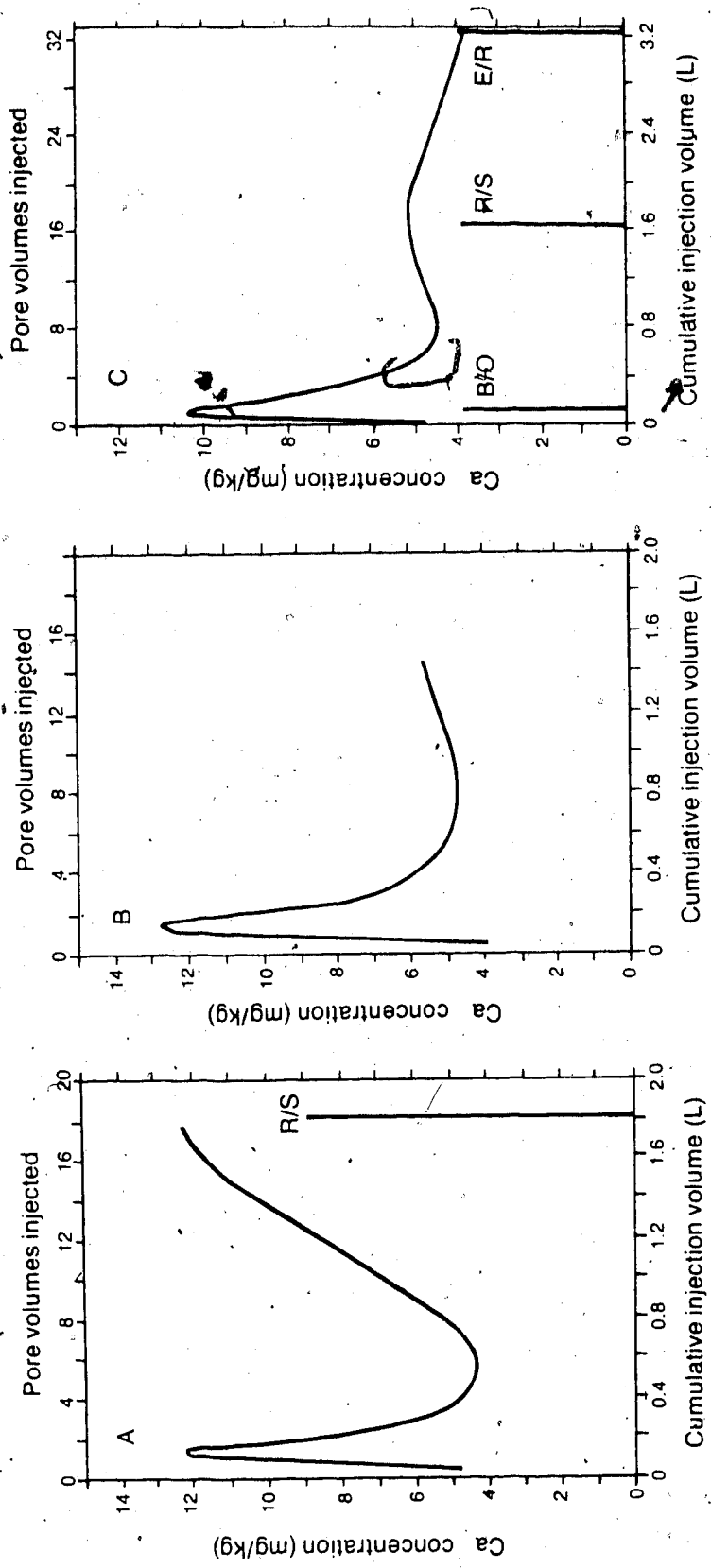
Figure 22. Calcium concentration in effluents of (a) run #2, (b) run #3 and (c) run #4. R/S = forced shutdown and restart. B/O = blow out. E/R = end of run.
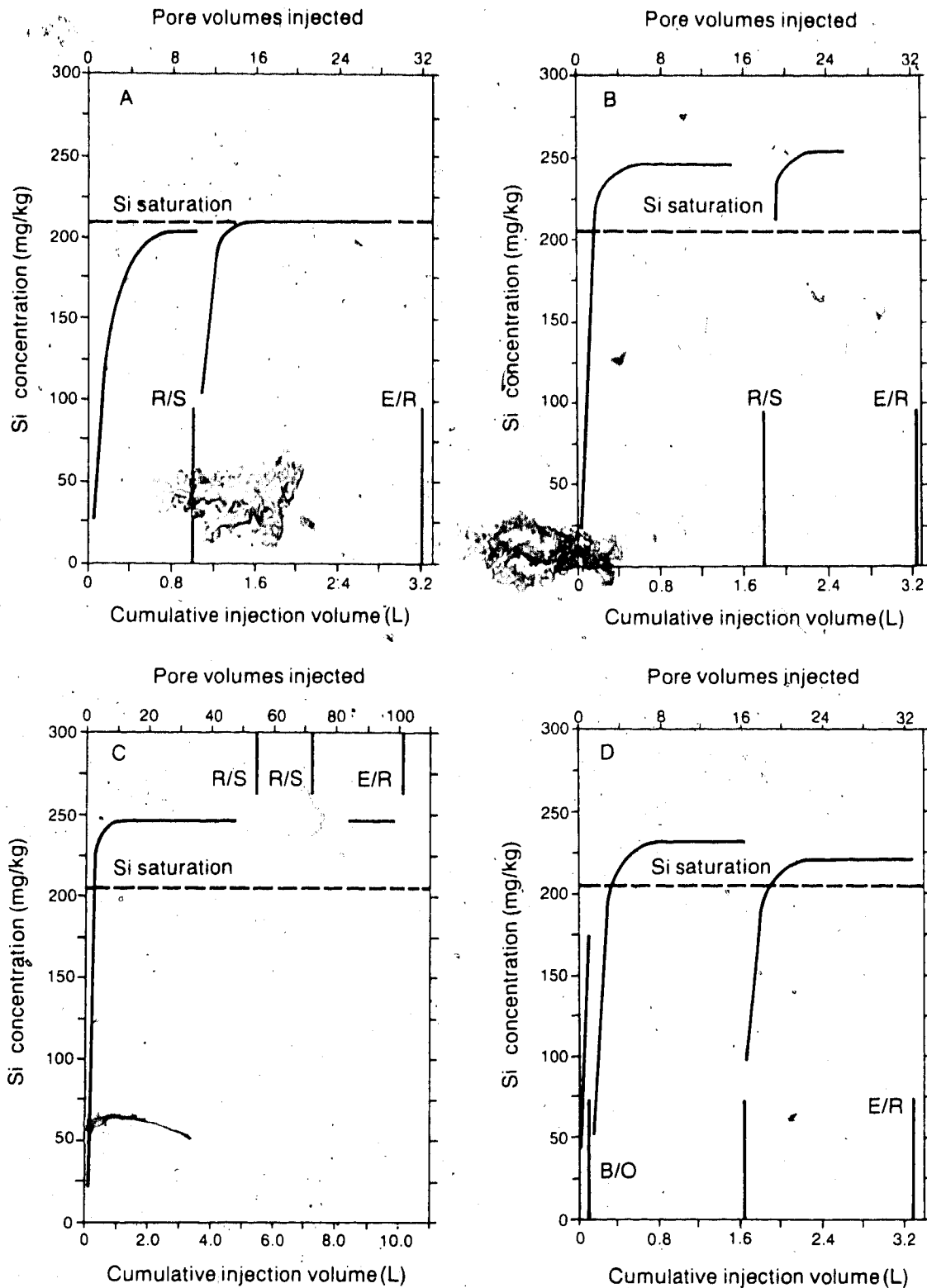
Figure 23. Silicon concentration in effluents of (a) run #1, (b) run #2. (c) run #3. and (d) run #4. Si saturation was determined using Figure 1 of Crerar and Anderson (1971) for neutral pH at 265°C. R/S = forced shutdown and restart. B/O = blow out. E/R = end of run.
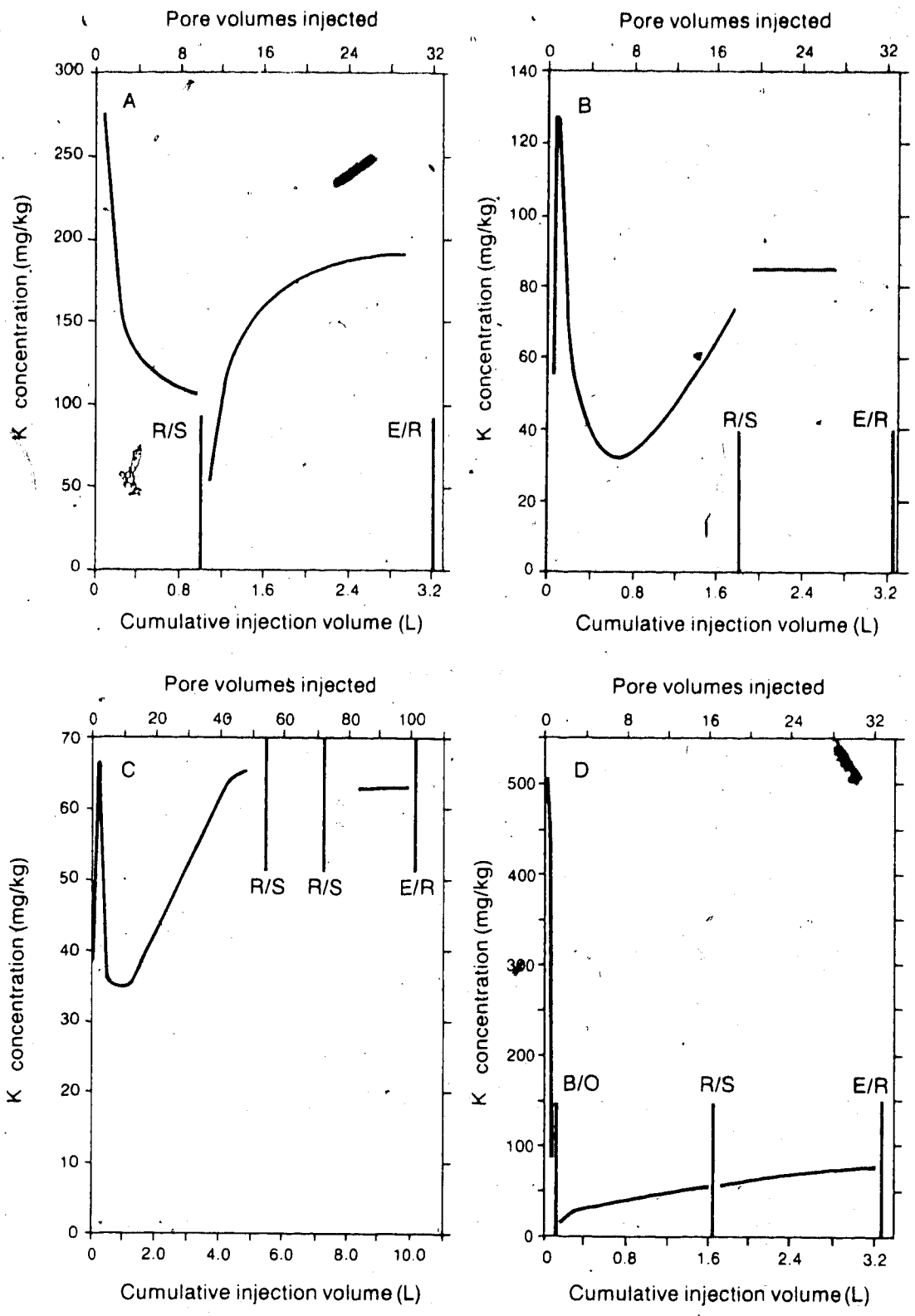
Figure 24. Potassium concentration in effluents of (a) run #1, (b) run #2, (c) run #3, and (d) run #4. R/S = forced shutdown and restart. B/O = blow out. E/R = end of run.

Calcium

The results for Ca, Si, and K concentrations in the production fluids are presented in the same format as the CO_2 results.

The results for run #1 are not presented because of measurement problems. The trends that developed in runs #2, #3 and #4 (Figure 22) were similar to each other. The initial maxima did not exceed 13 mg/kg and were reached before 0.2 l of fluid passed through the cores.

During run #2, the original maximum was followed by a decrease and a subsequent increase back to values approximately 12 mg/kg (Figure 22a).

Calcium concentration decreased rapidly after the initial high in runs #3 and #4 to values between 4 and 6 mg/kg (Figure 22b and c). These values were approximately stable for the duration of each run.

Silicon

In all four runs, Si concentration increased rapidly to levels that were constant for the duration of each run (Figure 23). The levels of constant Si concentration were highest for runs #2 (235-255 mg/kg) and #3 (245-250 mg/kg), followed by run #4 (230 mg/kg) and run #1 (205-215 mg/kg). Concentration values decreased below these levels only immediately after forced shutdowns.

Potassium

The rate of potassium concentration increase was greater than the other species studied. Potassium concentration was greatest at the onset of injection during runs #1 and #4, measured at 266 and 520 mg/kg, respectively (Figure 24). The amount of K in solution in the

production fluids of runs #2 and #3 increased to a maximum before 125 ml and 180 ml of injection fluid had been injected, respectively. The maximum concentration reached during run #2 was 124 mg/kg (Figure 24b) and during run #3 (Figure 24c) was 66 mg/kg.

After the initial highs, K concentration decreased rapidly during all four experiments to a minimum before gradually increasing to a relatively constant value of 190 mg/kg for run #1, 85 mg/kg for run #2, 63 mg/kg for run #3, and 75 mg/kg for run #4.

The pH of run #2 effluent was measured at two different injection volumes. The pH of run #3 and #4 effluent was measured once during the respective experiments. All measured values indicate that the effluent was acidic compared to injection fluid pH of 10.9 to 11.0 (Table 10).

E. Permeability Test Results

The permeability of the first three cores to injection fluid decreased during the course of the experiments (Figure 25). The permeability of core #4 was not determined because it was bitumen-saturated. The largest reduction occurred in core #2 where the permeability decreased 98%. The permeability of core #3 had decreased by 85% when it was measured about three-quarters through the run (see Appendix 1). The reduction in core #1 was 50%.

Table 10. Effluent pH of runs #2, #3 and #4 measured at different volumes of fluid injected.

Run #	Volume Injected (ml)	Effluent pH
2	820	5.3
2	3140	6.0
3	2945	5.3
4	2275	5.9
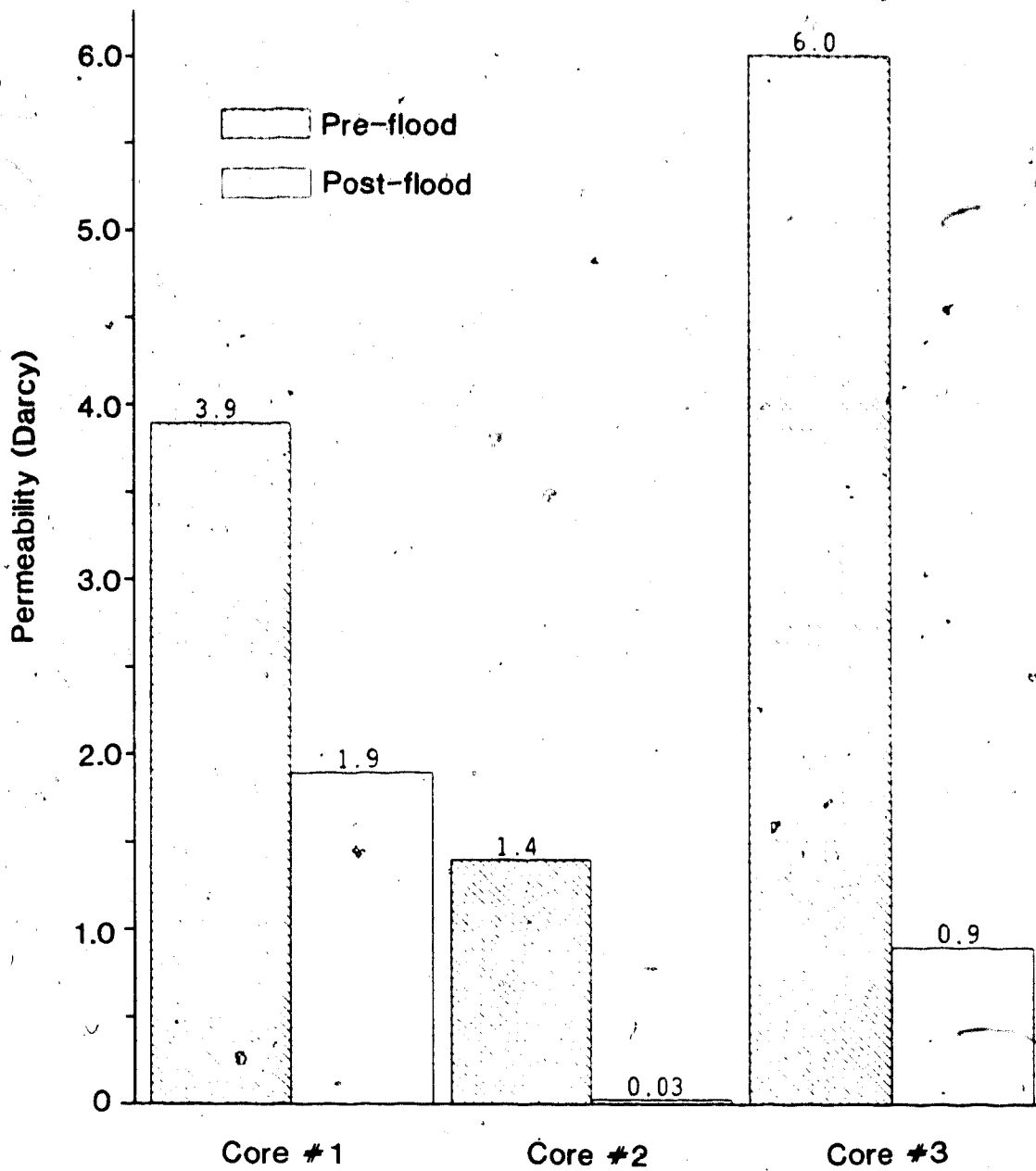
Figure 25. Pre- and post-flood permeabilities of cores #1, #2 and #3. The final permeability determination for core #3 was made after the second shut down (7274.1 ml). At this point 70% of the total volume of injection fluids had passed through the core. Values in darcys.

V. DISCUSSION

A. Mineral Reactions

Two observations indicate that dolomite dissolved during the experiments: (1) it is less abundant in the post-flood cores than in the pre-flood sand (Figure 14b) and (2) CO_2 was produced from the cores (Figure 21). Kaolinite is less abundant in the finer fractions of the post-flood cores relative to the pre-flood sand (Tables 8 and 9) indicating that it was dissolving. Two indirect observations suggest that quartz was dissolving: (1) silica saturation of the production fluids (Figure 23) and (2) pitted quartz surfaces (Plate 9).

Three different observations indicate that smectite and calcite formed during the experiments. First, the two minerals are more abundant in the post-flood cores than in the pre-flood sand (Figure 14). Second, both minerals have authigenic morphologies and occur in pore spaces (Plates 8b and 5c).

The third line of evidence indicating that calcite formed during the experiments involves isotope data. Friedman and O'Neil (1977) related the oxygen-isotope values of calcite and its crystallization fluid to temperature (T) by:

$$10^3 \ln\alpha_{A-B} = (2.78)10^6 T^{-2} - 2.89, \qquad (8)$$

where α_{A-B} is the oxygen-isotope equilibrium fractionation factor between calcite and water and T is expressed in $^\circ K$. The value of α_{A-B} is defined by:

$$\alpha_{A-B} = \frac{1000 + \delta_A}{1000 + \delta_B} \qquad (9).$$

The $\delta^{18}O_{SMOW}$ value of the water distilled to make the injection fluids is -17.0 (F.J. Longstaffe, personal communication). When the α_{A-B} value calculated based on that water value is used in equation 8, calculated temperatures of formation for calcite range between 240° and $275^\circ C$. This range corresponds to the experimental temperatures. The ranges of the $\delta^{13}C_{PDB}$ values for dolomite and calcite are close indicating that dolomite was the most probable source of carbonate for calcite.

Based on studies involving pure mineral mixtures, Levinson and Vian (1966) and Bayliss and Levinson (1971) postulated (unbalanced) reactions (1) and (10), respectively.

$$\text{dolomite + quartz + kaolinite + } H_2O =$$
$$\text{Ca+Mg-smectite + calcite + } CO_2 \qquad (1).$$
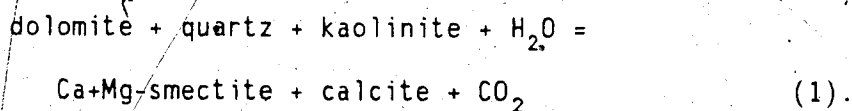
Calcite can then react in place of dolomite to yield:

$$\text{calcite + quartz + kaolinite =}$$
$$\text{Ca-smectite + } CO_2 + H_2O \qquad (10).$$
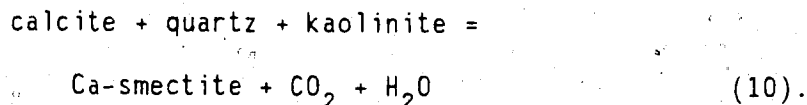
The Sedimentology Research Group (1981) proposed reaction (11) as the mechanism for smectite formation during a steam flood. The source of Na^+ was the injection fluids.

$$Na^+ + quartz + kaolinite =$$

$$Na\text{-smectite} + H_2O + H^+ \qquad (11).$$
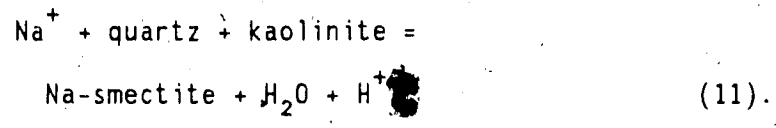
The balanced versions of these three reactions are given in Chapter 2.

The smectite produced during the experiments of this study was identified as dioctahedral. For the purpose of the following discussion, smectite composition is described as either beidellite (dioctahedral smectite with substitution in the tetrahedral layer) or montmorillonite (dioctahedral smectite with substitution in the octahedral layer).

Reactions (1), (10) and (11) were written in terms of simple smectite compositions, i.e., only one type of interlayer cation. It was determined using EDS that Na < Ca < Mg in the smectites produced during this study. Beidellite with Na:Ca:Mg = 1:1:2.5 would be formed by:

$$2.5MgCa(CO_3)_2 + 32H_4SiO_4 + 28Al_2Si_2O_5(OH)_4 + Na^+ =$$

$$\quad dolomite \qquad quartz \qquad kaolinite$$

$$24Na_{1/24}Ca_{1/24}Mg_{5/48}Al_{7/3}Si_{11/3}O_{10}(OH)_2 + 1.5CaCO_3 +$$

$$\quad\quad smectite \qquad\qquad\qquad calcite$$

$$3.5CO_2 + 95.5H_2O + H^+ \qquad (12).$$
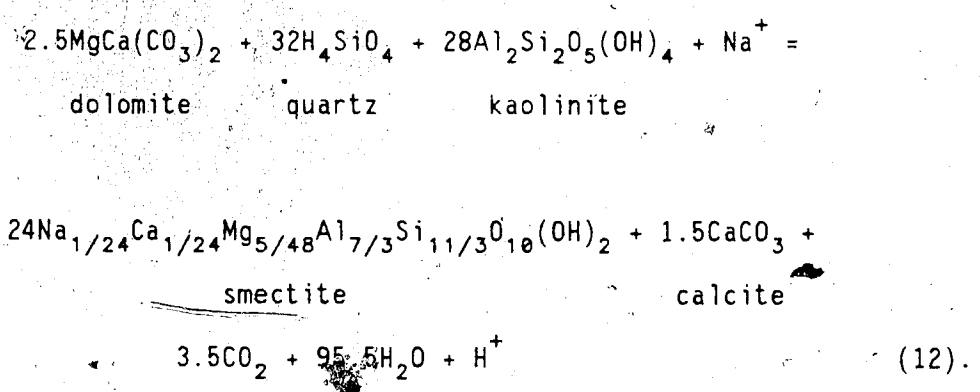
Montmorillonite with Na:Ca:Mg = 0.67:1:2.67 would be formed by:

$$4MgCa(CO_3)_2 + 28H_4SiO_4 + 10Al_2Si_2O_5(OH)_4 + Na^+ =$$

$$\quad dolomite \qquad quartz \qquad kaolinite$$

$$12Na_{1/12}Ca_{1/8}(Al_{5/3}Mg_{1/3})Si_4O_{10}(OH)_2 + 2.5CaCO_3 +$$

<div align="center">smectite   calcite</div>

$$5.5CO_2 + 63.5H_2O + H^+ \qquad\qquad (13).$$
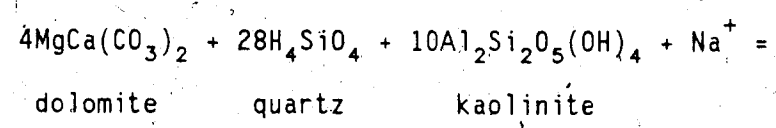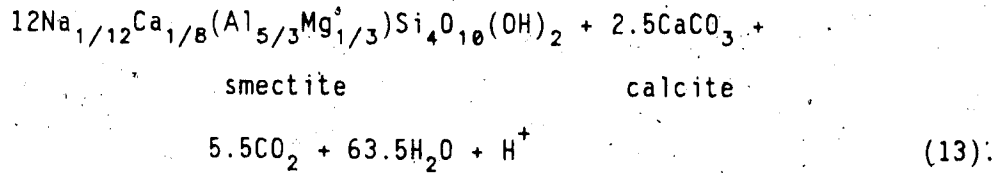
While reactions (12) and (13) are written in the form of solid to solid transformations, it is more likely that the mechanism is solution and reprecipitation (G. Bird, personal communication). Reaction (12) can be written as the sum of six reactions: three dissolution, two precipitation and one gas evolution. The reactions can be described as:

$$MgCa(CO_3)_2 = Mg^{2+} + Ca^{2+} + 2CO_3^{2-} \qquad\qquad (14),$$

$$Al_2Si_2O_5(OH)_4 + 5H_2O = 2H_4SiO_4 + 2Al(OH)_3 \qquad (15),$$

$$SiO_2 + 2H_2O = H_4SiO_4 \qquad\qquad (16),$$

$$Ca^{2+} + CO_3^{2-} = CaCO_3 \qquad\qquad (17),$$

$$1/8Na^+ + 1/8Ca^{2+} + 5/16Mg^{2+} + 7Al(OH)_3 + 11H_4SiO_4 =$$

$$3Na_{1/24}Ca_{1/24}Mg_{5/48}Al_{7/3}Si_{11/3}O_{10}(OH)_2 + 28.5H_2O + H^+ \qquad (18),$$

and $$CO_3^{2-} + 2H^+ = H_2CO_3 = H_2O + CO_2 \qquad\qquad (19).$$
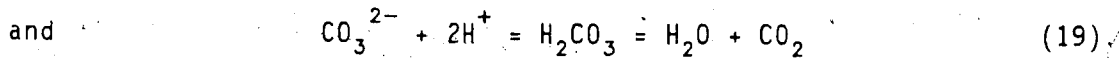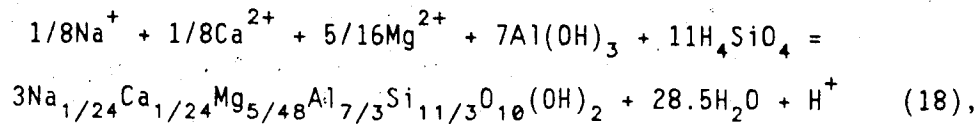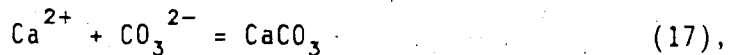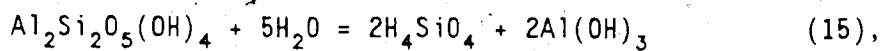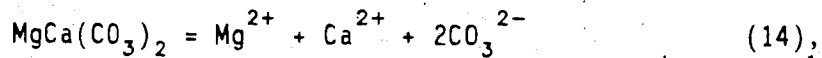
The carbon isotope values indicated that dolomite is the most likely source of carbon for calcite. Therefore, the carbonate ion of the product side of reaction 14 and the carbonate ion of the reactant

side of reaction 17 are the same. Since dolomite is the source of carbonate for calcite, it is also likely that it is the source of carbon for CO_2. The rapid evolution of CO_2 from the cores (Figure 21) indicates that dolomite dissolved quickly. It also appears that quartz dissolved quickly because silica concentration in the effluents rose to saturation levels before eight pore volumes (40 hours elapsed time) were passed through the cores.

B. Influent pH Effects

Carbonate solubilities decrease with increasing pH (Drever, 1982). This relationship accounts for a number of observations: CO_2 (wt%), dolomite, and calcite cement abundances are lowest in core #1 at the end of the run (Tables 7 and 6). Furthermore, the stable CO_2 concentration levels and Ca concentration are higher in the effluent of run #1 than in the effluents of the other runs (Figures 21 and 22). The injection fluid used in run #1 had the lowest pH (Table 3) resulting in more carbonate dissolution and the release of more CO_2 and Ca to solution than during the other runs.

Quartz solubility increases with pH (Busey and Mesmer, 1977). Silica concentration was higher in the effluents of runs #2, #3 and #4 than run #1 (Figure 23) because the injection fluid pH was higher. The relationship between higher injection fluid pH and higher Si saturation in effluents was observed by Reed (1979), McCorriston et al. (1981), Sydansk (1982), and Boon et al. (1983).

The effluents of runs #2, #3 and #4 became oversaturated with silica because the pH of the fluid decreased as it passed through the core. The effluent pH had dropped to between 5.5 and 6.0 before four

pore volumes of fluid were injected (Table 10). However, the dissolved silica levels did not decrease to quartz saturation. Bird and Boon (1985) showed that quartz dissolution follows a zero-order rate law and quartz precipitation follows a first-order rate law so that the reaction:

$$SiO_2 + 2H_2O \rightarrow H_4SiO_4 \tag{20}$$
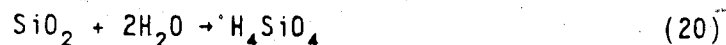
proceeds more rapidly than the reaction:

$$H_4SiO_4 \rightarrow SiO_2 + 2H_2O \tag{21}.$$

If the cores were longer or the residence time of the fluids were increased, then the precipitation kinetics would reduce the silica levels to quartz saturation. However, it is beyond the scope of this study to determine how long a core would have to be for silica precipitation to reach equilibrium.

Silica solubilities were equal in the effluents of runs #2 and #3 even though the fluids passed through core #3 four times faster (Reed (1979) made similar observations). Silica saturation was reached within five hours (residence time for the fluids in core #3) indicating that quartz dissolves rapidly at $265^{\circ}C$ and pH 11.

The silica saturation level also had an effect on the smectite-forming reactions. As quartz is dissolved (along with kaolinite and dolomite), reactions (12) and (13) proceed to the right. With higher silica saturation levels in higher pH solutions (Figure 23), reactions (12) and (13) proceed further to the right. This mechanism may account for the higher abundances of smectite and calcite and lower abundance of kaolinite in cores #2 and #3 compared to core #1 (Figure 14 and Table 8).

The observation that phillipsite was rare in core #1 (Plate 7) but common on the volcanic rock fragments of core #2 (plate 8f) can be attributed to higher pH conditions in run #2 since phillipsite is a product of the diagenesis of volcanogenic sandstones by basic fluids (Hay, 1966; Sheppard and Gude, 1968; and Hay and Sheppard, 1977). The mineral is less common in the production half of core #2 than in the injection half because pH decreased as the fluids passed through the core (effluent pH was between 5.5 and 6.0).

Potassium concentration in the effluent from each core reached a roughly stable level after approximately 16 pore volumes of fluid were injected (40 pore volumes for run #3; Figure 24). The K^+ levels at the end of runs #2, #3 and #4 were approximately 50% of the level reached during run #1. The higher K^+ concentration in run #1 effluent can be attributed to two factors. First, the stability of K-feldspar increases with pH (Helgeson et al., 1969). As K-feldspar dissolves, K^+ is released to solution. An increase in K-feldspar dissolution caused by lower pH results in higher K^+ concentrations. Secondly, K^+ that enters smectite interlayer positions is not carried from the core with the effluent. There is more smectite in cores #2 and #3 (Figures 16 and 18) and, therefore, more sites for K^+ to enter.

Three mineralogical trends in core #2 that indicate compositional changes of the injection fluid as it passed through the core are: (1) kaolinite abundance in the <2 μm fraction increases along the injection path of the core (Table 8); (2) smectite, in the <2 and 2-5 μm fractions, is more abundant in the inner two portions than in the outer two portions of the core (Figures 16 and 18); and (3) calcite abundance increases from the first to second quarter and then decreases through

the rest of the core (Figure 14c). When the hot caustic solution entered the core, it was undersaturated with silica, dolomite and kaolinite and therefore these minerals dissolved. As the fluids passed along the core, they became supersaturated with smectite and calcite which precipitated. By the time these two minerals crystallized, the injection fluids had reached the inner portion of the core. The smectite-producing reaction, such as reaction (12), was closer to equilibrium in the inner portions of the core resulting in less dissolution of reactant minerals as shown by the increase in kaolinite content. The decreased rate of dissolution as the fluids passed through the core resulted in a decreased rate of precipitation at the production end of the core as shown by lesser abundances of smectite and calcite in the production quarter relative to the inner quarters. By the time it had reached the production quarter of core #2, the composition of the injection fluid had become similar to the injection fluid used in run #1 (i.e., less reactive because the caustic was consumed).

C. Flow Rate Effects

The injection (flow) rate of run #3 was four times greater than run #2 (Table 3). Therefore, the time that the fluids were in core #3 and in contact with the grains was four times less than in core #2.

Kaolinite is less abundant in the <2 μm fraction of core #3 than in the other cores (Table 8) and the surfaces of quartz grains appear more pitted in core #3 (Plate 9) than in core #2.

Smectite is more abundant in core #3 than in any other core (Figures 16, 18 and 19) indicating that smectite-producing reactions occurred to the greatest extent in core #3. As a result, core #3 has

the greatest amount of material <20 μm (Figure 11). The greater abundance of smectite in core #3 resulted because 6.9 1 (57.6 PV) more fluid passed through it than core #2 (Table 3).

Albite overgrowths were observed in core #3 (Plate 9) but not in core #2. Injection fluids in core #3 travelled through a greater distance of the core before approaching equilibrium because the higher flow rate used in run #3 resulted in less contact time between the injection fluids and the core materials. This effectively extended the portion of core #3 that was at high enough pH for albite to form (Figure 26). The Sedimentology Research Group (1981) showed that albite is stable relative to smectite at elevated temperatures (>200°C) and pH. Boon et al. (1983) however, did not observe the formation of albite which they attributed to kinetic factors. The temperatures during run #3 (265°C) were greater than the temperatures of the experiments of Boon et al. (1983) which may account for the crystallization of albite during this study. However, Boon et al. (1983) relied on XRD, not SEM, to determine if albite had formed. Small amounts of albite growth, as observed in this study, could not normally be detected using XRD.

Phillipsite was observed in much greater abundance in core #2 than in core #3 suggesting that the kinetics of phillipsite crystallization are slow relative to run #3 residence time (5.7 hours) or the linear velocity of the fluids (4 cm/h[1]).

----

[1]$V = \frac{\text{injection rate}}{\text{effective area}}$ where effective area $= \frac{\text{cross-section area of core}}{\text{porosity} \div 100}$
and V = velocity. $V = (20 \text{ cm}^3/h)/(18.3 \text{ cm}^2 \cdot 0.27) = 4 \text{ cm/h}$.
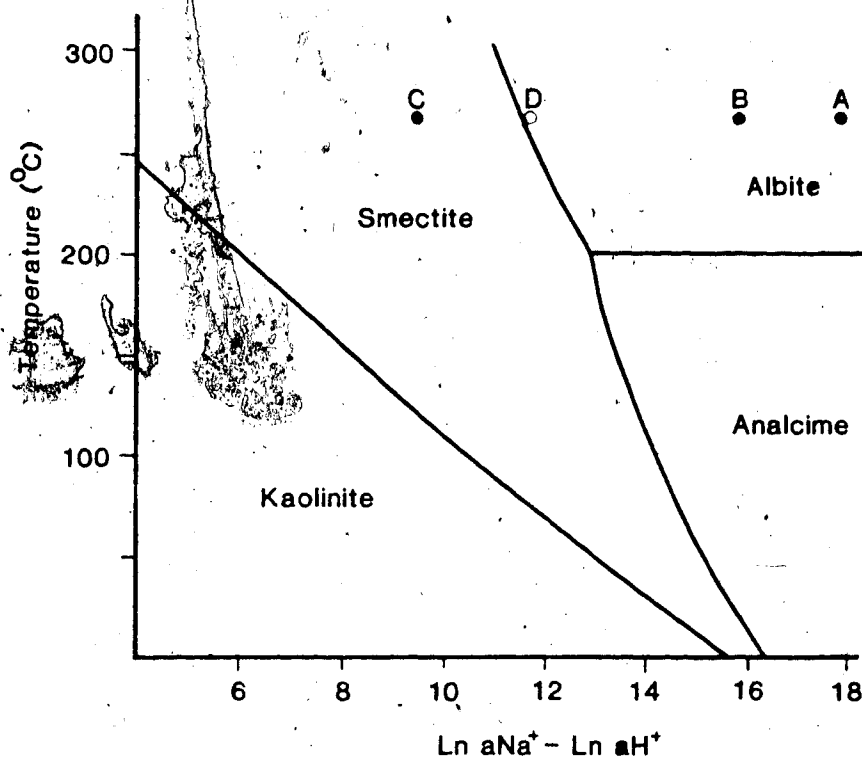
Figure 26. Phase relationships as a function of temperature relative to
the natural logarithm of the ratio of the activities of Na^+ to H^+.
Fluid pressure (H_2O) is 2MPa. Smectite has a Ca:Na ratio 1:1 and quartz
is present. As the pH of the injection fluid in runs #2 and #3
decreases by interaction with the core, the fluid composition moves
from A (pH=11), through B (pH=8.5) to C (pH=5.7 measured in effluent).
Point D represents the composition of the injection fluid used in run
#1 (pH=6.3). Modified after the Sedimentology Research Group (1981).

Boon et al. (1983) maintained that a higher injection rate decreases hydrothermal alteration because of lower residence times for the fluids. The stable level of potassium concentration was lowest in the effluent of the core subjected to the highest flow rate (core #3; Figure 24) because less K-feldspar (and illite?) was dissolving per unit volume of injection fluid.

The interactions that occurred along core #3 were similar to the interactions that occurred along core #2 except they were modified by the higher flow rate. The observations that:

(1) smectite abundance is high and kaolinite abundance is low in the <2 μm fraction throughout core #3 (Figure 16 and Table 8); and

(2) smectite abundance in the 2-5 μm fraction increases to the third quarter and then decreases in the production quarter (Figure 18); and

(3) calcite abundance increases to the third quarter and then decreases in the production quarter (Table 6)

indicate that equilibrium between core minerals and fluids was reached at greater distances travelled through core #3 than through core #2.

D. Bitumen Effects

The difference between runs #2 and #4 is that core #2 was packed with bitumen-free sand and core #4 was packed with bitumen-saturated sand (Table 3). Therefore, the presence of bitumen was responsible for the observed differences in post-flood core mineralogy and effluent chemistry between these two runs.

The overall smectite content of core #4 is lower and the kaolinite content in the <2 μm fraction is higher than in any other core (Tables 6 and 8) indicating that smectite-producing reactions occurred to the least extent in core #4.   Overall, core #4 has the least amount of material less than 20 μm (Figure 11) and the least developed rims on the framework grains.

The observation that CO_2 weight percent is greatest in core #4 (Figure 15) is further evidence of the lack of reactivity in the bitumen-saturated core. Petrography indicated that core #4 had the highest abundance of carbonate (dolomite) grains but the lowest abundance of calcite cement.   Boon et al. (1983) also observed a decrease in dolomite dissolution with bitumen present at 200°C.

Silica concentration in the effluent of run #4 (230 mg/kg) is lower than in run #2 (240 mg/kg) but higher than in run #1 (210 mg/kg; Figure 23) indicating that bitumen decreases the dissolution rate of quartz less than does a decrease of 4 pH units. Boon (1977) also observed a decrease in silica concentration with bitumen present.

The stable level of K^+ concentration is lower in the effluent of run #4 than in run #2 (Figure 24) indicating that bitumen decreases the solubility of K-feldspar.

The bitumen in core #4 limited the smectite-producing reactions relative to the bitumen-free cores. The amounts of dolomite and kaolinite are high in this core relative to the other cores (Tables 6 and 8). The greatest amount of smectite in the 2-5 and 5-20 μm fractions occurs in the injection quarter (Figures 18 and 19) indicating that, due to the reduction of reactivity between the core and fluids by bitumen "armouring", the reaction front (point of most intense authigenic

mineral precipitation) was confined to the entrance point of the fluids into the core. The low $\delta^{18}O_{SMOW}$ value of dolomite in sample 4.1 (Figure 20) indicates that dolomite in the injection portion of core #4 underwent isotopic exchange with the fluids to a much greater extent than did dolomite in the rest of the core.

'E. Effluent Chemistry

Potassium Concentrations

The high initial values of potassium concentration (Figure 24) are attributed to flushing of drilling fluid residue which apparently was completed after 300 ml (three pore volumes) of fluid injected. The bitumen-saturated core had the highest initial K^+ concentration because some of the contamination was removed from the bitumen-free cores by toluene extraction and permeability tests prior to their respective runs.

pH

Effluent pH was less than influent pH (Table 10) indicating that the pH of the injection fluids decreased as they passed through the cores. A number of mineral equilibria contribute to the reduction in pH by either consuming OH^- or producing H^+. One type of equilibria is the smectite-producing reaction (reaction 12 or 13) since H^+ is produced. Quartz solution lowers pH (Boon et al., 1983) by:

$$SiO_2 + 2H_2O = H_4SiO_4 \qquad\qquad (16)$$

$$H_4SiO_4 = H_3SiO_4^- + H^+ \qquad\qquad (22)$$

$$H_3SiO_4^- = H_2SiO_4^{2-} + H^+ \qquad\qquad (23).$$

The pH is also lowered by the production of CO_2.

F. Permeability Reduction

Laboratory studies in the past have indicated the potential for permeability loss when hot fluids come into contact with a formation (Boon, 1977; Perry and Gillott, 1979; Reed, 1979; Boon and Hitchon, 1983b). McCorriston et al. (1981) and Boon et al. (1983) measured permeability decreases in packed cores under laboratory core flood conditions and attributed them to fines dispersion. The Sedimentology Research Group (1981) completed a field study on the effects of steam flooding the Clearwater Formation and came to the conclusion that the process was responsible for a decrease in permeability of the reservoir.

One of the main factors in permeability decrease during a steam flood is the production of smectite (McCorriston et al., 1981; Sedimentology Research Group, 1981; Boon et al., 1983). Smectite, when fully hydrated, can decrease permeability fifty-fold (Waldorf, 1965).

The largest permeability reduction occurred in the cores that had the greatest increase in smectite content. Cores #2 and #3 had permeability decreases of 98% and 85% respectively (Figure 25). Smectite grew as pore-lining material in these cores by reaction of dolomite,

quartz and kaolinite. Smectite size increased in the post flood samples since smectite abundance increased in the 2-5 μm and 5-20 μm fractions and decreased in the <2 μm fraction (Figures 18, 19 and 16, respectively). The honeycomb morphology of this authigenic mineral creates a microporosity network that reduces permeability by constricting flow. The fabric is also responsible for retention of bitumen in the pores (Sedimentology Research Group, 1981).

As smectite hydrates, it occupies more pore volume, further reducing effective pore space. Osmotic swelling increases inversely with the square root of salt concentration (MacEwan and Wilson, 1980). The lower salt concentration of the injection fluid used in runs #2 and #3 compared to run #1 could have caused an increase in osmotic swelling (Figure 27), thereby contributing to greater permeability reduction.

Migration of fines and subsequent pore-throat clogging (Plates 7e and 8e) causes permeability reduction (Muecke, 1979; Sedimentology Research Group, 1981). Boon et al. (1983) observed fines dispersion in their flow experiment.

Phillipsite developed to the greatest extent in core #2 (Plate 8). The rod-like shape of this mineral appears fragile (Plate 8f), allowing for it to be dislodged from host volcanic fragments and accumulate at pore throats (Plate 8e). This mechanism may partially account for the large permeability reduction observed in core #2 (Figure 25).

The permeability of core #4 was not measured before nor after the experiment because permeabilities of bitumen-free and bitumen-saturated cores cannot be compared. However, a number of observations were made in core #4 that are associated with permeability reduction in the other cores including: the development of authigenic smectite with its
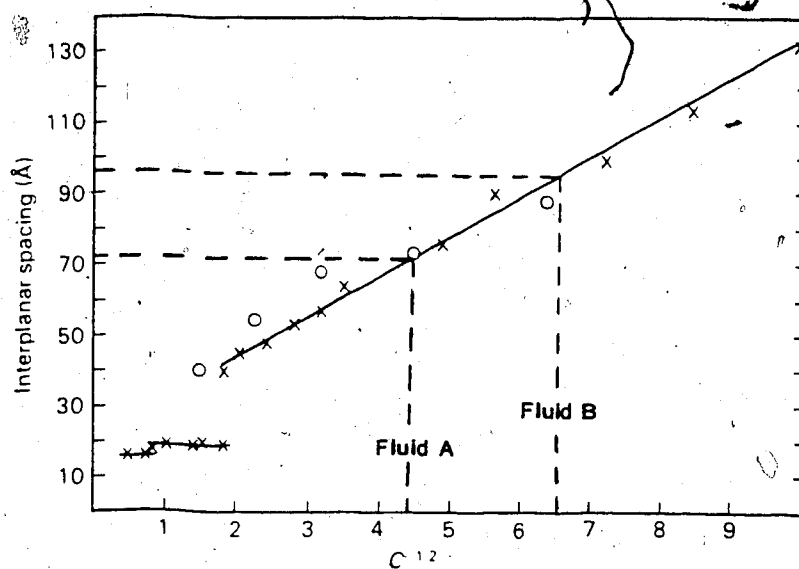
Figure 27. The mean interlayer spacing of montmorillonite increases with the reciprocal of the square root of NaCl concentration $(C^{-1/2})$. $C^{1/2}$ for injection fluid A (run #1) and fluid B (runs #2, #3 and #4) are 4.4 and 6.5 respectively. The lower salt concentration of the latter fluid is responsible for increased montmorillonite swelling (modified after MacEwan and Wilson, 1980). x = NaCl solutions. o = Na_2SO_4 solutions.

honeycomb fabric (Plate 10b); and migration of fines (Plate 10d). The same injection fluid was used in runs #2, #3 and #4 (Table 3), thus the potential for increased osmotic swelling exists (Figure 27).

Boon (1977) maintained that the precipitation of quartz as fluids (saturated with silica) move away from the point of injection to lower temperature areas of the reservoir may result in permeability reduction. This mechanism was not observed during the core floods because isothermal conditions prevailed. However, its potential for permeability reduction is considered minimal. The most silica was transported out of core #3, but the total (5.3 g[1]) was only 0.7% of the total core weight (794 g).

There is a possibility that part of the permeability decrease was a result of experimental procedure. The initial permeabilities of cores #1, #2 and #3 were 3.9, 1.4 and 6.0 Darcy, respectively. Permeability reduction was highest in the core with the lowest initial permeability. However, the variation in initial permeabilities is not considered a major factor because the initial permeability of core #3 was 1.5 times the initial permeability of core #1 yet the final permeability of core #3 was lower.

G. Comparison to Diagenetic Environments

Steam flooding accelerates and alters the diagenesis of a reservoir (Hitchon, 1977) and can be related to the diagenesis of volcanogenic sandstones and to the shallow diagenesis of volcanics by highly alkaline and saline groundwaters.

-----

[1] 0.245 g/kg Si saturation = 0.525 g/kg SiO_2 saturation
$(0.525$ g/l$)(10.1$ l injection volume$)$ = 5.3 g SiO_2 removed from core #3.

Galloway (1979) observed four stages of progressive diagenesis of arc-derived sandstones. The first two stages occurred during the experiments of this study: (1) the formation of pore-filling calcite; and (2) the development of clay (montmorillonite or chlorite) rims. Stages (3) and (4) (further cementation of and replacement of framework grains) did not occur because of the short duration of the experiments relative to burial diagenesis. Stage (1) may be transient during the core floods because calcite produced may be consumed with excess kaolinite and quartz to produce a Ca-rich smectite as in reaction (3).

The diagenesis of volcanoclastic sedimentary rocks is compared to the core floods because the Clearwater Formation contains up to 23% volcanic rock fragments (Table 5). Phillipsite, and other zeolites and feldspars, form rather than clay minerals because of high alkali ion to H^+ ratios (Sheppard and Gude, 1968) and low magnesium activity (Hay, 1966). Phillipsite formed in the injection half of core #2 and not in the production half because solution pH decreased as the fluids passed through the core, thereby decreasing the alkali-ion:H^+ ratio. The lack of phillipsite in the production half of the core was not caused by an increase in magnesium activity since magnesium concentration was measured at low values (<0.2 mg/kg) throughout the run.

VI. SUMMARY AND CONCLUSIONS

Four flow experiments using steam condensate were completed at elevated temperature ($265°C$) and pressures (6.2-8.3 MPa) in an auto-clave laboratory on material from the Clearwater Formation of the Cold Lake oil sands. Four parameters were varied in order to determine their effect on mineralogical reactions: pH of injection fluids (6.3 or 11); salinity of injection fluids (1400 or 3000 mg/kg NaCl); injection rate (1.2 or 4.8 pore volumes per day); and bitumen present or absent in the prepared cores.

All four experiments resulted in the following changes to the cores:

(1) a decrease in grain size;

(2) a decrease in dolomite abundance;

(3) a decrease in kaolinite abundance in the finer fractions;

(4) evolution of CO_2 from the cores;

(5) precipitation of smectite rims on framework grains.

(6) precipitation of calcite in the pores spaces; and

(7) a reduction in permeability

Furthermore, the effluent from each core was supersaturated with silica.

Based on the above observations and the low $\delta^{18}O$ values of calcite, two mass balance equations are proposed for the mineral reactions that occurred during the core floods:

$$2.5MgCa(CO_3)_2 + 32H_4SiO_4 + 28Al_2Si_2O_5(OH)_4 + Na^+ \rightarrow$$

dolomite   quartz   kaolinite

112

$$24Na_{1/24}Ca_{1/24}Mg_{5/48}Al_{7/3}Si_{11/3}O_{10}(OH)_2 + 1.5CaCO_3 +$$

beidellite   calcite

$$3.5CO_2 + 95.5H_2O + H^+$$

and/or

$$4MgCa(CO_3)_2 + 28H_4SiO_4 + 10Al_2Si_2O_5(OH)_4 + Na^+ \rightarrow$$

dolomite   quartz   kaolinite

$$12Na_{1/12}Ca_{1/8}(Al_{5/3}Mg_{1/3})Si_4O_{10}(OH)_2 + 2.5CaCO_3 +$$

montmorillonite   calcite

$$5.5CO_2 + 63.5H_2O + H^+.$$
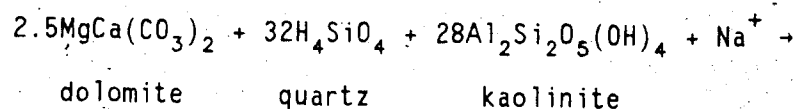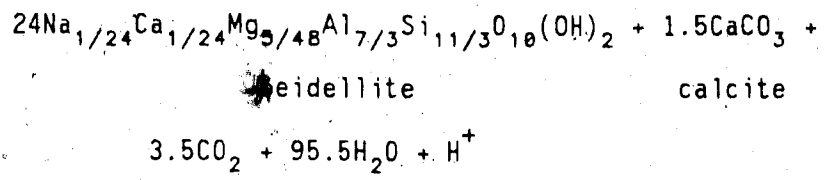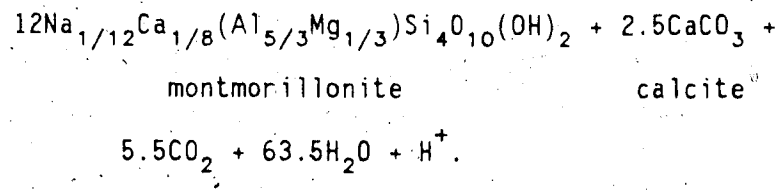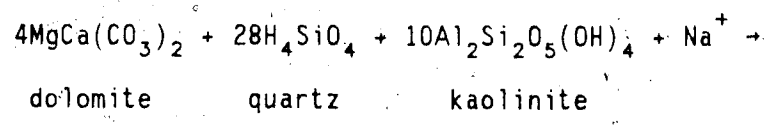
High initial CO_2 and Si concentrations in effluent suggest that the dissolution kinetics are rapid.

The pH of the injection fluid had the greatest effect on the smectite-producing reactions; high pH injection fluids resulted in greater dissolution of quartz and precipitation of smectite and calcite. The presence of bitumen decreased the extent to which the reactions occurred by armouring the grains. Higher flow rates resulted in greater volumes of fluids passing-through a core which caused greater mineral dissolution and precipitation relative to the slower flow rates.

Reactions such as the two listed above are most responsible for permeability damage by promoting smectite growth. Smectite increases the amount of material in the pore space and creates a microporosity network with its authigenic fabric that restricts flow and results in higher residual bitumen saturations.

A decrease in injection fluid salinity causes smectite swelling. This behavior decreases porosity (and permeability) because smectite occupies more pore space volume with increased hydration.

Migration-of-fines contributes to permeability reduction when the fines accumulate at and block pore throats.

The most permeability damage occurred to the core subjected to the high pH, low salinity injection fluid at low flow rates, followed by the core subjected to the high ph, low salinity injection fluid at high flow rates. The least damage occurred in the core subjected to the neutral pH, high salinity injection fluid at low flow rates. The permeability of the bitumen-saturated core was not measured. Visual observations made of that core suggest that permeability decreased to a lesser extent than in the other cores. These permeability results imply that higher flow rates reduce the effect of permeability reduction caused by high pH injection fluids.

The dissolution and reprecipitation of quartz is not considered to be a major cause of formation damage in the Clearwater Formation. The most silica transported out of a core during the course of an experiment, and therefore available for reprecipitation, was only 0.7% of the core weight.

VII. REFERENCES

Bayliss, P. and Levinson, A. A., 1971. Low temperature hydrothermal alteration synthesis from dolomite or calcite, quartz and kaolinite. Clays and Clay Minerals, 19, 109-114.

Bayliss, P. and Levinson, A. A., 1976. Mineralogical review of the Alberta oil sand deposits (Lower Cretaceous, Manville Group). Bulletin of Canadian Petroleum Geology, 24, 211-224.

Bird, G. W. and Boon, J. A., in press. 1985. Silica transport during steam injection into oil sands: I. Dissolution and precipitation kinetics of quartz-new results and review of existing data. Chemical Geology.

Boles, J. R., 1977. Zeolites in deep-sea sediments. In Mineralogy and geology of natural zeolites. Edited by F. A. Mumpton, Mineralogical Society of America Short Course Notes, 137-163.

Boon, J. A., 1977. Fluid-rock interactions during steam injection. In The oil sands of Canada-Venezuela. Edited by D. A. Redford and A. G. Winestock. Canadian Institute of Mining and Metallurgy Special Volume 17, 133-138.

Boon, J. A., Hamilton, T., Holloway, L. and Wiwchar, B., 1983. Reaction between rock matrix and injected fluids in Cold Lake oil sands - potential for formation damage. Journal of Canadian Petroleum Technology, 22(3,4), 55-66.

Boon, J. A. and Hitchon, B., 1983a. Application of fluid-rock reaction studies to in situ recovery from oil sand deposits, Alberta, Canada- I. Aqueous phase results for an experimental-statistical study of water-bitumen-shale reactions. Geochimica et Cosmochimica Acta, 47, 235-248.

Boon, J. A. and Hitchon, B., 1983b. Application of fluid-rock reaction studies to in situ recovery from oil sand deposits, Alberta, Canada- II. Mineral transformations during an experimental-statistical study of water-bitumen-shale reactions. Geochimica et Cosmochimica Acta, 47, 249-257.

Bowman, C. W., Humphreys, R. D. and Mossop, G. D., 1983. Oil sands technology and economics. Short course sponsored by the Alberta Research Council, 287p.

Busey, R. H. and Mesmer, R. E., 1977. Ionization equilibria of silicic acid and polysilicate formation in aqueous sodium chloride solutions to 300°C. Inorganic Chemistry, 16, 2444-2450.

Carrigy, M. A., 1963. Criteria for differentiating the McMurray and Clearwater Formations in the Athabasca oil sands. Research Council of Alberta Bulletin 14, 32p.

Craig, H., 1957. Isotopic standards for carbon and oxygen and correction factors for mass-spectrometric analysis of carbon dioxide. Geochimica et Cosmochimica Acta, 12, 133-149.

Craig, H., 1961. Standard for reporting concentrations of deuterium and oxygen-18 in natural waters. Science, 133, 1833-1834.

Crerar, D. A. and Anderson, G. M., 1971. Solubility and solvation reactions of quartz in dilute hydrothermal solutions. Chemical Geology, 8, 107-122.

Davies, D. K., Almon, W. R., Bonis, S. B. and Hunter, B. E., 1979. Deposition and diagenesis of Tertiary-Holocene volcaniclastics, Guatemala. In Aspects of diagenesis. Edited by P. A. Scholle and P. R. Schluger. Society of Economic Paleontologists and Mineralogists Special Publication No. 26, 281-306.

Drever, J. I., 1982. The geochemistry of natural waters. Englewood Cliffs, New Jersey: Prentice-Hall, Inc., 388p.

Energy Resources Conservation Board, 1983. Alberta's reserves of crude oil, oil sands, gas, natural gas liquids, and sulphur at December 31, 1983.

Farouq Ali, S. M., 1974. Application of in situ methods of oil recovery to tar sands. In Oil sands, fuel of the future. Edited by L. V. Hills. Canadian Society of Petroleum Geologists Memoir #3, 199-211.

Folk, R. L., 1968. Petrology of Sedimentary Rocks. Austin Texas: Hemphill's Book Store, 179p.

Friedman, I. and O'Neil, J. R., 1977. Compilation of stable isotope fractionation factors of geochemical interest. In Data of geochemistry. Edited by M. Fleischer. United States Geological Survey Professional Paper, 440-KK, 6th edition.

Galloway, W. E., 1979. Diagenetic control of reservoir quality in arc-derived sandstones: implications for petroleum exploration. In Aspects of diagenesis. Edited by P. A. Scholle and P. R. Schluger. Society of Economic Paleontologists and Mineralogists Special Publication No. 26, 251-262.

Harrison, D. B., Glaister, R. P. and Nelson, H. W., 1981. Reservoir description of the Clearwater oil sand, Cold Lake, Alberta, Canada. In The future of heavy crude and tar sands. New York: McGraw-Hill, 262-279.

Hay, R. L., 1966. Zeolites and zeolitic reactions in sedimentary rocks. Geological Society of America Special Paper 85, 130p.

Hay, R. L., 1978. Geological occurrence of zeolites. In Natural zeolites: occurrence, properties, use. Edited by L. B. Sand and F. A. Mumpton. New York: Pergamon Press, 135-143.

117

ography and geology of natural zeolites. Edited by F.
    A. Mumpton. Mineralogical Society of America Short Course Notes, 93-
    102.

Hebner, B., Bird, G. W. and Longstaffe, F. J., 1985. Fluid/pore-mineral
    transformations during simulated steam injection; implications for
    reduced permeability damage. Paper 85-36-50 presented at the 36th
    Annual Meeting of the Petroleum Society of the Canadian Institute of
    Mining and Metalurgy.

Helgeson, H. C., Brown, T. H., and Leeper, R. H., 1969. Handbook of
    theoretical activity diagrams depicting chemical equilibria in
    geologic systems involving an aqueous phase at one atm. and $0°$ to
    $300°C$. San Francisco: Freeman, Cooper and Co., 253p.

Hitchon, B., 1977. Geochemical aspects of in-situ recovery. In The oil
    sands of Canada-Venezuela. Edited by D. A. Redford and A. G.
    Winestock. Canadian Institute of Mining and Metallurgy Special
    Volume 17, 80-86.

Ignasiak, T. M., Kotlyar, L., Longstaffe, F. J., Strausz, O. P. and
    Montgomery, D. S., 1983. Separation and characterization of clay
    from Athabasca asphaltene. Fuel, 62, 353-362.

Jardine, D., 1974. Cretaceous oil sands of western Canada. In Oil
    sands, fuel of the future. Edited by L. V. Hills. Canadian Society
    of Petroleum Geologists Memoir #3, 50-67.

Kramers, J. W., 1974. Geology of the Wabasca A oil sand deposit (Grand
    Rapids Formation). In Oil sands, fuel of the future. Edited by L. V.
    Hills, Canadian Society of Petroleum Geologists Memoir #3, 68-83.

Levinson, A. A. and Vian, W., 1966. The hydrothermal synthesis of
    montmorillonite group minerals from kaolinite, quartz and various
    carbonates. The American Mineralogist, 51, 495-498.

Longstaffe, F. J., 1983. Stable isotope studies of diagenesis in clas-
    tic rocks. Geoscience Canada, 10, 43-58.

MacEwan, D. M. C. and Wilson, M. J., 1980. Interlayer and intercalation
    complexes of clay minerals. In Crystal structures of clay minerals
    and their x-ray identification. Edited by G. W. Brindley and G.
    Brown. Mineralogical Society of London Monograph No. 5, 495p.

McCorriston, L. L., Demby, R. A. and Pease, E. C., 1981. Study of
    reservoir damage produced in heavy oil formations due to steam
    injection. SPE Paper #10077.

Mellon, G. B., 1967. Stratigraphy and petrology of the Lower Cretaceous
    Blairmore and Manville Groups, Alberta foothills and plains.
    Research Council of Alberta Bulletin 21, 270p.

Minken, D. F., 1974. The Cold Lake oil sands: geology and reserves estimate. In Oil sands, fuel of the future. Edited by L. V. Hills. Canadian Society of Petroleum Geologists Memoir #3, 84-99.

Muecke, T. W., 1979. Formation fines and factors controlling their movements in porous media. Journal of Petroleum Technology, 31, 144-150.

Mumpton, F. A. and Ormsby, W. C., 1976. Morphology of zeolites in sedimentary rocks by scanning electron microscopy. Clays and Clay Minerals, 24, 1-23.

Outtrim, C. P. and Evans, R. G., 1977. Alberta's oil sands reserves and their evaluation. In The oil sands of Canada-Venezuela. Edited by D. A. Redford and A. G. Winestock. Canadian Institute of Mining and Metallurgy Special Volume 17, 36-66.

Perry, C. and Gillott, J. E., 1979. The formation and behavior of montmorillonite during the use of wet forward combustion in the Alberta oil sand deposits. Bulletin of Canadian Petroleum Geology, 27, 314-325.

Putnam, P. E. and Pedskalny, M. A., 1983. Provenance of Clearwater sandstones, Cold Lake, Alberta, with comments on feldspar composition. Bulletin of Canadian Petroleum Geology, 31, 148-160.

Reed, M. G., 1979. Gravel pack and formation sandstone dissolution during steam injection. SPE Paper #8424.

Schumacher, M. M., 1978. Enhanced oil recovery secondary and tertiary methods. New Jersey, Noyes Data Corporation, 206p.

Sedimentology Research Group, 1981. The effects of in situ steam injection on Cold Lake oil sands. Bulletin of Canadian Petroleum Geology, 29, 447-478.

Settari, A. and Raisbeck, J. M., 1981. Analysis and numerical modeling of hydraulic fracturing during cyclic steam stimulation in oil sands. Journal of Petroleum Technology, 33(11), 2201-2212.

Sheppard, R. A. and Gude, A. J., 1968. Distribution and genesis of authigenic silicate minerals in tuffs of Pleistocene Lake Tecopa, Inyo County, California. United States Geological Survey Professional Paper 597, 38pp.

Surdam, R. C. and Boles, J. R., 1979. Diagenesis of volcanic sandstones. In Aspects of diagenesis. Edited by P. A. Scholle and P. R. Schluger. Society of Economic Paleontologists and Mineralogists Special Publication No. 26, 251-262.

Sydansk, R. D., 1982. Elevated-temperature caustic/sandstone interaction: implication for improving oil recovery. Society of Petroleum Engineers Journal, 22(4), 453-462.

Thompson, M. and Walsh, J. N., 1983. A handbook of inductively coupled plasma spectrometry. Glasgow and London: Blackie, 274p.

Travis, R. B., 1955. Classification of rocks. Quart. Colorado School of Mines, 50(1).

Tremaine, P. R., Isaacs, E. E., and Boon, J. A., 1983. Hydrothermal chemistry applied to in situ bitumen recovery. Chemistry in Canada, 35(4), 29-33.

Waldorf, D. M., 1965. Effect of steam on permeabilities of water-sensitive formations. Journal of Petroleum Technology, 17(11), 1219-1222.

Walters, L. J., Claypool, G. E. and Choquette, P. W., 1972. Reaction rates and δO^{18} variation for the carbonate-phosphoric acid preparation method. Geochimica et Cosmochimica Acta, 36, 129-140.

Williams, G. D., 1963. The Manville Group (Lower Cretaceous) of central Alberta. Bulletin of Canadian Petroleum Geology, 11, 350-368.

VIII. APPENDIX 1: DETAILS OF ANALYTICAL METHODS

A. Hydrometer Analysis

Hydrometer analysis was used to determine the percentage of fine-grained material in each sample. Between 30 and 50 grams of material from each sample was soaked in 125 ml of a 4% sodium hexametaphosphate solution for approximately 8 hours to disperse the particles. After the soaking period, the material was ultrasonically disaggregated to ensure thorough dispersion of the clay-sized particles. The solution was placed in a 1l graduated cylinder and diluted with distilled water to 1000 ml (sample cylinder). A 1l graduated cylinder was filled only with 125 ml of 4% sodium hexametaphosphate and 750 ml of distilled water (control cylinder).

To begin the analysis, the sample cylinder was agitated and the contents were allowed to settle. Measurements were taken with a hydrometer at 0.25, 0.5, 1.0, 2.0, 5.0, 10.0, 15.0, 30.0, 60.0, 120.0, 240.0, 480.0, 1440.0 minutes elapsed time of both the sample and control cylinders. Temperatures of the solutions in both cylinders were also recorded. The following calculations were performed from these data:

(1) The hydrometer readings of the sample cylinder were corrected for variations in temperature and for the density of the sodium hexametaphosphate solution (temperature corrected sample reading minus control reading);

(2) Calibrated tables were used to convert the corrected sample hydrometer readings to values of effective depth;

(3) The maximum particle diameter still in suspension at a specified time was calculated by multiplying the specific gravity of that particle (assume 2.65) by the square root effective depth divided by the specified time;

(4) To calculate the percentage of material still in suspension at a specified time, the corrected hydrometer reading was divided by the weight of the sample (determined before addition of sodium hexametaphosphate solution).

The percentage of material still in suspension represents the percentage of sample that is less than the calculated particle size diameter. Plots were constructed consisting of smooth curves drawn through points of particle size diameter versus percentage of material still in suspension.

In the case of samples 1.1, 1.4, 2.1 and 2.4 a variation of this method was used because of a sample availability. The fraction from the catch pan (from wet sieve analysis) was dispersed and analyzed with a hydrometer by the procedure outlined above. To calculate the percentages of material finer than the calculated particle size diameter, the percentages from the hydrometer calculations were multiplied by the

weight percent of the <38, μm fraction (catch pan fraction) determined in the wet sieve analysis.

B. Wet Sieve Analysis

Approximately 100 grams of sample was weighed to 0.01 g, placed in a mixture of 400 ml H_2O plus 10 ml isopropanol, and boiled. The following sieves (in U.S. standard size #) were weighed and stacked in descending order with the largest sieve on top: 18; 25; 35; 45; 60; 80; 120; 170; 230; 325; and 400.

The analysis was initiated by transferring the sample to the top (largest) sieve. The sample was washed through the sieve using a fine spray of water and a rubber policeman until the water leaving the base of the sieve was clear. The bottom of the sieve was rinsed and the sieve (with the sample material retained by it) was dried in an oven. This procedure was repeated for each sieve down through the stack. The contents of the catch pan were dried with infra-red light.

All the sieves and the catch pan were weighed once again. The amount of material retained by each sieve was calculated by subtracting the pre-sieving weight from the post-sieving weight. The net weights were summed and the net weight of each sieve or pan was divided by the sum net weight to yield the fractional percentage of material retained by each sieve. To obtain the cumulative percentage retained by each sieve, the fractional percentage of that sieve and all larger sieves were added together. The value obtained corresponds to percentage of sample that is coarser than the size of that sieve. To obtain a distribution of percentage less than (the grain size represented by the sieve), the cumulative percentage retained by each sieve was subtracted from 100%.

The last step in the calculation was not in keeping with standard wet sieve calculations but enabled easier graphical comparison of the wet sieve data with hydrometer data.

C. Petrographic Study

Because none of the samples (pre- or post-flood) were well-indurated, epoxy grain mounts were made. Thin sections were cut from these mounts. The color of the mounting medium is blue; blue in the thin section photographs does not represent porosity nor stain. The fact that some samples appear more porous than others is a remnant of the mounting process. All photographs were taken with a Wild MPS 51S Spot Camera mounted on a Leitz OrthoTux II POL-BK Microscope.

D. Gravimetric CO_2 Analysis

Gravimetric CO_2 analysis was used to determine the CO_2 content (weight %) of a sample and, if the type of carbonate present was known, then the weight percent of the carbonate could be calculated. The procedure is based on evolving CO_2 from the sample with concentrated HCl and then trapping the CO_2 for weight measurement.

Five (5) to 10 g of sand were dried at $110°C$ for one hour and then dessicated. The sand was weighed to the nearest 0.0001 g and placed in a 100 ml three-necked round bottom flask. One neck of the flask was connected in series with a conden er, four successive U-tubes and a rotameter. The first U-tube in series was filled with drierite (anhy-drite), the second and third were filled 3/4 with ascarite (NaOH-covered asbestos) and 1/4 with drierite, and the last U-tube was filled with drierite. A U-tube filled with drierite and ascarite was placed on-line before the round bottom flask. N_2 gas, attached to this first U-tube, was used to purge, the entire system and to carry the evolved gasses through the series of four U-tubes. The two U-tubes containing ascarite on-line after the flask were weighed before the analysis began.

To start the analysis, 6N HCl was added to the sand in the round bottom flask. This resulted a reaction between the acid and the carbo-nate in the sample:

$$MCO_3 + HCl = MCl_2 + H_2O + CO_2,$$
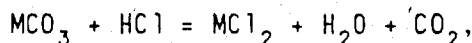
where M represents the cation in the carbonate. The water evolved was trapped by the drierite and the CO_2 evolved was trapped by the ascar-ite. HCl was added to the sand until gas was no longer evolved (bub-bling ceased). At this point, the solution with the sand in the flask was boiled for 15 minutes. The two ascarite tubes were taken off-line and weighed to determine the weight increase that occurred due to the following reaction:

$$2NaOH + CO_2 = Na_2CO_3 + H_2O.$$

The weight % CO_2 in the sand was calculated by dividing the weight increase of the two ascarite-filled U-tubes by the original sand sample weight. This quotient was multiplied by 100 to obtain a percentage figure.

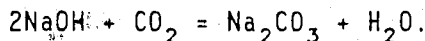The weight percent of calcite or dolomite (if it was determined that either one was present) could be calculated from the weight per-cent of CO_2 given that the molecular weights of CO_2, calcite and dolo-mite are 44.01 g/mol, 100.09 g/mol, and 184.41 g/mol respectively.

(1) calcite   wt% $CaCO_3$ = 100.09(wt% CO_2)/44.01.
(2) dolomite   wt% $MgCa(CO_3)_2$ = 184.41(wt% CO_2)/2(44.01)

E. Backpack X-ray Diffraction Analysis

Backpack diffractograms were obtained to determine the mineralogy of each sample. Two grams of sample were crushed with a mortar and pestal to pass a #325 sieve. Non-oriented XRD samples were then pre-pared from the powders so as to measure the hkl reflections. XRD pat-terns were obtained with a Philips diffractometer using Co K_α radiation generated at 50 kV and 20 mA with one degree divergent slits and a time constant of 2. The scan and chart speeds were 1° 2θ/min and 600 mm/h, respectively. Humidity of the chamber was not controlled.

F. Clay Mineral Analysis

The composition and relative abundances of the clay minerals were determined using the following procedure. Approximately 25 g of sand was soaked in a 125 ml solution of 4% sodium hexametaphosphate over-night. Ultrasonic disaggregation was then used to ensure that the clay-size particles were thoroughly dispersed. This solution was placed in a 1l graduated cylinder or settling column and diluted to 1000 ml with distilled water.

Three size fractions were collected from each sample by gravitational settling ($<2\mu m$, 2-5 μm and 5-20 μm) using Stoke's Law to ca late the settling rate of each size fraction in distilled water. The settling procedure was repeated three times for each size fraction to ensure that all the desired portion was collected. The various size fractions were then treated with 1% sodium hypochlorite and heated to 65 C for 48 hours to destroy organic material.

Two separate aliquots of the ⬛ μm fraction were rinsed with dis-tilled water to remove the sodium hexametaphosphate and the sodium hypochlorite. One portion was saturated with potasium (2M KCl solution for three hours) and the other was saturated with calcium (2M $CaCl_2$ solution for three hours). These samples were then thoroughly washed of excess potassium or calcium with distilled water and then freeze-dried. The resulting material was deposited onto a ceramic disc by suction. This procedure resulted in the preferred basal orientation of the clays. The 2-5 μm and 5-20 μm fractions were rinsed, freeze-dried and deposited onto ceramic discs in the Na-saturated form (from the sodium hexametaphosphate and the sodium hypochlorite). XRD patterns were collected under the same conditions outlined in the preceding section.

Less Than 2 μm Fraction

Since the <2 μm fraction contained mostly clay minerals, the samples underwent a series of XRD treatments following the method of Ignasiak et al. (1983) to distinguish the clay minerals present. Each clay mineral shows characteristic basal reflections for each treatment.

Semi-quantitative estimates of clay mineral abundances were prepared using peak heights and appropriate form factors for clay mineral crystallinities (Don Scafe, personal communication). The calculation procedure is outlined below.

(1) A smooth baseline was drawn beneath the first order peaks on the glycolated and K-550 C patterns.

(2) Measurements for the kaolinite, illite and montmorillonite peaks were taken from the glycolated pattern. The peak height was measured by subtracting the intensity of the baseline (or back-ground) from the intensity the peak.

(3) The measurement for the chlorite peak was taken from the K-550°C pattern in the same manner that the other peaks were measured

(note: the machine settings should be the same when both types of diffractograms were generated).

(4) Form factors were calculated as follows:

(a) Illite (10 Å clay) was used as an internal standard and assigned a form factor of 1.000;

(b) Smectite form factor = $\dfrac{\text{height of smectite peak}}{4 \times \text{height of illite peak}}$

(c) Chlorite form factor = $\dfrac{\text{height of chlorite peak}}{3 \times \text{height of illite peak}}$

(d) Kaolinite form factor = $\dfrac{\text{height of kaolinite peak}}{2.5 \times \text{height of illite peak}}$

(5) The form factors were summed and the individual form factors were divided by the sum to yield preliminary relative abundances.

(6) To account for overlap of the chlorite 002 peak on the kaolinite 001 peak, the preliminary chlorite abundance was subtracted from the preliminary kaolinite abundance. All of the subsequent abundances were summed again and the individual abundances were divided by the new sum to yield the relative abundances of the clay minerals present.

This method is generally reproducible to within ±10%.

Two(2)-5 and 5-20 μm Fractions

The 2-5 and 5-20 μm fractions were not saturated with calcium or potassium (but with Na); the semi-quantitative method for calculating relative abundances of clay minerals in the <2 μm fraction was not used. Instead, the clay mineralogy of these portions was characterized by smectite:illite and kaolinite:illite ratios. These ratios were calculated using peak intensities from two diffractograms:

(1) Na-disc maintained at 54% humidity ($2°-60°$ 2θ range);
(2) Na-disc heated to $550°C$ for one hour and maintained at 0% humidity ($2°-35°$ 2θ range).

The intensity of the smectite peak was calculated by subtracting the intensity of the 14.4 Å peak on the diffractogram collected at $550°C$ from the intensity of the 15.0 Å peak on the diffractogram collected at room temperature.

The intensities of the kaolinite and illite peaks equal the intensities of the 7.2 Å and 10.2 Å peaks, respectively, on the room temperature diffractogram.

The smectite:illite and kaolinite:illite ratios were calculated by dividing the appropriate peak intensities. These intensities were not corrected using form factors in the manner used for the <2 μm fraction.

G. Scanning Electron Microscopy (SEM)

Scanning electron micrographs were taken of all the samples (i.e., pre-flood sand without bitumen, pre-flood sand saturated with bitumen, post-flood non-bitumenous sand, and post-flood bitumenous sand).

Mounts of bitumen-free sand were made by gluing the sand to stubs with a silver-based paint. Sand samples that had significant amounts of bitumen present were placed in vacuum at $30^\circ C$ for two days to remove the light petroleum ends. These samples were then mounted on stubs in the same manner as the bitumen-free samples were. All the mounts were sputter-coated twice with gold before being analyzed. The micrographs were taken with a Cambridge F250 scanning electron microscope. Energy dispersive analysis was completed with a Kevex micro-X 7000.

H. Stable Isotope Analysis of Carbonates

The oxygen- and carbon-isotope composition of the carbonates were determined by reacting crushed rock samples with phosphoric acid (method after Walters et al., 1972). The isotope data are given in δ notation with respect to Bellemnitella americana from the Pee Dee Formation (PDB) for carbon (Craig, 1957) and Standard Mean Ocean Water (SMOW) for oxygen (Craig, 1961). A more detailed treatment of the use of stable isotopes in diagenetic interpretation is given by Longstaffe (1983).

I. Preparation Procedure For Fluid Analyses

Two different methods were used to prepare the production fluid samples for Total Inorganic Carbon (TIC) and Inductively Coupled Argon Plasma (ICP). The type of method used depended on whether the fluid sample was collected during a bitumen-free or bitumen-saturated experiment.

The following procedure was used for fluid samples collected during bitumen-free experiments. The volume of the production fluid sample was measured. Recorded volumes of a 0.1N NaOH and phenolphthalein red solution were added to the samples. This converted all the CO_2 to bicarbonate by the reaction:

$$CO_2 + NaOH = HCO_3^- + Na^+.$$
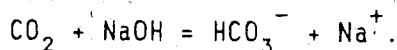
The endpoint of the reaction was reached when the solution turned from red to clear. An aliquot (5 ml) was then taken for TIC analysis. The remaining portion of the solution was acidified with concentrated nitric acid and an aliquot was taken for ICP analysis. The volumes of NaOH and HNO_3 added to the production fluid samples were recorded in order to determine the dilution factors when calculating actual concentration.

This method of sample preparation was altered somewhat to accommodate the bitumen. The CO_2 was extracted from the production fluid accumulators under vacuum and then trapped in a bubble chamber with the

NaOH solution. An aliquot of the solution in the bubble chamber was taken for TIC analysis. It was later determined that this method was faulty. The fluid remaining in the sample accumulator was acidified with the concentrated HNO_3 and sent for ICP analysis. The main difference, then, between the two methods of sample preparation is aliquots for ICP analysis of bitumen-free fluid samples were brought to basic (with NaOH) and subsequently acidified whereas the samples taken for ICP analysis from the bitumen experiment were not taken to basic with NaOH.

J. Total Inorganic Carbon Analysis

The concentration of inorganic carbon in the production fluid samples was determined using a Dohrmann DC-80 Automated Laboratory Total Organic Carbon Analyzer complete with a Horiba Model PIR-2000 General Purpose Infrared Gas Analyzer. All the inorganic carbon was converted to carbon dioxide by reaction with nitric acid (HNO_3) present in a persulfate (S_2O_8) solution. The amount of carbon dioxide generated could be quantitatively determined using an infrared detector (Horiba Infrared Gas Analyzer).

K. Inductively Coupled Argon Plasma Analysis

The cation concentrations of the fluid samples were determined with a Bausch and Lomb Model 34000 Inductively Coupled Plasma Spectrometer. The optical path was 1 m, the grating was 1080 lines/mm and the primary slit was 20 μm. Operating conditions were (Ed Zacharuk, personal communication):

        .incident power - 1200 watts
        collant gas flow - 10.5 l/min
        nebulizer gas flow - 1 l/min
        plasma gas flow - 0.75 l/min
        sample uptake - 1.8 ml/l
        sampling time - three 10 s integrations
        observation height - 14 mm above load coil
        observation temperature - 6000 K to 8000 K

The reader is referred to Thompson and Walsh (1983) for a detailed discussion of ICP analysis.

L. Permeability Measurements

Permeability measurements were conducted at room temperature with the differential pressure transmitter loop part of the apparatus. These measurements were based on the expression of Darcy's Law for fluid flow through a porous medium:

$$K = \frac{\eta Q L}{A \cdot dp}$$

        where: K = permeability (darcys)
               η = fluid viscosity (centipoise)
               Q = flow rate (cm/s)

$$L = \text{length of the core (cm)}$$
$$A = \text{area of the core base (cm}^2)$$
$$dp = \text{pressure drop across the core (atm).}$$

Because of the weak concentrations of NaCl and NaOH in the injection fluids, the value for viscosity (η) was taken as the viscosity of distilled water. The value of the flow rate was the rate at which the fluid was injected into the core. This value was changed during the course of the permeability determination in order to check the reproducibility of the tests (permeability of the cores should have changed with flow rate). Both L and A were measured directly from each core after the cores were removed from the apparatus. The one variable that was measured during the permeability tests was the pressure drop across the core (dp). The procedure of dp measurement is outlined in Chapter 3.

The permeability of core #4 was not measured because bitumen was present in the core. The value calculated would have been a relative permeability. Also, the procedure would have displaced some of the bitumen from the core.

M. Problems Encountered During Experiments

During each experiment, pressure conditions became such that the experiment had to be shut down (ruska pump and oven turned off). The fault was found and repaired. The experiments were restarted in the same manner that they were initially started.

The cause of the shut down was the same for runs #1 and #2. The injection line burst due to corrosion from the injection fluids. Corrosion was a result of fluid vaporization which caused increased salt concentration in the injection line at the point of vaporization. This bursting occurred at 1004.6 ml cumulative fluid injected in the first experiment and at 1803.1 ml cumulative fluid injected during the second experiment.

The third experiment was shut down twice because a leak developed in the lead core sleeve. The stainless steel sleeve tore the first time at 5485.1 ml cumulative fluid injected. The core was repaired by molding a teflon sleeve around the torn lead sleeve. The second shut down occurred at 7274.1 ml fluid injected because the teflon sleeve broke. The teflon sleeve was replaced with another teflon sleeve which held for the duration of the experiment. However, the permeability of the core was determined after the second shut down (at 7274.1 ml injected) because uncertainty existed as to whether a major core rupture might occur, thereby eliminating the possibility of a final permeability determination.

Two different types of problems were encountered during the fourth experiment, the second resulting in a shut down. The first problem occurred at 122.8 ml cumulative fluid injected when production pressure was lost in one of the effluent accumulators. This caused a rapid escape of the production fluids (including bitumen) from the core. The

accumulator was immediately taken off-line and the pressure was manually restored. The second shut down occurred at 1648.9 ml cumulative fluid injected when the injection line burst in the same manner that it burst during the first and second experiments. Once again, the line was replaced and the experiment was restarted and run to its duration.

IX. APPENDIX 2: DATA TABLES

Table 2-1. Grain size analysis of the pre-flood sand and core #1 using hydrometer settling. PF = pre-flood sand.

size fraction μm	PF	wt % less than			
		1.1	1.2	1.3	1.4
105	20		25	30	
76	10		19	22	
54	7		16	17	
38	6		14		
24			12	14	
17	5				
14				12	
10	4				
7		5.6	9		6.5
5	3	5.4		8	6.3
3		3.5	5		5.2
2	2				4.6
1			4		4.3

Table 2-2. Grain size analysis of core #2 using hydrometer settling.

size fraction μm	wt % less than			
	2.1	2.2	2.3	2.4
103		29	24	
74		17	15	
52		16	13	
37		15	12	
23		14		
17		12		
10		10		
7	3.5		11	5.0
5	2.6	7	9	4.9
3	2.5	6	8	3.4
2	2.3			2.9
1	1.9		7	2.6

Table 2-3. Grain size analysis of core #3 using hydrometer settling.

size fraction μm	wt % less than			
	3.1	3.2	3.3	3.4
100	29	26	30	34
71	18	18	21	25
51	16	15	16	20
36	14		15	18
23		14		17
17			14	16
13		13		
7	13	12	13	14
5		11		13
3	12			
1	11		12	

Table 2-4. Grain size analysis of core #4 using hydrometer settling.

size fraction μm	wt % less than			
	4.1	4.2	4.3	4.4
103	28	28	28	28
74	15	15	15	16
53	9	8	11	11
38	8	7	8	8
24	7	6		
17			7	7
14	6	5	6	
7				5
5	4		5	
3			4	4
2	3	3	3	
1				3

Table 2-5. Grain size analysis by wet sieving. PF = pre-flood sand.

size fraction μm	PF	1.1	1.4	wt % less than 2.1	2.4	3.1	3.4	4.1	4.4
1000	99.4	99.8	99.3	99.2	99.1	99.5	99.4	99.5	99.9
710	98.6	99.4	98.4	98.4	97.7	98.3	98.2	98.5	99.7
500	98.4	99.0	97.7	97.7	96.3	97.4	97.2	97.4	99.4
350	97.0	98.5	96.7	96.8	95.2	96.2	95.8	96.3	99.1
250	83.8	92.2	88.4	89.1	87.5	87.7	87.2	91.7	95.2
177	45.0	62.6	56.5	59.0	56.9	57.7	57.0	67.9	72.0
125	24.5	31.8	27.1	29.7	26.5	29.6	26.9	38.6	40.5
88	10.0	19.5	17.2	16.6	15.5	17.6	14.2	19.4	21.6
62.5	5.6	12.0	12.0	9.5	9.5	10.5	7.9	9.0	9.8
44	4.6	9.7	10.1	7.8	7.8	8.5	6.4	7.0	7.2
38	4.1	8.9	9.4	7.3	7.3	7.7	5.8	6.0	6.3

Table 2-6. Carbonate oxygen and carbon isotope values for selected samples. Values given in permill (parts per thousand). PF = pre-flood sand.

Sample	Dolomite $\delta^{18}O_{SMOW}$	$\delta^{13}C_{PDB}$	Calcite $\delta^{18}O_{SMOW}$	$\delta^{13}C_{PDB}$
PF	24.4	0.0		
1.1	18.8	-0.3	-9.4	-1.9
1.4			-10.8	-3.1
2.1	16.1	-0.6		
2.4	13.5	-0.6	-10.6	-1.9
3.2	19.0	-0.4		
3.4	14.6	-0.5		
4.1	1.7	-1.4		
4.3	16.4	-0.3		
4.4	17.0	-0.2		

Table 2-7. CO$_2$ and cation concentrations in run #1 production fluids. Concentration values in mg/kg. nd = below detection limit.

Sample Interval ml of injection fluid		CO2	Ca	Si	K	S	Li	Fe	B
0.0-	69.6	272							
69.6-	116.0	2231	12	48	266	143	3.1	137	55
116.0-	143.3	4018							
143.3-	186.1	5126	15	120	163	94	3.8	106	54
186.1-	212.0	8624							
212.0-	260.9	3919	24	159	179	55	5.2	57	45
260.9-	288.3								
288.3-	322.2	7370							
322.2-	540.7	1792	33	188	113	23	3.5	22	23
540.7-	584.5	1313	71	171	118	24	3.3	1	13
584.5-	616.3	1909	40	202	116	17	3.6	86	13
616.3-	663.9	1173							
663.9-	924.8	846	54	179	114	11	3.4	5	9
924.8-	948.8	711							
948.8-	1004.6								
1004.6-	1047.0		63	12		5	nd	1	1
1047.0-	1164.4	569	46	112	60	4	nd	69	2
1164.4-	1497.2	1105	40	208	138	6		20	2
1497.2-	1539.2	1072	47	217	152	29	1	6	1
1539.2-	1766.0	1307	62	184	174	3	1	13	1
1766.0-	2612.2								
2612.2-	2647.1	1246	33	239	189	3	1	1	1
2647.1-	3211.5								

Table 2-8. CO_2 and cation concentrations in run #2 production fluids. Concentration values in mg/kg. nd = below detection limit.

Sample Interval ml of injection fluid		CO_2	Ca	Si	K	S	Li	Fe	B
0.0-	45.6								
45.6-	69.0	536	5.6	20	58	50	0.3	1	15
69.0-	100.2	2393							
100.2-	122.9	4962	10.0	118	124	125	1.2	4	41
122.9-	143.9								
143.9-	164.9	7500	12.0	191	99	89	1.0	3	45
164.9-	186.7	7040							
186.7-	204.8	8660	8.8	229	70	39	0.7	1	35
204.8-	225.3								
225.3-	245.8	10500	7.4	225	59	32	nd	1	24
245.8-	255.3	7715							
255.3-	286.8								
286.8-	307.3	5677	5.7	225	45	21	0.5	nd	10
307.3-	512.9	3182	4.7	242	40	17	0.6	1	5
512.9-	588.6	1830							
588.6-	677.4	1734	3.7	246	31	12	0.5	<1	1
677.4-	757.5	1348	7.3	193	32	9	0.6	28	1
757.5-	821.4	1786	5.6	235	35	11	0.6	1	1
821.4-	885.8	1804	5.9	227	34	7	0.6	1	1
885.8-	923.6	1496	6.4	237	36	8	0.6	1	1
923.6-	1375.8	1190	7.8	236	45	7	1.0	4	1
1375.8-	1498.6								
1498.6-	1535.5	455	11.7	246	60	9	1.2	2	1
1535.5-	1635.1								
1635.1-	1803.1	190	12.2	257	73	13	1.3	3	1
1803.1-	1921.1								
1921.1-	1962.4	276	25.3	236	85	12	1.7	1	1
1962.4-	2290.5								
2290.5-	2328.5	337	18.4	225	85	6	2.4	1	1
2328.5-	3260.8								

Table 2-9. CO_2 and cation concentrations in run #3 production fluids. Concentration values in mg/kg. nd = below detection limit.

Sample Interval ml of injection fluid		CO_2	Ca	Si	K	S	Li	Fe	B
0.0-	39.1								
39.1-	59.6	723	8.0	35	32	28	nd	4	5
59.6-	78.1	734							
78.1-	104.0	1210	5.2	21	43	66	0.5	2	15
104.0-	121.1								
121.1-	141.6	3260	12.5	77	55	127	1.0	4	31
141.6-	162.1	4465							
162.1-	178.9	6400	12.5	165	66	104	1.0	3	41
178.9-	207.1	7760							
207.1-	229.3								
229.3-	249.6	12860	7.0	183	59	32	nd	1	29
249.6-	271.2	15196							
271.2-	286.0								
286.0-	296.0	10433	9.1	217	51	26	nd	2	24
296.0-	316.0	5173							
316.0-	500.4	2487	5.8	236	41	23	0.6	1	7
500.4-	529.0	2933							
529.0-	555.1	2383	6.1	237	38	19	0.6	2	2
555.1-	630.5	2218							
630.5-	674.4	1886	4.8	235	35	15	0.6	1	1
674.4-	980.0	1354							
980.8-	1020.4								
1020.4-	1107.6	924	5.1	245	35	11	0.6	1	1
1107.6-	1529.8	771	5.4	246	36	8	0.7	1	1
1529.8-	4390.9								
4390.9-	4456.1	82	14.2	248	65	15		<1	<1
4456.1-	9887.7								
9887.7-	9970.4	277	6.0	247	63	3	0.3	<1	<1
9970.4-	10148.4								

Table 2-10. Cation concentrations in run #4 production fluids. Concentration values in mg/kg. nd = below detection limit.

Sample Interval ml of injection fluid		Ca	Si	K	S	Li	Fe	B	Mg	Al
0.0-	12.5	5.0	34	520	155	1.0	1.	330	1.7	nd
12.5-	43.9	7.0	39	475	265	1.8	12	126	1.7	3.3
43.9-	67.7									
67.7-	122.8	10.4	158	108	100	1.0	4	133	1.2	0.7
122.8-	138.6									
138.6-	157.7	7.2	54	12	33	0.2	6	42	2.2	15.4
157.7-	183.6									
183.6-	260.9	8.7	140	24	38	0.2	1	42	1.8	0.7
260.9-	279.7									
279.7-	385.5	6.6	205	28	37	0.4	1	66	1.0	1.2
385.5-	751.5	4.8	230	34	23	0.4	nd	22	0.3	0.4
751.5-	1237.1	4.6	230	42	13	0.6	nd	2	0.4	0.3
1237.1-	1648.9	5.0	230	51	7	0.9	<1	1	0.5	nd
1648.9-	1656.5									
1656.5-	1675.7	7.9	104	42	8	0.6	2	1	1.4	0.6
1675.7-	1783.5									
1783.5-	2274.7	4.9	215	62	3	1.0	1	1	0.4	nd
2274.7-	2742.6	4.5	215	68	3	0.9	1	1	0.4	nd
2742.6-	3287.8	4.0	215	74	4	0.9	<1	1	0.4	nd